

BIOGEOCHEMICAL CONTROLS OF URANIUM  
REMEDICATION AND TRANSPORT

by  
Martin A. Dangelmayr

A thesis submitted to the Faculty and the Board of Trustees of the Colorado School of Mines in partial fulfillment of the requirements for the degree of Doctor of Philosophy (Environmental Science and Engineering).

Golden, Colorado

Date \_\_\_\_\_

Signed: \_\_\_\_\_  
Martin A. Dangelmayr

Signed: \_\_\_\_\_  
Dr. Linda Figueroa  
Thesis Advisor

Signed: \_\_\_\_\_  
Dr. James Stone  
Thesis Advisor

Golden, Colorado

Date \_\_\_\_\_

Signed: \_\_\_\_\_  
Dr. Terri Hogue  
Professor and Head  
Department of Civil and Environmental Engineering

## ABSTRACT

In the U.S. almost 140 sites have been contaminated by uranium mining and milling operations or by the storage of radioactive materials. *In-situ* recovery (ISR) facilities still face challenges restoring water to pre-mining conditions and leave behind elevated uranium concentrations. Bioremediation and reactive transport modeling are potential tools to mitigate the impact of uranium contamination on human and environmental health, through their ability to immobilize uranium and assess the effectiveness of natural uranium attenuation. This project investigated biogeochemical aspects of both active and natural remediation of uranium contaminated subsurface for two field sites: The Smith Ranch Highland (SRH) site in WY, and the Rifle, Integrated Field Research Challenge (IFRC) site in CO. Our project objectives were to study the transformation of organic substrate during biostimulation and assess uranium retardation due to sorption with sediments taken from an ISR site. This thesis presents two research projects that address the remediation and risk assessment of uranium contaminated sites.

The first project evaluated the impact of added organic carbon on the long-term biogeochemical attenuation of uranium in the subsurface of a former mill tailings site. Fluorescence and specific ultraviolet absorption (SUVA) analyses were used together with dissolved organic carbon (DOC) measurements to track organic carbon dynamics during and post-biostimulation of the 2011 Rifle IFRC experiment. An electron mass balance was performed on well CD01 to determine if any carbon sinks were unaccounted for. DOC values increased to 1.76 mM-C during biostimulation, and 3.18 mM-C post-biostimulation over background DOC values of 0.3-0.4 mM-C. Elevated DOC levels persisted 90 days after acetate injections ceased. The electron mass balance revealed that assumed electron acceptors would not

account for the total amount of acetate consumed. Fluorescence spectra showed an increase in signals associated with soluble microbial products (SMP), during biostimulation, which disappeared post-biostimulation despite an increase in DOC. SUVA analyses, indicated that DOC present post-biostimulation is less aromatic in nature, compared to background DOC. Our results suggest that microbes convert injected acetate into a carbon sink that may be available to sustain iron reduction post-stimulation

The second project consisted of two sets of column experiments and attempted to evaluate the impact of alkalinity and pH on the sorption of uranium in sediments from an ISR site. The ability of thermodynamic models to predict uranium behavior under conditions relevant to ISR restoration sites was also tested. Sediments at three different depths from a monitoring well at the SRH site were used in nine column studies and six batch experiments to study the sorption capacity of SRH sediments and estimate uncertainties associated with fitted parameters. Sediments were characterized by X-Ray Diffraction (XRD) and X-Ray Fluorescence (XRF) for dominant mineralogy and Brunauer-Emmett Teller (BET) measurements to determine sediment surface area. Uranium transport in the columns was modeled with PHREEQC using a generalized composite surface complexation model (GC SCM). A parameter estimation program (PEST) was coupled to PHREEQC to derive best parameter fits according to correlation coefficients and lowest sums of residuals squared.

In the first set of sorption experiments a GC SCM utilizing one, two, and, three generic surfaces, was evaluated in 5 column studies to find the simplest model with the best fit. A 2-pK model with strong and very strong sorption sites was found to produce model results in best agreement with observed data. Uranium breakthrough was delayed by a factor of 1.68, 1.69 and 1.47 relative to the non-reactive tracer for three of the 5 experiments at an alkalinity of 540 mg/l.

while a sediment containing smectite and kaolinite retained uranium by a factor of 2.80 despite a lower measured BET surface area. Decreasing alkalinity to 360 mg/l from 540 mg/l in the kaolinite containing sediments increased retardation by a factor of 4.26. Model fits correlated well to overall BET surface area in the three columns where clay content was less than 1%. For the sediment with clay, models consistently understated uranium retardation when reactive surface sites were restricted by BET results. Calcite saturation was shown to be a controlling factor for uranium desorption as the pH of the system changed to a lower value. A pH of 6 during a secondary background water flush remobilized previously sorbed uranium resulting in a secondary uranium peak at twice the influent concentrations. The first set of sorption experiments demonstrated the potential of GC SCM models to predict uranium transport in sediments with homogenous mineral composition, but highlighted the need for further research to understand the role of sediment clay composition and calcite saturation in uranium transport.

The second set of experiments consisted of duplicate column studies on two sediment depths. Columns were flushed with synthesized restoration waters at two different alkalinities (160 mg/l CaCO<sub>3</sub> and 360 mg/l CaCO<sub>3</sub>) to study the effect of alkalinity on uranium mobility. Low alkalinity (160 mg/l CaCO<sub>3</sub>) water at pH of 7.5 was introduced after 143 hours, to mimic background water entering the restoration zone. Uranium breakthrough occurred 25% - 30% earlier in columns with 360 mg/l CaCO<sub>3</sub> over columns fed with 160 mg/l CaCO<sub>3</sub> influent water. Fitted models produced R<sup>2</sup> values of > 0.9 for all columns using a 2-surface site model with strong and very strong sorption sites. The results demonstrated that the GC SCM approach is capable of modeling the impact of carbonate on uranium in flow systems. Derived site densities for the two sediment depths were between 135 and 177 μmol-sites/kg-soil, showing similar sorption capacity despite heterogeneity in sediment mineralogy. Model sensitivity to alkalinity

and pH was shown to be moderate compared to fitted site densities, when calcite saturation was allowed to equilibrate. Calcite kinetics emerged as a potential source of error when fitting parameters in flow conditions. Fitted results were compared to data from batch experiments conducted on SRH sediments prior, and column studies from the first set of experiments, to assess variability in derived parameters. Parameters from batch experiments were lower by a factor of 1.5 to 3.9 compared to column studies completed on the same sediments. The difference was attributed to errors in solid-solution ratios and the impact of calcite dissolution in batch experiments. Column studies conducted at two different laboratories showed almost an order of magnitude difference in fitted site densities suggesting that methodology may play a bigger role in column sorption behavior than actual sediment heterogeneity. Our results demonstrate the necessity for ISR sites to remove residual  $p\text{CO}_2$  and equilibrate restoration water with background geochemistry to reduce uranium mobility. In addition, the observed variability between fitted parameters on the same sediments highlights the need to provide standardized guidelines and methodology for regulators and industry when the GC SCM approach is used in subsequent risk assessments.

This study demonstrates the impact of biogeochemical parameters on uranium remediation and transport at current and former mining and milling sites. Subsurface bioremediation projects need to incorporate microbial transformation of injected organic carbon into conceptual models and operational procedures. Furthermore, the potential of thermodynamic models to predict uranium behavior at ISR restoration sites was shown to depend highly on accurate representation uranium geochemistry and experimental methodology to derive sorption parameters. The work herein advises regulators and industry on the best practices for the management of uranium contaminated field sites to protect the public health and the environment.

## TABLE OF CONTENTS

ABSTRACT.....	iii
LIST OF FIGURES.....	xi
LIST OF TABLES.....	xiii
ACKNOWLEDGMENTS.....	xv
CHAPTER 1 LITERATURE REVIEW OF URANIUM BIOGEOCHEMISTRY: CHALLENGES FOR REMEDIATION AND RISK ASSESSMENT.....	1
1.1 Uranium contamination from uranium mining and milling operations.....	1
1.2 Overview of uranium biogeochemistry.....	2
1.3 Bioremediation challenges: Organic carbon dynamics.....	4
1.4 Risk assessment and transport modeling on ISR sites.....	8
1.5 Scope and purpose of study.....	11
CHAPTER 2 CHARACTERIZING ORGANIC CARBON DYNAMICS DURING BIOSTIMULATION OF A URANIUM CONTAMINATED FIELD SITE...	15
2.1 Introduction.....	15
2.2 Methods.....	19
2.2.1 Site description and field experiment.....	19
2.2.2 Sample collection and preparation.....	20
2.2.3 Groundwater chemical analysis.....	20
2.2.4 Organic acids, TOC, and SUVA analyses.....	21
2.2.5 Fluorescence analysis and EEM regional integration.....	21

2.2.6	Microbial stoichiometries and conceptual model.....	22
2.3	Results.....	25
2.3.1	General performance.....	25
2.3.2	Organic Carbon.....	25
2.3.3	Electron utilization accounting.....	28
2.3.4	SUVA 254 nm results.....	28
2.3.5	Excitation-emission matrices and regional intensities.....	29
2.4	Discussion.....	30
CHAPTER 3 LABORATORY COLUMN EXPERIMENTS AND TRANSPORT MODELING TO EVALUATE RETARDATION OF URANIUM IN AN AQUIFER DOWNGRAIENT OF A URANIUM IN-SITU RECOVERY SITE.....		40
3.1	Introduction.....	40
3.2	Methods.....	43
3.2.1	Site Description.....	43
3.2.2	Sediment core collection.....	44
3.2.3	Sediment core analysis.....	45
3.2.4	Ground water preparation.....	46
3.2.5	Column setup.....	47
3.2.6	Column operation.....	49
3.2.7	Column transport modeling.....	50

3.3 Results.....	52
3.3.1 Sediment analysis and estimation of site densities.....	52
3.3.2 Column operation.....	53
3.3.3 Column modeling.....	58
3.4 Discussion.....	60
3.4.1 Effect of sediment heterogeneity on uranium breakthrough.....	60
3.4.2 Effect of reductive processes on uranium breakthrough.....	66
3.4.3 Effect of alkalinity on uranium breakthrough.....	68
3.4.4 Effect of calcite on uranium sorption.....	70
3.5 Conclusions.....	72
 CHAPTER 4 UNCERTAINTY AND VARIABILITY IN LABORATORY DERIVED SORPTION PARAMETERS FROM A URANIUM IN-SITU RECOVERY SITE.....	 75
4.1 Introduction.....	75
4.2 Methods.....	78
4.2.1 Sediment collection and characterization.....	78
4.2.2 Column preparation.....	80
4.2.3 Column operation and water analysis.....	81
4.2.4 Modeling and parameter fitting.....	82
4.3 Results.....	86

4.3.1	Experimental results.....	87
4.3.2	Modeling and fitting results.....	91
4.4	Discussion.....	93
4.4.1	Modeling effects of carbonate dynamics on uranium transport.....	93
4.4.2	Model sensitivity to carbonate dynamics.....	96
4.4.3	Significance of calcium carbonate dynamics for ISR restoration.....	99
4.4.4	Modeling desorption hysteresis.....	100
4.4.5	Cross-comparison between different sorption experiments.....	101
4.4.6	Uncertainty in upscaling parameters to field sites.....	106
4.5	Conclusion.....	106
<b>CHAPTER 5 SUMMARY REMARKS AND FUTURE RESEARCH NEEDS</b>		<b>108</b>
<b>APPENDIX A BATCH SORPTION STUDY AND RESULTS.....</b>		<b>112</b>
A.1	Sediment collection.....	112
A.2	Batch experiment methods.....	112
A.3	Batch experiments results.....	113
<b>APPENDIX B PHREEQC INPUT FILES FOR COLUMN MODELING .....</b>		<b>116</b>
<b>APPENDIX C COPYRIGHT PERMISSION TO REPRINT.....</b>		<b>122</b>
<b>LITERATURE CITED.....</b>		<b>123</b>

## LIST OF FIGURES

Figure 2.1	Well Gallery of 2011 “Best Western” biostimulation experiment at the Rifle, IFRC field site .....	20
Figure 2.2	Example EEM of well CD04 delineating operationally defined fluorescent regions I-V for regional integration.....	23
Figure 2.3	Conceptual model of SMP production during biostimulation.....	24
Figure 2.4	SO <sub>4</sub> <sup>2-</sup> , Fe(II), and acetate concentrations for wells CD01, CD04, and CD07 over the observation period.....	26
Figure 2.5	UO <sub>2</sub> <sup>2+</sup> concentrations for wells CD01, CD04, CD07 and CU01 over the observation period.....	27
Figure 2.6	Non-acetate DOC concentrations (mM-C/l) for wells CD01, CD04, CD07 and background values.....	27
Figure 2.7	Electron accounting for well CD01 of electrons available from consumed acetate and electrons utilized by sulfate, iron, and uranium reduction.....	29
Figure 2.8	EEMs for observation well and well CD04, 16, 67 and 105 days into biostimulation.....	31
Figure 2.9	Relative fluorescence of region IV for wells CD01, CD04, and CD07.....	32
Figure 2.10	Relative fluorescence of region V for wells CD01, CD04, and CD07.....	32
Figure 2.11	Excitation Emission matrix for well CD07 on day 282 of the experiment.....	33
Figure 3.1	Map of the Smith-Ranch Highland uranium ISR facility with pertinent wells...	44
Figure 3.2	Uranium and tracer data and model fit for column experiment MU3 A.....	56
Figure 3.3	Uranium and tracer data and model fit for column experiment MU3 .....	56
Figure 3.4	Uranium and tracer data and model fit for column experiment MU3 C.....	57
Figure 3.5	Uranium and tracer data and model fit for column experiment MU10 A.....	57

Figure 3.6	Uranium and tracer data and model fit for column experiment MU10 B.....	58
Figure 3.7	Picture of sediment core from depth 191.2-191.5 m below surface.....	61
Figure 3.8	Picture of sediment core from depth 191.5-192.1 m below surface.....	61
Figure 3.9	Picture of sediment core from depth 192.4-192.7 m below surface.....	62
Figure 4.1	Influent alkalinity (mg/l CaCO <sub>2</sub> ) and pH for all four column experiments.....	83
Figure 4.2	Uranium and tracer data and model fit for column experiment 192 HAW.....	89
Figure 4.3	Uranium and tracer data and model fit for column experiment 192 LAW.....	89
Figure 4.4	Uranium and tracer data and model fit for column experiment 193 HAW.....	90
Figure 4.5	Uranium and tracer data and model fit for column experiment 193 LAW.....	90
Figure 4.6	Model alkalinity (mg/l CaCO <sub>3</sub> ) and pH versus measured alkalinity and pH for column experiment 192 HAW.....	94
Figure 4.7	Model alkalinity (mg/l CaCO <sub>3</sub> ) and pH versus measured alkalinity and pH for column experiment 192 LAW.....	94
Figure 4.8	Model alkalinity (mg/l CaCO <sub>3</sub> ) and pH versus measured alkalinity and pH for column experiment 193 HAW.....	95
Figure 4.9	Model alkalinity (mg/l CaCO <sub>3</sub> ) and pH versus measured alkalinity and pH for column experiment 193 LAW.....	95
Figure 4.10	Sensitivity analysis of alkalinity, pH, and site density on column model 192 HAW with calcite equilibrium.....	97
Figure 4.11	Sensitivity analysis of alkalinity, pH, and site density on column model 192 HAW without calcite equilibration.....	98
Figure A.1	Sorption isotherm for batch experiment on sediment 192.....	114
Figure A.2	Sorption isotherm for batch experiment on sediment 193.....	115

## LIST OF TABLES

Table 3.1	Ionic constituents of waters used as column influent.....	46
Table 3.2	Experiment summary table of sediment depth, column flow rate, porosity, experiment duration, alkalinity (mg/l CaCO <sub>3</sub> ), and pH for each column.....	48
Table 3.3	Pertinent equilibrium and sorption reactions added to PHREEQC database.....	51
Table 3.4	Total organic carbon and BET results for sediments sections.....	54
Table 3.5	XRF results showing elemental constituents of sediment sections .....	54
Table 3.6	XRD results showing mineralogy of sediment sections used in column experiments.....	55
Table 3.7	R values and SORS of each surface site model for each column experiment....	55
Table 3.8	Calculated uranium recoveries for each column experiment.....	55
Table 3.9	Fitted site densities for strong and very strong sites for all columns.....	59
Table 4.1	Sediment characterization by XRF, BET, and TOC for three sediment.....	79
Table 4.2	Sediment mineralogy by XRD analysis for three sediment.....	79
Table 4.3	Chemical constituents of influent restoration and background water.....	81
Table 4.4	Pertinent equilibrium reactions added to the PHREEQC database.....	84
Table 4.5	Sediment size fractions for depths 192 m and 193 m below surface.....	88
Table 4.6	Summary table of pore volumes, retardation factors, fitted site densities, R <sup>2</sup> and SORS values for best model fits.....	88
Table 4.7	Uranium and calcium recoveries for each column experiment.....	88
Table 4.8	Summary table of sediment depths, influent alkalinities, influent calcite saturation, and porosities for each column experiment.....	91

Table 4.9	Cross comparison of fitted site densities for column and batch experiments.....	102
Table A.1	Results for batch sorption experiments for sediment depth 191 m.....	113
Table A.2	Results for batch sorption experiments for sediment depth 193 m.....	114

## ACKNOWLEDGMENTS

First and foremost, I want to give special thanks to my advisor Dr. Linda Figueroa who supported me for a long time and whose guidance and advice on thinking like a scientist shaped all the research and writing herein. Also appreciated were her limitless patience and tolerance for my ornery tirades and stubbornness whenever things didn't go quite well. Thank you for not giving up on me. I also want to give special thanks to Dr. James Stone for the opportunity to work on the Smith-Ranch Highland project and cracking the whip on me to get my Ph.D. finished. Without his help and support this thesis would not have happened. I want to acknowledge Dr. Paul Reimus, Dr. Ray Johnson and Dr. Jim Clay for their valuable insights into uranium geochemistry and transport modeling and their help in writing my publications. I also want to acknowledge my committee members Dr. James Ranville, Dr. Jonathan O. Sharp, and Dr. Christopher Bellona for the help they lent me

I am grateful to Dr. Barbara Moskal and the Trefny Institute who provided me not only with funding, but also with a breath of fresh air during my time as a Ph.D. student. Lastly, a credit to my family for lending an ear to those frustrations and complaints that seem to accompany every Ph.D.

Funding for this research was provided by a grant from Power Resources, Inc., and by the University of Wyoming, School of Energy Resources. Additional financial support was supplied by the Trefny Institute, Colorado School of Mines and the SmartGeo project, a program funded by the National Science Foundation.

## CHAPTER 1

### LITERATURE REVIEW OF URANIUM BIOGEOCHEMISTRY: CHALLENGES FOR REMEDIATION AND RISK ASSESSMENT

#### **1.1 Uranium contamination from uranium mining and milling operations**

Contamination of groundwater by uranium remains an environmental problem that exists in all areas that are host to identified uranium resources (Mangini et al. 1979, Sheppard and Evenden 1988, USGS 2009). The release of uranium from mining and milling operation has resulted in elevated concentrations in groundwater aquifers at 27 sites managed by the Uranium Mill Tailings Radiation Control Act (UMTRCA). In addition, the Department of Energy oversees the management of 107 sites contaminated by radioactive materials from nuclear weapons research and nuclear waste storage facilities. The estimated clean-up cost for all those sites reaches to a trillion U.S. dollars (Lloyd and Renshaw 2005, Long et al. 2006). Presently 40 new applications for Uranium mills and mining sites have been submitted in the U.S and the demand for nuclear power is likely to increase as industrialized and developing nations strive to wean themselves off fossil fuels, due concerns over climate change. This increase in Uranium mining activity and generation of nuclear waste, will lead to more contamination than is already present, and will require state-of-the-art remediation technologies and tools for risk assessment to protect public health.

*In-situ* recovery (ISR) now accounts for most of the uranium produced in the U.S., and about half of the uranium produced worldwide (Macfarlane and Miller 2007, Mudd 2014). ISR

involves the injection of  $O_2$ ,  $CO_2$ , and either  $NaHCO_3$  or  $H_2SO_4$  fortified water (i.e., lixiviant) into a uranium-bearing ore zone to oxidize and solubilize the uranium (Pelizza 2008). The solubilized uranium is then pumped to the surface, extracted, and processed into uranium oxide. This process avoids excavation or the processing of solid ores and does not leave behind open pits, shafts or tailing piles. While ISR is a non-intrusive method to extract uranium from the subsurface, it alters the geochemistry of the ore zone significantly during operation and mobilizes contaminants such as arsenic, selenium, radon, and uranium (Hall 2009). The industry restoration practice to reduce contaminant concentrations can vary, but commonly involve a combination of groundwater withdrawal to replace the existing groundwater, treatment of the groundwater by reverse osmosis, and the use of chemical reductants (such as  $H_2S$ ) to induce reducing conditions on aquifer waters and sediments (Osiensky and Williams 1990, Catchpole and Kuchelka 1993, Abitz and Kooyoomjian 2011). These practices work well to significantly reduce constituent concentrations, however, they typically do not succeed in lowering concentrations of all species to pre-mining ‘baseline’ levels. As a consequence, industry may have to apply for alternate concentration limits for contaminants of concern and demonstrate the closed ISR sites do not pose risks to adjacent aquifers (Borch, et al. 2012, Hall 2009).

## **1.2 Overview of uranium biogeochemistry**

Several thermodynamic processes determine the mobility of uranium in the subsurface. Transport models commonly account for sorption, precipitation, and the aqueous chemistry of Uranium. Aqueous U(VI) in the subsurface is typically present in its oxidized state as the uranyl ion ( $UO_2^{2+}$ ). U(VI) may be reduced to U(IV) through abiotic or microbial processes in the subsurface, if redox potentials are low enough (Anderson and Lovley 2002, Gorby and Lovley,

1992, Lovley and Phillips 1992, Liger et al. 1992, Behrends et al. 2005, Wersin et al. 1994) though abiotic processes occur at significantly lower rates than microbially facilitated uranium reduction (Behrends et al 2002). The reduction of  $\text{UO}_2^{2+}$  to U(IV) can occur at an Eh of 0.273 V under acidic conditions (Bratsch et al. 1989), which can make uranium reduction more thermodynamically favorable than the reduction of Iron(III) hydroxides. Uranium bioreduction has been demonstrated in bench-scale studies (Gorby and Lovley 1992, Lovley and Philips 1992, Gu et al. 2005, Komlos et al. 2008) and field systems at the Integrated Field Research Challenge (IFRC) sites at Oak Ridge, TN and Rifle, CO (Anderson et al. 2003, Elias et al. 2003, Vrionis et al. 2005, Williams et al. 2011, Bao et al. 2014, Tang et al. 2013) and studies have shown that it can be carried out by iron reducers (IRB), sulfate reducers (SRB) and even methanogenic communities (Bond and Lovley 2002). Reduced uranium is commonly assumed to precipitate out of solution as uraninite possibly providing a stable sink for uranium transport (Lovley et al. 1992), though several studies have noted that U(IV) may also bond to biomass (Bernier-Latmani et al 2010) or aggregate into mobile nano-particulates (Suzuki et al. 2002).

U(VI) readily sorbs to Fe-containing minerals, (Barnett et al. 2002; Cheng et al. 2007; Ho and Miller, 1986, Waite et al. 1994) clays (Ames et al. 1983, Bachmaf et al. 2011, Echevarria et al. 2001, Missana, et al. 2004, Payne et al. 2004), quartz (Prikryl et al. 2001, Fox et al. 2006, Dong and Wan 2014) and natural organic matter (Evans et al. 2011, Lenhart and Honeyman, 1999, Mibus et al. 2007), which may slow down uranium movement. Research literature has demonstrated that the bioavailability and mobility of aqueous uranium is highly dependent on alkalinity and pH due to the preferred formation of stable ternary uranyl-carbonate complexes with calcium and magnesium (Bargar et al. 2000, Bernhard et al. 2001, Brooks et al. 2003 Dong et al. 2006, Guillaumont and Mompean 2003). This causes alkalinity, calcium concentrations and

pH to be controlling parameters for the sorption of uranium to mineral phases since the neutral and negatively charged ions of  $\text{Ca}_2\text{UO}_2(\text{CO}_3)_3$  and  $\text{CaUO}_2(\text{CO}_3)_3^{2-}$  are unlikely to adhere to the surfaces of negatively charged metal oxide minerals (Dong and Brooks, 2008, Fox et al. 2006). The effect of these species on sorption have been investigated by several other studies (Nair and Merkel 2011a, 2011b, Stewart et al. (2010)) which showed that uranyl-calcium-carbonate species can reduce total sorption by as much as 90% while increasing sorption kinetics by a factor of two (Nair and Merkel 2011(b)). Calcium-carbonate-uranyl complexes are also less bioavailable to reduction (Brooks et al. 2002) and can drive down the redox potential of the U(VI) species into an Eh range of -0.05 to - 0.15 (Ginder-Vogel et al. 2006). The biogeochemistry of uranium is very complex and the existence of calcium-carbonate-uranyl ternary species, means uranium bioavailability and sorption behavior may change with shifting geochemical conditions

### **1.3 Bioremediation challenges: Organic carbon dynamics**

While uranium reduction can occur abiotically (Liger et al. 1999, Jang et al. 2008) microbially driven uranium reduction has been shown to occur more efficiently and quickly (Gorby and Lovley 1992, Lovley and Philips 1992, Behrends et al. 2005, Gu et al. 2005) and can be induced by the addition of a carbon-based electron donor into the subsurface. As a result, uranium bioreduction has been proposed as a remediation strategy for uranium contaminated groundwater (Anderson et al. 2002, Elias et al. 2003, Vrionis et al. 2005). Despite its promising applications, uranium bioreduction still faces several challenges that make implementation uncertain. One problem is the changes in sediment porosity that may occur during biostimulation as a consequence of microbial growth and mineral precipitation (Anderson et al. 2003, Bao et al. 2014). The resulting overstimulation of the aquifer has diverted plumes away from remediation

zones and monitoring wells (Seifert and Engesgaard 2007, Seifert and Engesgaard 2012). Another difficulty is present in the efficient delivery and distribution of carbon sources to the remediation zone (Williams et al. 2011) as bioreduction has been shown to occur in hot zones of high microbial activity (Bao et al. 2014). In addition, maintaining reducing conditions past active remediation remains challenging (Yabusaki et al. 2007, Komlos et al. 2008). In field studies at Rifle IFRC, CO, uranium concentrations returned to background values after the injection of the soluble carbon source was terminated (Williams et al. 2011, Yabusaki et al. 2007). Uranium reduction is not exclusive to any specific microbial species and may be mediated by microbially produced organic substances or occur abiotically altogether. As a consequence, remediation designs need to look at bioremediation from a systems perspective that ties uranium removal efficiency, microbial growth, and changes in sediment porosity to easily measurable field parameters that can be incorporated into decision making frameworks.

Organic carbon plays a crucial role in bioremediation, regulating both redox conditions and biomass growth. Little research, however, has paid attention to the substrate utilization pathways that occur during biostimulation. Nor has there been significant focus on the carbon and electron mass balances that have been shown to contain unknown carbon sinks (Komlos et al. 2008, Regberg et al. 2011). The wastewater treatment literature has long recognized that microbes convert their primary organic substrate (e.g., acetate) into a range of soluble microbial products (SMP) and solid organic matter (Barker and Stuckey 1999, Aquino and Stuckey. 2008, Ni et al. 2009(a), Wang et al. 2009, Ni et al. 2010(a)). The production of these organic compounds during biostimulation constitutes a possible carbon sink that could contribute to aquifer clogging (in the case of solid phase organic carbon) or provide additional bioavailable carbon post-stimulation (Tian 2008, Wang et al. 2007). Research on anaerobic chemostats has shown that

between 3% - 37% of supplied COD can be shuffled into the production of soluble microbial products (SMP) (Aquino and Stuckey 2003), with higher percentages occurring in N-starved systems (Aquino and Stuckey 2003), systems with microbial toxins such as Cr(VI) (Aquino and Stuckey 2004(a)) and during sulfate reduction (Patidar et al. 2008). In addition, soluble organic matter (microbially or terrestrially produced) can affect bioremediation by increasing uranium mobility or decreasing uranium bioavailability through the formation of soluble organic-U(VI) compounds (Ganesh et al. 1998, Francis 1998, Artinger et al. 2002, Gu et al. 2005(a)). Post-stimulation these SMPs may be the sole carbon source in the system while solid phase organic matter produced during the growth phase may be utilized as an electron donor to maintain reducing conditions (Krishna et al. 1999, Wang et al. 2007, Tian 2008). Studying the transformation pathways of organic substrates and the characteristics of SMPs in biostimulated systems can address some of the fundamental challenges that keep uranium bioremediation from being accepted by regulators and industry.

SMP comprise a complex mixture of organic compounds that include proteins, fulvic-like substances, biomass decay products, polysaccharides and extracellular polymeric substances (EPS). (Barker and Stuckey 1999, Lapsidou and Rittmann 2002a, Aquino and Stuckey 2008) which may have varying degrees of bioavailability and chemical characteristics. For convenience, microbial process modeling frameworks group SMP into two operationally defined categories utilization associated products (UAP) and biomass associated products (BAP) (Lapsidou and Rittmann 2002b). UAP consist of organic compounds that facilitate growth, such as enzymes and siderophores, metabolic intermediates or end products (Barker and Stuckey 1999). UAP are released only during the growth stage in significant quantity and their production is proportional to the rate of substrate utilization (Lapsidou and Rittmann 2002). UAP can be a measurable

carbon sink during active metabolism consuming between 5%-20% of supplied substrate (Aquino and Stuckey 2004(a), Ni et al. 2009(a)). BAP are released through the degradation of biomass, which can include cell lysis products as well EPS released through hydrolysis or degradation (Namkung and Rittmann 1986, Ni et al. 2010). Estimating the fraction of substrate shuffled into BAP is difficult since most BAP stems from the solubilization of solid phase carbon (EPS and cell mass). Based on models of anaerobic, acetate-fed chemostats, however BAP can constitute up to 42% of SMP (Aquino and Stuckey 2008). Naturally in the absence of substrate, BAP will dominate SMP composition. UAP and BAP stem from different microbial mechanisms and their characteristics and bioavailability may vary from each other. Understanding both the character and production rates of UAP and BAP in biostimulated systems is necessary to determine potential impacts SMP may have on the efficiency and longevity of uranium bioremediation.

The complex composition of SMPs has led to the use of spectroscopic bulk characterization to elucidate major features of soluble compounds in microbially active systems (Chen et al 2003(a), Chen et al 2003(b), Sheng et al 2006, Wang et al. 2009, Wang et al. 2010, Ni et al 2009b, 2010b). Two spectroscopic bulk methods used to characterize SMP are Excitation-Emission Matrices (EEM) and specific ultraviolet absorption (SUVA). (Jarusutthirak et al. 2007, Wang et al. 2010, Ni et al. 2010(b)). EEMs are three dimensional landscapes that plot a sample's fluorescence intensity to the corresponding emission and excitation wavelength (Fellman et al. 2010, McKnight et al. 2003). EEMs produce characteristic peaks at specific ex/em regions that have been associated with tryptophan-like (peak B at 280/340), tyrosine-like (peak B at 270/310), humic-like (peak C at 340/440 and peak A at 260/460), and fulvic-like (peak M at 310/390) compounds (Fellman et al. 2010). Furthermore, specific regions in those

EEMs are correlated with either microbially produced organic matter or terrestrial organic matter (Chen et al 2003(a)). High SUVA values have been shown to indicate greater amounts of aromatic functional groups in DOC as well (Weishaar et al. 2003). Reduced levels of aromaticity in DOC would make it more bioavailable and could indicate the presence of BAP or low-molecular weight compounds.

#### **1.4 Risk assessment and transport modeling on ISR sites**

Risk assessments normally employ reactive fate and transport models to approximate uranium movement through the aquifer. A plethora of geochemical and hydrological processes can affect uranium transport. Sorption to mineral surfaces remains an important mechanism that can lead to a significant retardation of uranium in groundwater (Davis et al. 2004) and is an important focus of reactive-transport models (Davis et al. 2007). The industry and its regulators (Environmental Protection Agency (EPA), Nuclear Regulatory Committee (NRC), and state agencies) are currently working toward an ISR regulatory framework that considers best mining and restoration practices, the need to protect groundwater resources, the realities of geochemical changes resulting from ISR mining, and relative risks to the environment and the public.

Reactive fate and transport models (RTM) have the potential to inform stakeholders on the risk that mining operations pose to downgradient aquifers and the EPA's Proposed Rulemaking for 40 CFR Part 192, 82 FR 7400 suggests extensive geochemical modeling to assess ISR site closure.

However, currently there are no standardized methods or even guidelines to conduct these transport models that could demonstrate industry compliance with these regulatory requirements (NRC Staff comments). The lack of accepted modeling assumptions and practices, such as which thermodynamic databases to include, what kind of sorption models to apply, and what methods

to use to determine important parameters, can produce significant variability and uncertainties in final model predictions. In addition, inherent variability in experimental designs and scale dependent uncertainty can introduce further errors when transferring bench-scale experiments to the field scale (Miller et al. 2011). These challenges pose liability issues for regulators and industry when models fail to predict plume behavior, and license applications could get bogged down in debates over the applicability of certain modeling assumptions or procedures.

ISR alters the geochemistry of ore zones significantly, and the injection of CO<sub>2</sub> as lixiviant leaves behind elevated concentrations of uranium, alkalinity, calcium and a pH often one unit below background values. At the SRH site restored ore zones reported a Ca<sup>2+</sup> and alkalinity range from 120-400 mg/l and 180-800 mg/l CaCO<sub>3</sub> respectively, while pH ranged from 6.0-6.5 (Jim Clay Personal communications). As a consequence, the ratio of uranyl, uranyl-carbonate, and calcium-carbonate-uranyl ternary species at ISR sites may vary significantly during the restoration and monitoring phase. These changes in aqueous chemistry mean that traditional K<sub>d</sub> approaches for modeling sorption are inadequate for restored ISR sites where geochemical conditions may shift when background water mixes with restoration water.

A range of theoretical models of varying complexity and accuracy have been proposed to simulate metal sorption onto mineral surfaces. Generalized surface complexation models (GC SCM) have become favored by many researchers due to its semi-empirical nature and relative ease to incorporate into transport calculations (Davis and Curtis 2003, Davis et al. 2004, Kohler et al. 1996, Zhang et al. 2009, Waite et al. 2000). GC SCM models rely on experimental data to estimate important sorption parameters such as sorption site density and equilibrium constants. This approach has the advantage of incorporating experimental verifications of the model from the beginning, compared to component additive surface complexation models (CA SCM) that

rely on assumed sorption mechanisms based on the observed mineralogy of soil cores (Davis et al. 2004, Davis et al. 2009, Payne et al. 2006). However, experimentally derived sorption parameters are highly dependent on experimental designs and methods of parameterization, which can make them difficult to transfer between systems of different mineralogy or geochemistry and introduce experimental uncertainties and errors. The use of CA SCM faces different challenges. Several studies have demonstrated that estimations of surface areas can depend highly on the method used and give inconsistent results with soils of heterogeneous mineral compositions since clay swelling and mineral coatings may alter measured and actual surface areas (Maček et al. 2013, Macht et al. 2011, Metz et al. 2002, Yukselen-Aksoy et al. 2010). As a consequence, theoretical surfaces used for sorption models may not match with those actually available in the field system. Furthermore, CA SCM require extensive sediment characterization to decompose complex heterogeneous materials into individual components, or require modelers to make assumptions about the presence of dominant sorbents (Payne et al. 2013). CA SCM have been shown to incur higher errors than the GC SCM approach (Miller et al. 2011), with prediction being off by almost 2 orders of magnitude compared to 1 order of magnitude for GC SCM models (Payne et al. 2006). For ISR sites the use of GC SCM may be more robust, since extensive sediment characterization may be cost prohibitive compared to experimental batch studies and the GC SCM approach has a better track record for accurate predictions (Miller et al. 2011).

Chapter 3 presents a study published in *Applied Geochemistry* that investigated the applicability of GC SCM to uranium transport in ISR relevant conditions. Column studies were conducted and modeled with a 1-site, 2-site, and 3-site GC SCM. Parameters were derived for each surface site and evaluated based on best fits. Chapter 4 continues to examine uranium

retardation due to sorption in column studies. Uncertainties in the parameter estimation process were assessed by comparing laboratory and bench scale studies completed at different laboratories on similar sediments.

### **1.5 Scope and purpose of this study**

The overarching goals of this research project to elucidate the biogeochemical controls of uranium fate and transport as it relates to the restoration of legacy and active mining and milling sites. Bioremediation and uranium retardation due to sorption are key retardation mechanism that can safeguard human health and environment from uranium contamination of groundwater. However, both bioremediation and transport models that incorporate sorption face significant challenges when trying to implement them in remediation designs or risk assessments. The impact on substrate transformations on bioremediation efficacy remains poorly understood, while uranium transport predictions still face uncertainties with regards to replicability and effects of geochemistry. This project tries to address these challenges by studying the carbon cycle of a biostimulation experiment and assessing the replicability of laboratory derived sorption experiments. The knowledge herein will fill crucial gaps of our understanding of uranium biogeochemistry and its impact on uranium fate and transport at uranium mining and milling sites.

Chapter 2 of this work investigated the transformations of acetate during the biostimulation of a uranium contaminated aquifer at the Rifle, IFRC site in Colorado. Our goal was to determine, if SMP production represent a significant and measurable carbon sink during biostimulation and a significant source of DOC post- biostimulation. We hypothesized that acetate and DOC measurements would show elevated non-acetate, organic carbon concentrations during and post-

biostimulation attributable to SMP production. Furthermore, an electron mass balance was performed to reveal the existence of carbon sinks not related to microbial growth. Microbial stoichiometries were used to derive carbon consumption due to biomass growth based on changes in measured electron acceptor concentrations ( $\text{Fe}^{2+}$  and  $\text{SO}_4^{2-}$ ). The hypothetical acetate consumption was then compared to actual acetate concentrations in an observation well to detect any excess substrate utilization. The chapter also evaluates the applicability of spectroscopic techniques to characterize SMP in this biostimulated system with regards to their origin and bioavailability. Fluorescence EEMs and SUVA were used to characterize SMPs and determine if spectroscopic techniques can differentiate between UAPs and BAP production during biostimulation. We postulated that fluorescence spectroscopy would be able to detect characteristic microbial signatures during biostimulation while SUVA would reveal post-stimulation SMPs to be more bioavailable than background DOC. The research herein present novel insights into the organic carbon dynamics of reductive bioremediation systems.

Investigating whether and when SMPs are bioavailable will help optimize remediation schemes by reducing the need for injecting excess electron donor. The presence and character of missing carbon sinks will show whether microbially produced solid phase organic carbon may be available as an electron donor post-stimulation. In addition, fluorescence signatures could be used to monitor the status of SMP and provide indicators when organic substrate injections need to be turned on or off, to keep microbial growth active or to prevent overstimulating the system.

Chapter 3 and 4 present laboratory and modeling studies that investigated the applicability of sorption models to uranium transport in ISR relevant conditions. Column experiments were conducted with sediments collected from the SRH site that received synthetic and sampled groundwater contaminated with uranium. A PHREEQC 1-D transport model was coupled to a

parameter fitting software (PEST) to derive best fits to measured data based on lowest SORS and  $R^2$  values. Our goal was to test the ability of GC SCM models to predict uranium behavior under conditions of shifting alkalinity and pH and to determine key geochemical components that show the greatest sensitivity to uranium retardation.

Chapter 3 describes five column studies that were modeled with a 1 pK, 2 pK and 3 pK GC SCM based on the conceptual model proposed by Davis et al (2004). The inherent non-uniqueness of the solution space of GC SCMs requires the number of fitting parameters to be limited to the minimum necessary to represent observed data (Payne et al 2013). One purpose of the study was to determine the number and types of reactions needed to produce acceptable model fits. The extend of influent alkalinity on uranium retardation was also investigated. Two columns packed with sediment from the same borehole and depth received an influent alkalinity that differed by a factor of two. We hypothesized that uranium would elute earlier in the column with higher alkalinity. In addition, the role of calcite in regulating uranium desorption was investigated in one of the column experiments. Influent pH and alkalinity were adjusted to produce three different stages with varying degrees of over and undersaturation with respect to calcite. Calcite dissolution was expected to induce the desorption of previously immobilized uranium due to the increase in alkalinity and pH.

Chapter 4 continues to study uranium retardation due to sorption in column studies. One focus of the 4<sup>th</sup> chapter was to investigate the effect of shifting geochemistry during uranium transport. Two duplicate column experiments using two different sediment sections from an un-impacted monitoring well were subjected to variable influent alkalinity and pH that simulated the influx of background water into the restored mining zone. GC SCM models were used to capture the behavior of uranium transport under these variable geochemical conditions. We predicted

that GC SCM was capable of simulating not just uranium breakthrough, but expected desorption behavior that may result from the introduction of background water into the system. In addition, the replicability of the GC SCM approach was studied to evaluate the replicability of experimentally derived sorption parameters across different laboratory set-ups. The uncertainties in the parameter estimation process were assessed by comparing laboratory and bench scale studies completed at different laboratories on similar sediments. Data from the 5 prior column experiments in chapter 3 together with six batch experiments, were fitted with the same approach used in chapter 4. The fitted parameters were then compared to each other to test whether different experiments on the same sediment would still give the same fitted sorption parameters.

This research helps industry and regulators determine what geochemistry (pH, calcite saturation, and alkalinity) to aim for during the restoration process and what tools to use (such as pCO<sub>2</sub> stripping or blending restoration water with background water) to inhibit uranium transport. In addition, the research shows whether GC SCM approach can be used to accurately scale batch experiments to column and field systems and whether experimentally derived sorption parameters will provide replicable results across laboratories.

## CHAPTER 2

# CHARACTERIZING ORGANIC CARBON DYNAMICS DURING BIOSTIMULATION OF A URANIUM CONTAMINATED FIELD SITE

Manuscript in preparation

Martin A. Dangelmayr<sup>1</sup>, Linda A. Figueroa<sup>1\*</sup>, Kenneth Williams<sup>2</sup>, Phillip Long<sup>3</sup>

<sup>1</sup> Department of Civil and Environmental Engineering, Colorado School of Mines, 1500 Illinois St, Golden, CO 80401, USA

<sup>2</sup> Earth Sciences Division, Lawrence Berkeley National Laboratory, Berkeley, California 94720, USA

<sup>3</sup> Lawrence Berkeley National Laboratory, 1 Cyclotron Road, Berkeley, California 94701, USA

### 2.1 Introduction

Contamination of groundwater by uranium remains a ubiquitous environmental challenge in all areas that are host to identified uranium resources and novel management and remediation technologies are needed to protect human health and the environment (Mangini et al. 1979, Sheppard and Evenden 1988, USGS 2009). The microbial reduction and subsequent precipitation of the uranyl ion has been suggested as a possible remediation strategy (Anderson and Lovley 2002, Gorby et al 1992) and been the subject of study at the Integrated Field Research Challenge (IFRC) sites at Rifle, CO for over a decade (Anderson et al. 2003, Williams et al 2013). Despite its promising applications, uranium bioreduction still faces several challenges that complicate long-term sustainability in the field and application by the remediation industry. Sediment porosity can decrease during biostimulation as a consequence of microbial growth and mineral precipitation (Englert et al 2009, Li et al. 2009 Seifert et al. 2007, Seifert et al. 2012). The resulting overstimulation of the aquifer may divert plumes away from remediation zones and

monitoring wells. In addition, maintaining reducing conditions past active remediation remains difficult. During field studies at Rifle IFRC, CO, uranium concentrations returned to background values after the injection of the carbon source was terminated (Williams et al. 2011 Yabusaki et al. 2007) leading to an increase in groundwater uranium concentrations. To make bioreduction a viable remediation tool for a variety of uranium contaminated sites, the long-term stability and tendency for aquifer clogging need to be addressed.

The wastewater treatment literature has long recognized that microorganisms convert their primary organic substrate (e.g., acetate) into a range of solid-phase and soluble microbial products (SMP) (Barker and Stuckey 1999, Aquino and Stuckey. 2008, Ni et al. 2009(a), Wang et al. 2007, Ni et al. 2010(a)). The production and character of these microbially produced organic matter during bioreduction remains poorly understood. Nor has there been significant focus closing the carbon and electron mass balances that have been shown to contain missing carbon sinks (Komlos et al. 2008, Regberg et al. 2011). The production of these organic compounds during biostimulation constitutes a possible carbon sink that could contribute to aquifer clogging as extracellular polymeric substances (EPS). More importantly, during periods of excess carbon availability bacteria have been shown to shuffle electrons into the production of storage polymers, which may allow for continued microbial activity after injection of acetate is stopped (Krishna et al. 1999, Freguia et al. 2007, Wang et al. 2007). Studying the transformation pathways of organic substrates and the characteristics of microbially produced organic matter in biostimulated systems can address some of the fundamental challenges that keep uranium bioremediation from being accepted by regulators and industry.

Soluble microbial products (SMP) comprise a complex mixture of organic compounds that include proteins, fulvic-like substances, biomass decay products, polysaccharides and

extracellular polymeric substances (EPS) (Barker and Stuckey 1999, Aquino and Stuckey 2008), which may have varying degrees of bioavailability and chemical characteristics. For convenience, microbial process modeling frameworks group SMP into two operationally defined categories UAP and BAP (Lapsidou and Rittmann 2002). UAP are produced only during the growth stage in significant quantity and consist of organic compounds such as enzymes and siderophores, metabolic intermediates or end products (Barker and Stuckey 1999). UAP can be a measurable carbon sink during active metabolism consuming between 5%-20% of supplied substrate (Aquino and Stuckey 2004(a), Ni et al. 2009(a)). BAP are released through the degradation of biomass, which can include cell lysis products as well as the hydrolysis of microbially produced solid phase organic carbon such as EPS (Namkung and Rittmann 1986, Ni et al. 2010). Naturally in the absence of substrate, BAP will dominate SMP composition. Since UAP and BAP stem from different microbial processes they may serve as additional indicators to determine when and where microbes are actively growing. In addition, the bioavailability of DOC might change when SMP composition shifts from UAP to BAP and potentially impact the longevity of the remediation design.

The complex composition of SMPs has led to the use of spectroscopic bulk characterization to elucidate major features of soluble compounds in microbially active systems. Two spectroscopic bulk methods used to characterize SMP are 3-dimensional excitation-emission matrix fluorescence spectra (EEM) and specific ultra-violet absorption at 254 nm wavelengths (SUVA). (Sheng et al 2006, Henderson et al. 2009, Ni et al. 2009(b) Wang et al. 2010, Ni et al. 2010(b)). EEMs are three dimensional landscapes that plot a sample's fluorescence intensity to the corresponding emission and excitation wavelength (Fellman et al. 2010, McKnight et al. 2003). Specific regions in those EEMs have been shown to correlate with

either microbially produced organic matter or terrestrial organic matter (Chen et al 2003, Sheng et al 2006, Wang et al. 2009). SUVA 254 nm values have linked to a higher fraction of aromatic structures in DOC (Weishaar et al. 2003). A change in observed SUVA values could then indicate a shift in the bioavailability of SMPs during or post-biostimulation (Marschner et al. 2003, Kang et al. 2013). Spectroscopic techniques might offer new insights into the carbon dynamics of a biostimulated system both during active remediation and post-stimulation.

The purpose of this study was to determine, if in-situ biostimulation would produce SMP in measurable quantities and how long production of SMP would persist once acetate addition was terminated. In addition, an attempt was made to close the carbon and electron mass balance for the biostimulated system to detect possible carbon sinks that are not accounted for solely by biomass growth and substrate utilization. Dissolved organic carbon and acetate were measured to estimate the amount of SMP. A conceptual model was used to divide SMPs into two pools based on the postulated origin: UAP and BAP. Bulk analyses were used to characterize SMP by spectroscopic properties. Fluorescence spectroscopy was used to differentiate between UAP and BAP by EEMs characteristics while SUVA was used to assess aromaticity and hence bioavailability of SMP compared to background DOC. We postulate that SMP maintain reducing conditions post-stimulation, by providing a continued and bioavailable carbon source after acetate injections have ceased, and that fluorescence spectroscopy could be used as an indicator of active microbial growth due to the presence of microbial signatures associated with UAP production. In addition, the carbon mass balance shows electron sinks unaccounted for by microbial biomass production or dissolved organic carbon alone, which could be indicative of the formation of a solid phase carbon sink, such as storage polymers.

## 2.2 Methods

### 2.2.1 Site description and field experiment

The Rifle, IFRC site was home to a uranium and vanadium mill whose tailings leached significant contamination into the groundwater. The site was cleaned up under UMTRA (Uranium Mine Tailing Reclamation Act) between 1992 and 1996 by removing the nearly 5 million tons of tailings. However, residual uranium present in the subsurface aquifer was not removed and the Rifle, IFRC site has been used to study uranium bioreduction extensively. The Rifle, IFRC site offered a unique opportunity to improve our understanding of the carbon cycle during and after biostimulation. The Rifle, IFRC site field experiment conducted in Fall 2011 on the “Best Western” well gallery was used to examine the organic carbon dynamics during bioremediation. The Rifle, IFRC site has been described extensively in prior literature (Bao et al. 2014, Anderson et al. 2003, Williams et al. 2011). Meanwhile, details of the well gallery, in addition to the biostimulation experiment conducted a year prior to this research, are provided in Bao et al (2014). Figure 2.1 (page 20) depicts the well gallery studied for the 2011 experiment. The gallery was aligned with the average groundwater flow direction at the site based on historic trends observed in years prior. Injection wells are denoted as CG, while observation and background wells have the CD and CU prefix, respectively. Acetate and bromide injection occurred over a 72-day period from 8/23/2011 to 11/3/2011. The Injection solution contained 150 mM Sodium Acetate and 20 mM Sodium Bromide and was delivered at an estimated flow rate to achieve groundwater concentrations of approximately 15 mM and 2 mM, respectively. Groundwater samples were collected before, during and after the 2011 acetate injection experiment.

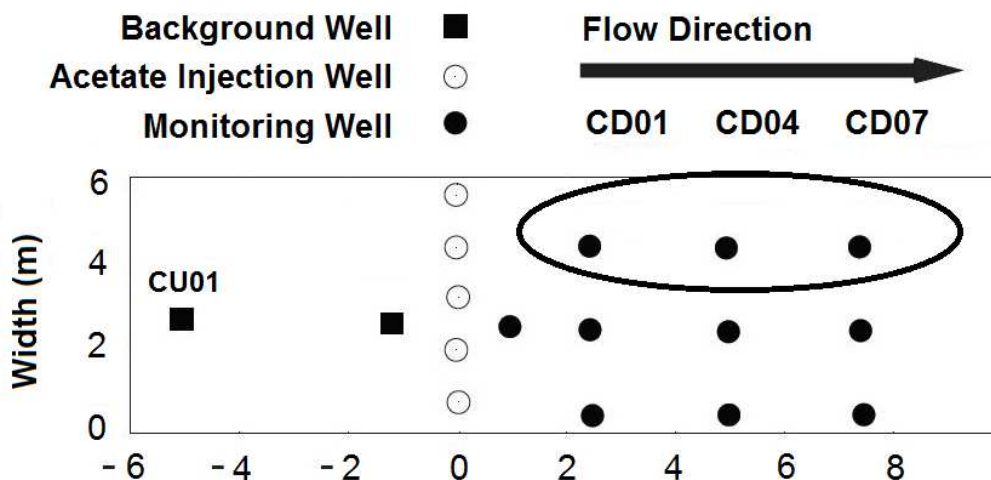


Figure 2.1: Depiction of the portion of "Best Western" well gallery used for biostimulation with relevant observation wells CD01, CD04, CD07 and background well CU01 locations noted.

### 2.2.2 Sample collection and preparation

Pumped groundwater samples (after ~ 12 L of purge volume) were taken from selected wells (CU01, CD01, CD04 and CD07). Samples for acetate, bromide, and geochemical analysis were taken at least weekly over the 210 days of this investigation. Samples for anion and total inorganic carbon (TIC) analysis were filtered (PTFE; 0.45 $\mu$ m) and stored in refrigerated, no-headspace HDPE and glass vials, respectively, until analysis. Samples for organic carbon analysis were collected in brown 100 mL glass on a biweekly to monthly interval during biostimulation and a bimonthly interval post-stimulation. Samples were filtered in the laboratory with a 0.45  $\mu$ m filter within 48 hours after sampling and stored at 4° C.

### 2.2.3 Groundwater chemical analysis

Acetate, bromide, and sulfate were measured using an ion chromatograph (ICS-2100, Dionex, CA) equipped with an AS18 column. TIC values (carbonates, bicarbonates, and dissolved carbon dioxide) were determined by sample acidification and sparging with the

subsequent quantification of evolved CO<sub>2</sub> (TOC-VCSH, Shimadzu, Corp.) Samples for cation analysis (including uranium) were filtered (PTFE; 0.45µm) and acidified (0.2mL 12N HNO<sub>3</sub> per 20mL sample), with concentrations determined using ion coupled plasma mass spectrometry (ICP-MS) (Elan DRCII ICP-MS, Perkin Elmer, Inc.).

#### **2.2.4 Organic acids, TOC, and SUVA analyses**

An Aminex HPX-87H ion-exclusion column (Bio-Rad) with a UV/VIS detector was used to determine concentrations of organic acids (acetic, oxalic, citric, formic, succinic, and propionic acid) in collected samples. DOC concentrations were analyzed using a Shimadzu TOC-500 analyzer with a high sensitivity catalyst. Total Fe of filtered samples was measured using a Perkin-Elmer Optima 3000 ICP-AES (EPA Method 6010B). Absorbance measurements were taken with a Perkin Elmer scanning UV-Vis Spectrophotometer for wavelength 254 nm in a 1 cm long cuvette. Specific UV absorbance (SUVA) values were calculated by dividing absorbance values by non-acetate DOC concentrations and the path length of the cuvette. Absorbance values were corrected for measured Fe concentrations using the method described in Weishaar et al. (2003).

#### **2.2.5 Fluorescence analysis and EEM regional integration**

Excitation-emission matrices (EEM) were obtained by scanning samples over an excitation (ex) range of 240-450 nm (10 nm intervals) and an emission (em) range of 280-550 nm (2 nm intervals) using a JY-Horiba/Spex Fluoromax-4 Spectro fluorometer. A blank (MilliQ water) was scanned prior to each run and subtracted from each sample EEM to account for Raleigh scattering. The area under the Raman peak (ex 350 nm) of the same-day blank was used to

normalize the intensities of all samples and a UV-Vis scan was used to apply an inner-filter correction to the EEMs. Since the same instrument was used for all fluorescence analyses, the EEMs used in this study are comparable to each other. Prior to fluorescence analysis all samples were acidified to pH 3-3.3 and adjusted to room temperature 15 min prior to analysis to reduce the effect of ion quenching (Chen et al 2003, Ohno et al. 2009) and increase fluorescence intensity. Samples were not diluted to a common DOC concentration since intensities all but vanished whenever dilutions of higher than 2x were applied.

EEMs were divided into five characteristic fluorescence regions (Figure 2.2 on page 23) based on operationally defined excitation and emission boundaries by Chen et al. (2003). Regions I, II, and IV have been linked to protein-like compounds while regions III and V have been attributed to the presence of humic and fulvic acids. The cumulative fluorescence intensities for each region were calculated by integrating intensities within the defined boundaries in MATLAB. Further details on the integration method can be found in Chen et al. (2003). Of specific interest to this study were changes in intensity of the biostimulation impacted wells relative to EEMs found in upgradient background well CU01. As a consequence, cumulative intensities in regions IV and V were divided by average cumulative intensities in region IV and V found in background samples taken periodically.

### **2.2.6 Microbial stoichiometries and conceptual model**

Microbial equations for iron (Eq. 2.1), sulfate (Eq. 2.2), and uranium reduction (Eq. 2.3) are presented on page 23. Stoichiometries are based on methods in Rittmann and McCarty (2001) using standard free energy corrected to pH 7 and an efficiency of 0.6 with the exception of iron reduction, which was based on an efficiency of 0.42. (Yabusaki et al. 2007).

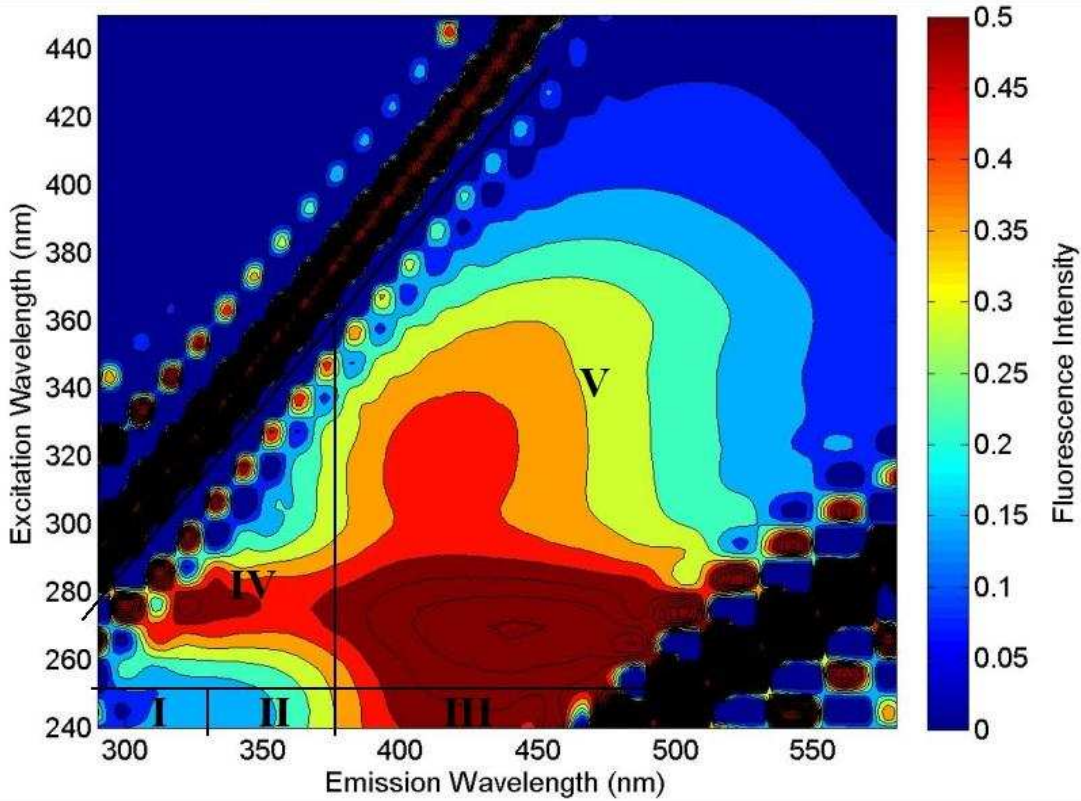
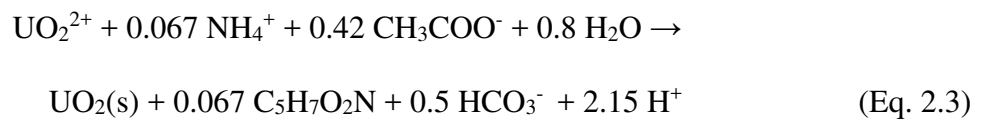
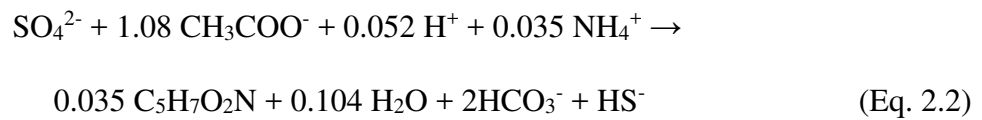
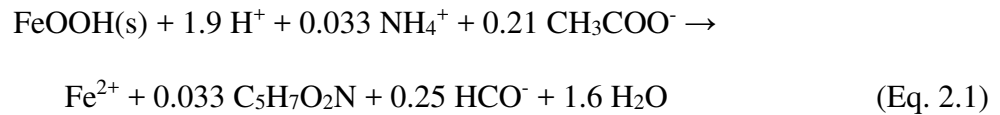


Figure 2.2: A depiction of regions and common peaks in an EEM for well CD04. Regions I, II, IV and Peaks B are usually associated with organic matter of microbial origin. Regions III and V as well as Peaks C, M, and A indicate humic and fulvic like materials.



The microbial stoichiometries were used to relate electron donor consumed to electron acceptor utilized, based on measured concentrations in the groundwater. The theoretical acetate utilization for each well could then be calculated through measured Fe(II),  $\text{SO}_4^{2-}$  and uranium

concentrations and compared to actual acetate concentrations.

SMPs can be calculated by the difference between measured DOC and acetate concentrations if the result is significantly above background DOC observed in well CU01. A conceptual model for the expected production of soluble microbial products during and after acetate injection is given in Figure 2.3. The SMP components are based on a modeling framework proposed by Lapsidou and Rittmann (2002) where SMP is divided into two fractions based on origin. Utilization associated products (UAP) are produced as part of microbial growth. In a biostimulated system the relative fraction of UAP is expected to increase after a lag with acetate injection, plateau when acetate utilization reaches steady state, and decline to zero after acetate injection is terminated. Biomass associated products (BAP) stem from the degradation and solubilization of biomass. The fraction of BAP is expected to contribute to a small fraction of SMP during acetate injection but dominate post-stimulation as accumulated biomass and solid-phase organic carbon begins to degrade.

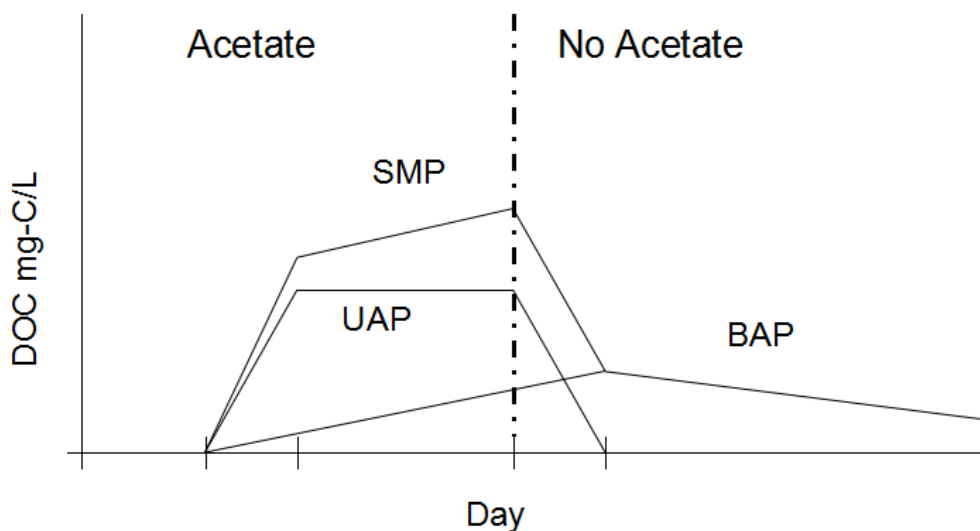


Figure 2.3: A hypothetical composition of SMP during the biostimulation event relating UAPs and BAPs to overall SMP production.

## **2.3 Results**

### **2.3.1 General performance**

Biotransformations stimulated by acetate injection were assessed by analyzing acetate, bromide tracer, ferrous iron, organic carbon, uranium and sulfate concentrations. Acetate, Fe(II), and sulfate are shown in Figure 2.4, for observation wells CD01, CD04, and CD07. Uranium concentrations in observation wells and background wells are shown in Figure 2.5. Acetate and bromide concentration by day 120 were zero. Data for the inorganic indicators are presented from the day of initial acetate injection until 210 days after acetate injection was terminated. The production of ferrous iron and removal of uranium are still evident at day 282 relative to background.

### **2.3.2 Organic Carbon**

Non-acetate DOC was calculated by subtracting measured acetate concentrations as mM-C from the measured DOC (mM-C) and is presented in figure 2.6 (page 26). DOC concentrations in observation wells were compared to DOC from background well CU01. Any organic carbon above background values was considered to be of microbial origin (SMP) produced during biostimulation. Determining non-acetate DOC concentrations was difficult for CD01 during the first 28 days, since acetate concentrations ranged up to 300 mg-C/l. Small instrument errors in either DOC or acetate would have overshadowed actual non-acetate DOC. Most observation wells experienced elevated DOC values ranging from 0.67 mM-C up to 1.76 mM-C during biostimulation and reaching up to 3.18 mM-C 32 days after injections ceased in well CD07. DOC concentrations in background well CU01 remained between 0.3 and 0.4 mM-C throughout the experiment. Elevated DOC concentrations persisted 169 days into the experiment.

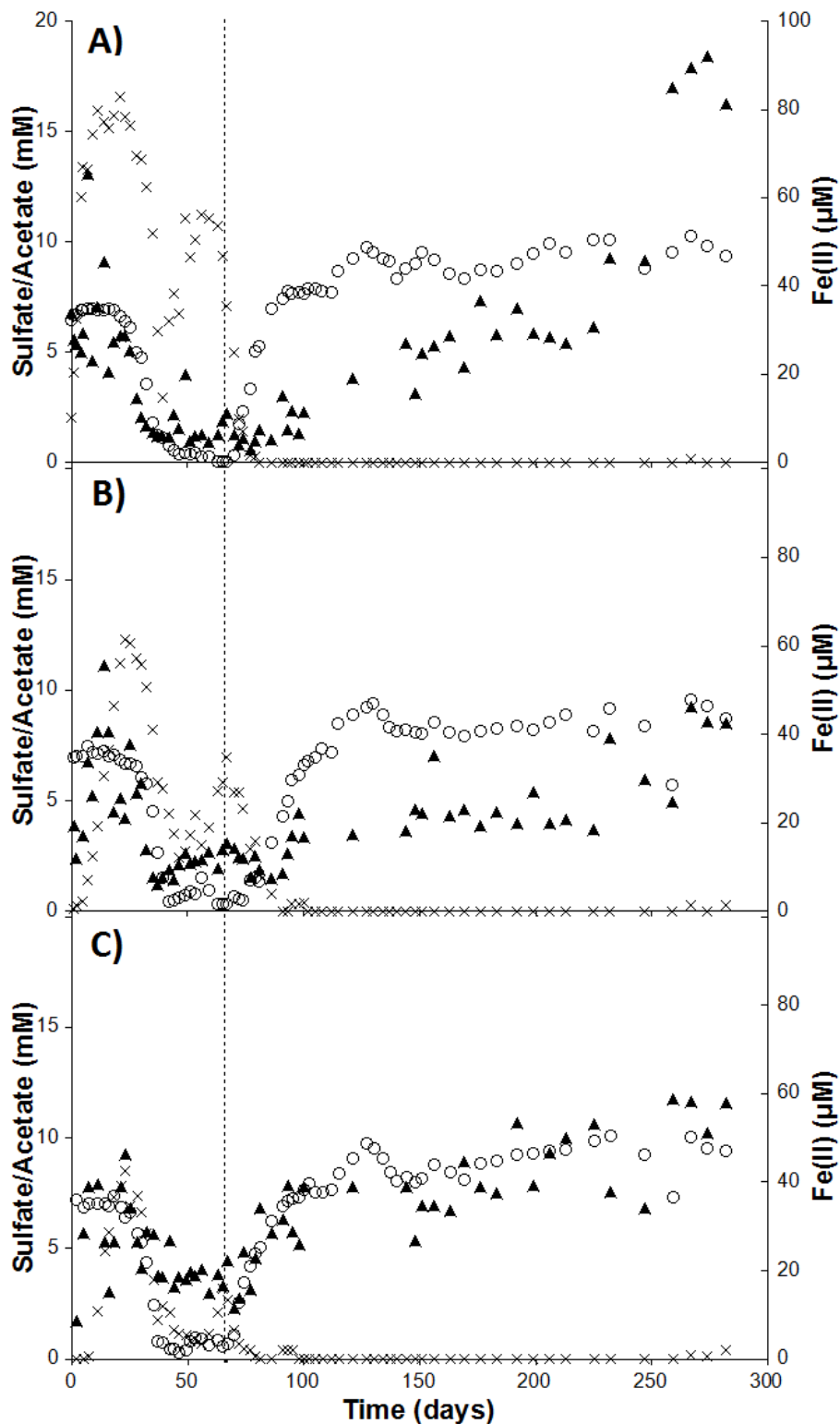


Figure 2.4: Acetate (x), Fe(II) (▲) and SO<sub>4</sub><sup>2-</sup> (○) concentrations for wells CD01 (A), CD04 (B), and CD07 (C). Acetate and sulfate concentrations are given in mM, while Fe(II) concentrations are in µM. The dotted line shows the end of the stimulation period.

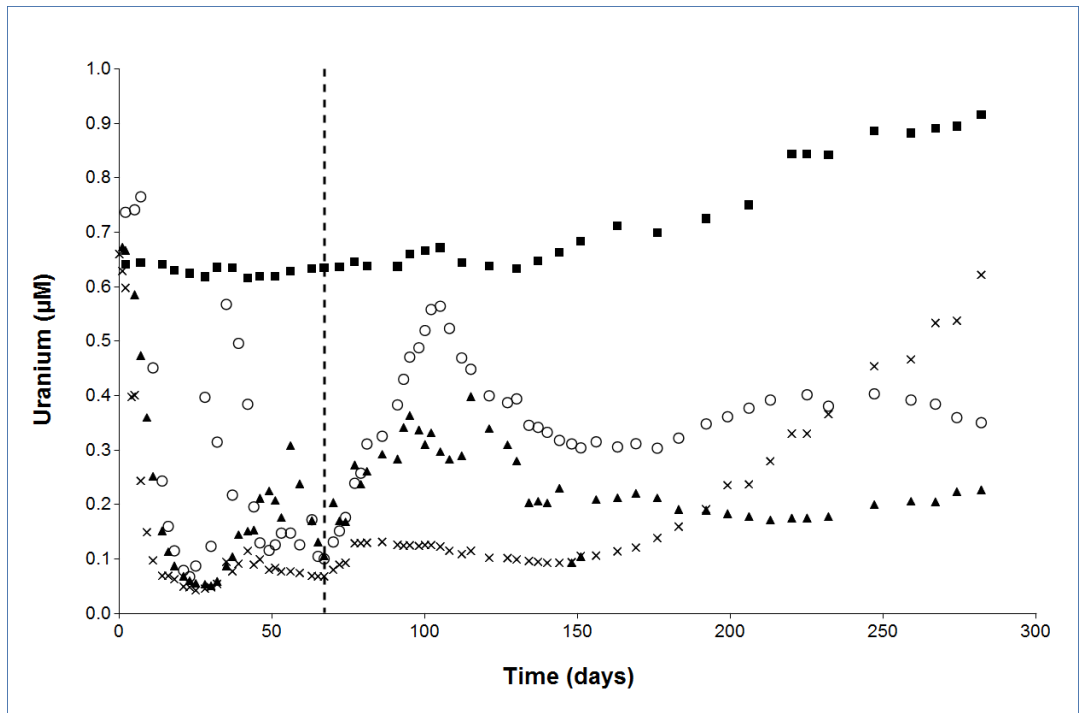


Figure 2.5: Dissolved uranium concentration at wells CD01 (x), CD04 (▲) and CD07 (○) as well as background well CU01 (■) over the 282 days of the carbon cycling investigation.

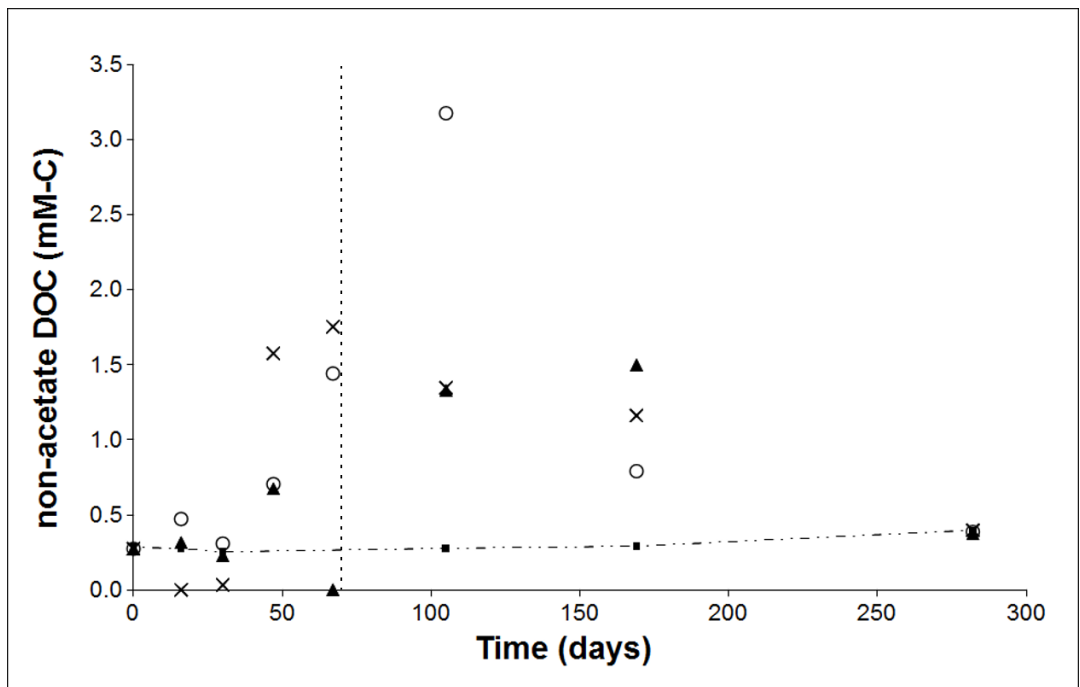


Figure 2.6: Non-acetate carbon concentrations (as mM-C) for wells CD01 (x), CD04 (▲), CD07 (○), and background well CU01 (■, dashed line), from initial acetate injection through 210 days after injection ended. The dotted line at 72 days represents the end of the acetate injection period.

### **2.3.3 Electron utilization accounting**

Acetate utilization was analyzed for CD01 because of the difficulties in estimating hypothetical acetate influent past the 1st observation well. An Ac:Br molar ratio of 7.5:1 was used to estimate an expected acetate concentration for well CD01. Electron equivalents of donor utilized, were based on 8 electron equivalents per mole of acetate. Utilization of electrons for the three important electron acceptors in the system was derived from stoichiometric equations 1-3. Sulfate utilization was calculated by subtracting measured  $\text{SO}_4^{2-}$  values from the average background value of 7.5 mM from well CU01 from day 0 to day 72. Fe(III) utilization was calculated from the production of Fe(II). Uranium utilization was calculated by subtracting the measured uranium values from the average uranium concentrations in well CU01. Estimated total electrons utilized for iron and uranium was less than 0.1 mM of electrons. Figure 2.7 shows the electrons utilized for sulfate reduction during acetate injection. On average a daily 20.8 mM of electrons (or 5.2 mM-C) remained unaccounted for throughout the injection period for well CD01. Electron deficits ranged from 0.6 mM-C on day 4 to 9.2 mM-C on day 30. Between 3.0 mM and 8.4 mM carbon was unaccounted for during the first 20 days of stimulation, before sulfate reduction became observable.

### **2.3.4 SUVA 254 nm results**

SUVA values in the background well CU01 ranged from 1.6 to 2.0 throughout the experiment. SUVA values for observation wells fluctuated during biostimulation from 0.64 to 2.98. The fluctuations are most likely due to difficulties in estimating accurate non-acetate DOC concentrations during the first 47 days due to the high acetate load. Post-stimulation values for observation wells on days 105 and 169 hovered between 0.39 and 0.58.

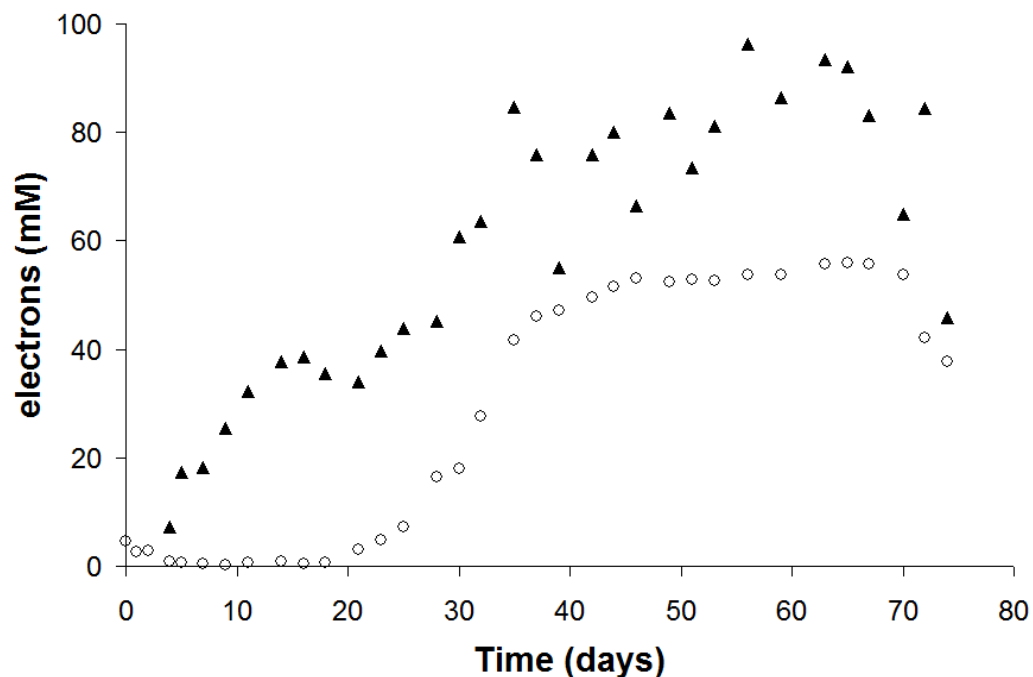


Figure 2.7: Electrons available from consumed acetate (▲) and electrons utilized for sulfate, uranium, and iron reduction (○) versus time for well CD01. Assumed background  $\text{SO}_4^{2-}$  concentration of 7.5 mM, were calculated from the average  $\text{SO}_4^{2-}$  values for CU01 from day 0 to day 72.

### 2.3.5 Excitation-emission matrices and regional intensities

EEMs for the background well CU01 on day 16 and observation well CD04 on days 16, 67, and 282 are presented in figure 2.8 on page 31. Well CD04 showed a well-defined fluorescence peak in the excitation emission (ex/em) region IV on day 67 when sulfate reduction dominated acetate consumption (Fig 2.8 C). Fluorescence intensity was already elevated in region IV 16 days after the onset of biostimulation, though the EEM did not show a characteristic peak as on day 67 yet (Fig 2.8 B). During biostimulation EEMs of background well CU01 (Fig 2.8 A) did not show any significant deviations from each other in either region IV or V. By day 105 or 33 days post-stimulation, the EEM for CD04 were indistinguishable from EEMs for background well CU01, with fluorescence intensity in region IV disappearing almost entirely. Similar trends were observed in wells CD01 and CD07 as well, though not all EEMs exhibited characteristic

peaks. Regional intensities for all observation wells, as a ratio of the average regional intensity of background well CU01, are shown on page 32 in figure 2.9 (for region IV) and 2.10 (for region V). Fluorescence intensities for humic and fulvic peaks (characteristic for region V) increased during biostimulation as well and returned to background values for all three observation wells. At day 282 (or 210 days post-stimulation) a marked difference appeared in well CD07 (Figure 2.11, page 33). Fluorescence peaks in region IV and II increased to values 5x observed in the background well and showed characteristic peaks in the 350 nm emission range that were not observed even during biostimulation. In addition, signatures in region V (typically associated with humic and fulvic acids) disappeared. EEMs for wells CD01 or CD04 did not show any similar characteristics on day 282, and were almost identical to EEMs for background well CU01.

## **2.4 Discussion**

The goal of the Rifle field experiments was to promote the reduction of uranium from the ground water plume. Acetate was added above the estimated stoichiometric requirement for the microbial reduction of iron, uranium and sulfate. The highest amount of uranium was removed during acetate injection, however, measurable uranium reduction continued to occur 100 days after acetate injections were terminated (Figure 5). Fe(II) measurements peaked at 64.2  $\mu\text{M}$  in well CD01 seven days after the injection period started and remained elevated for the first 21 days at approximately 28  $\mu\text{M}$  (Figure 4). Meanwhile background Fe(II) values for well CU01 remained within a range of 0.9 to 13.6  $\mu\text{M}$  during the entire observation period of 282 days. Sulfate reduction became noticeable after 28 days in well CD01. By day 42 all wells experienced a 90% reduction in measured sulfate concentration. Iron reduction was difficult to assess during sulfate reduction because the formation of ferrous sulfide precipitates would have removed Fe(II)

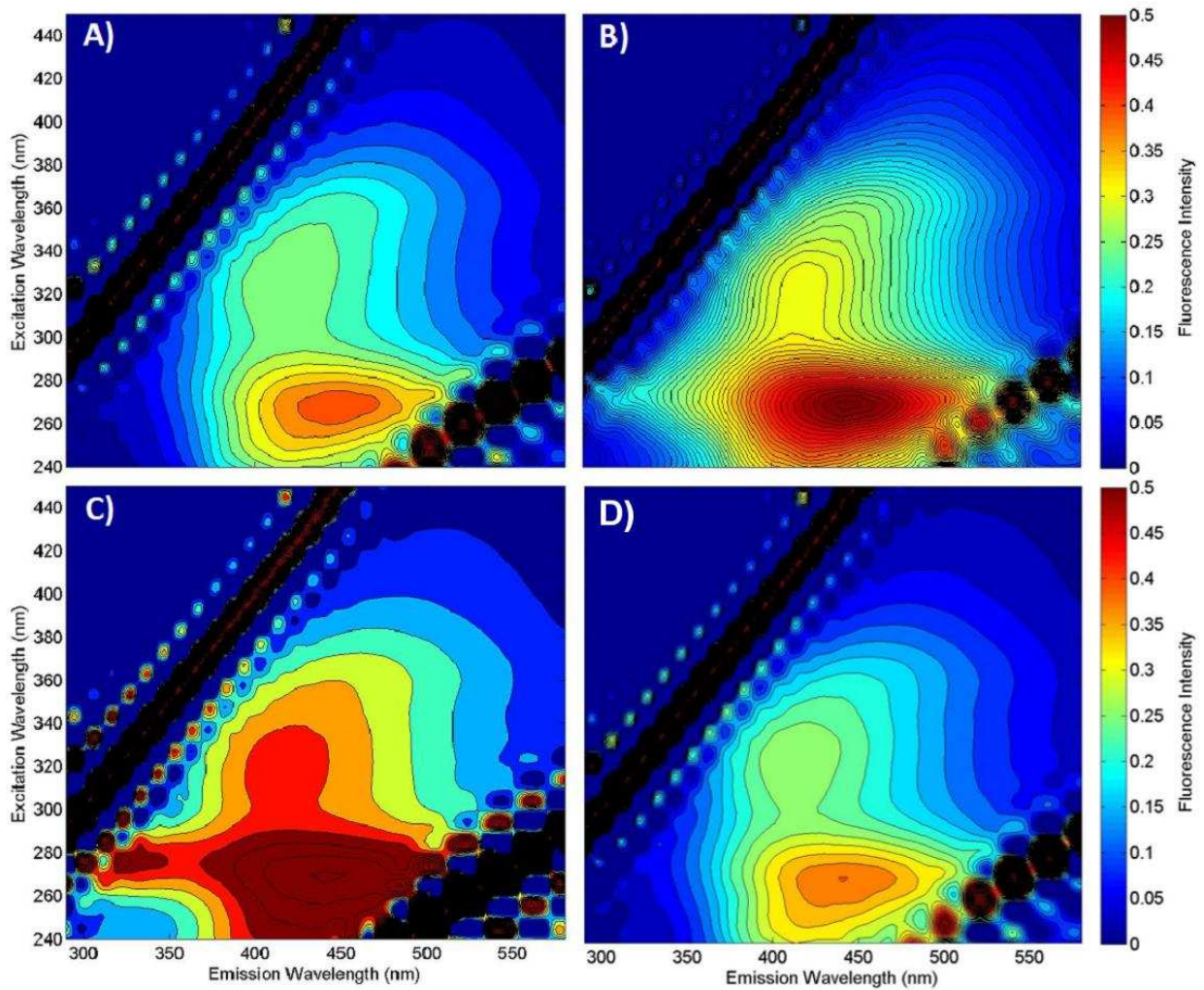


Figure 2.8: EEMs for observation well (A) and well CD04, 16 days into biostimulation (B). EEM of observation well CD04 on day 67 (C) and day 105 (D) into biostimulation.

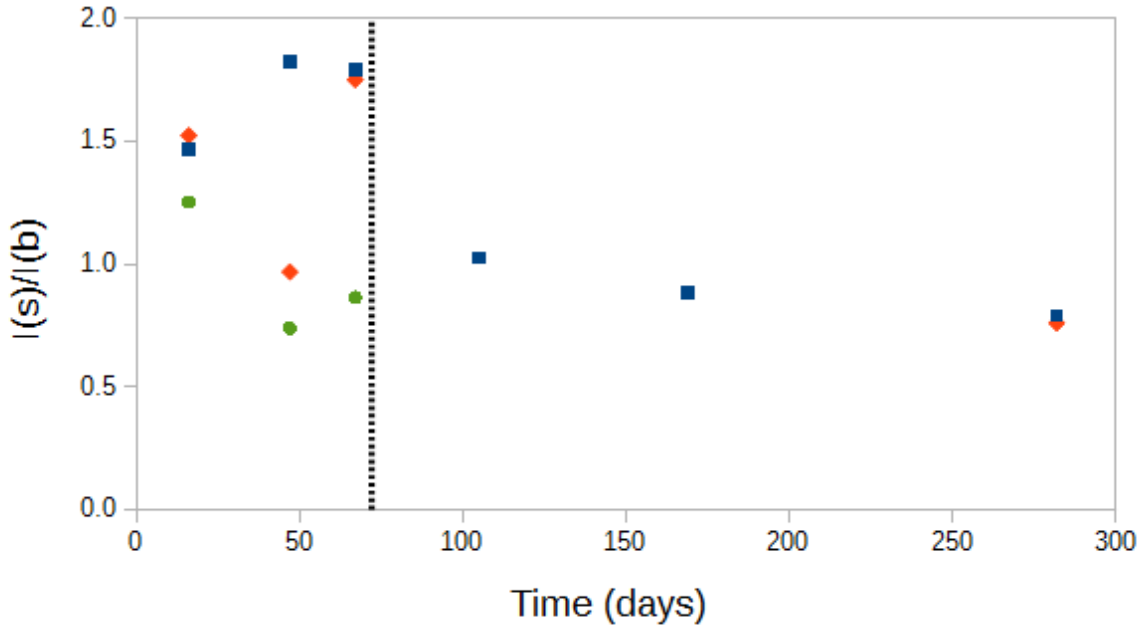


Figure 2.9: Intensities of region IV in EEM samples from wells CD01 (■, blue), CD04 (◆, red), CD07 (●, green) as a ratio of the average intensity of EEMs from background well CU01. The dotted line at 72 days indicates the end of the stimulation period.

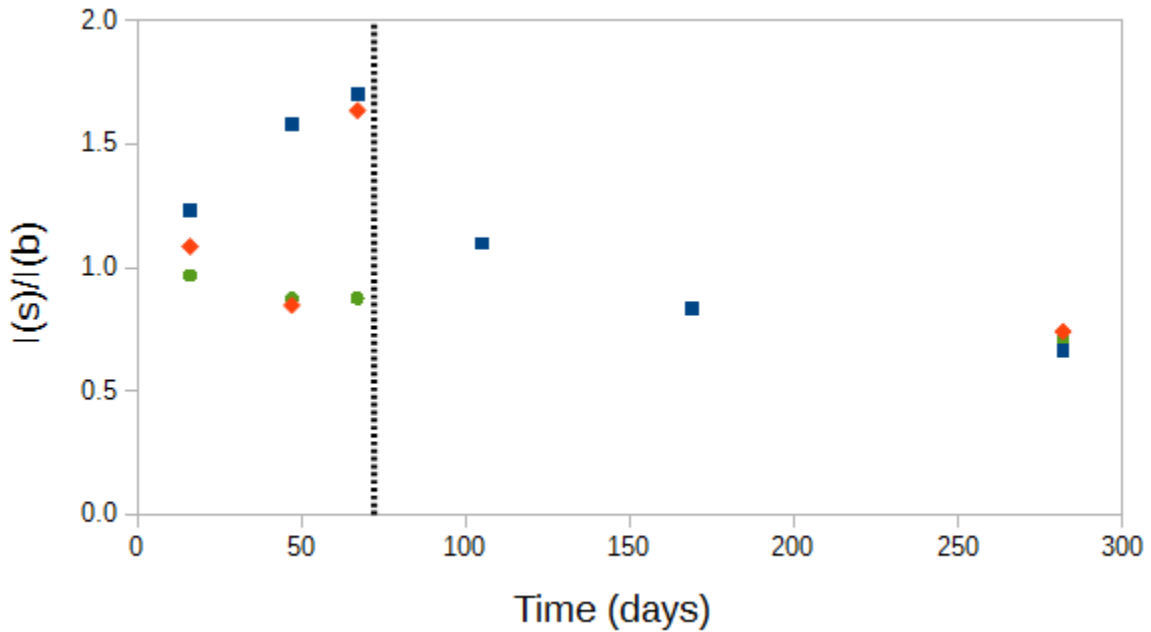


Figure 2.10: Intensities of region V in EEM samples from wells CD01 (■, blue), CD04 (◆, red), CD07 (●, green) as a ratio of the average intensity of EEMs from background well CU01. The dotted line at 72 days indicates the end of the stimulation period.

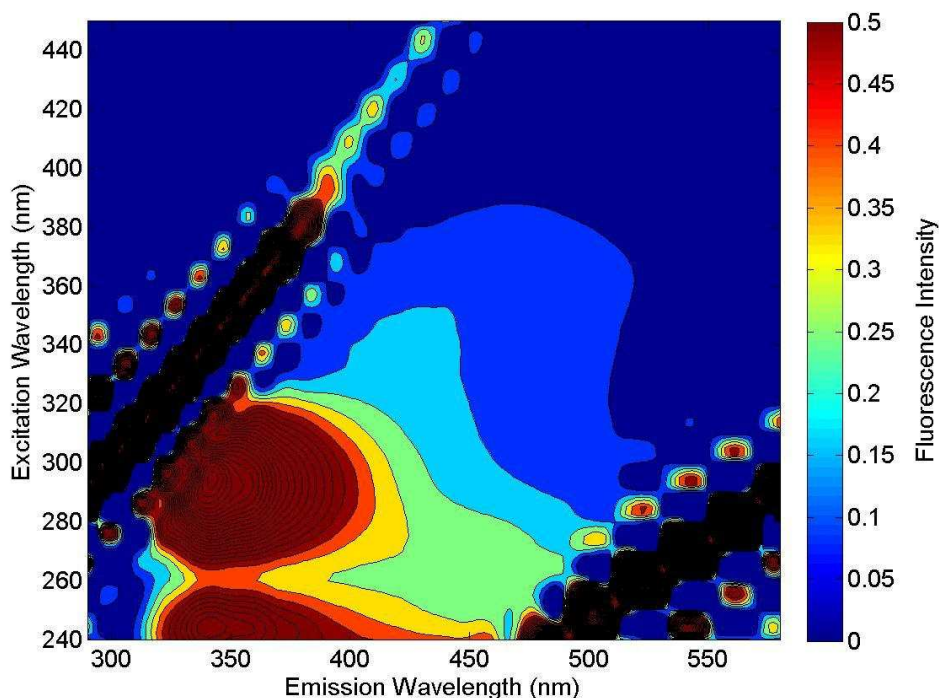


Figure 2.11: EEM spectra for well CD07 at day 282.

from solution. However, significant Fe(II) production was observed even after acetate injections were terminated. Fe(II) concentrations remained at approximately 20-40  $\mu\text{M}$  in all wells after day 100 (28 days post-stimulation) and even surpassed Fe(II) concentration during biostimulation in well CD01 on day 259 (or 187 days post-stimulation). The persistence of uranium and iron reduction in the absence of added acetate, suggests that other forms of organic carbon were available to uranium and iron reducing bacteria post-stimulation

The electron mass balance showed that the measured consumption of electron acceptors failed to account for a significant fraction of the acetate consumed in well CD01. During the initial iron reduction period (approximately day 7 to day 30) 88% (+/- 13%) of electrons donated from acetate were not utilized for microbial growth based solely on the stoichiometries in equations 2.1-2.3. During sulfate reduction, (approximately days 44 to 72), an average of 33% of the consumed acetate still remained unaccounted for. These results hint that an unknown electron

sink exists that was active within the first week of acetate injection (prior to sulfate reduction) and continued through the injection period. Other experimental systems studying uranium bioreduction also documented an incomplete carbon mass balance relative to the measured change in identified electron acceptors. Komlos et al. (2008) observed that only 1 to 1.5 % of acetate was consumed by sulfate, iron, and uranium reduction. Regberg et al. (2011) could account for only 28% of acetate consumed by iron reduction in column experiments.

Methanogenesis has been suggested as a possible sink for acetate during biostimulation (Regberg et al. 2011, Komlos et al. 2008) and has been shown to occur concurrently with sulfate and iron reduction in saturated aquifer sediment (North et al. 2004, Gu et al. 2005(b), Williams et al. 2011). However, it is unlikely that methane production could explain the significant gap in the electron mass balance observed in this experiment. Methanogens and SRBs grow slowly compared to IRB (Capone et al. 1988, Gu et al. 2005(b), Williams et al. 2011). Yet, a 33 mM electron gap in acetate utilization to relative to terminal electron acceptors (TEAP) consumption occurred 16-days after biostimulation. In addition, an average 20.8 mM of electrons, or 2.6 mM acetate were unaccounted for during the biostimulation period. If methanogenesis was responsible for that loss well CD01 would have produced roughly 2.4 mM of methane (or 52 mL CH<sub>4</sub> per liter of groundwater) each day. However, the highest methane concentration measured in well CD04 was only ~15 μM twenty days post-stimulation. Our results suggest that an unaccounted for carbon sink exists during biostimulation, assuming that iron and sulfate reduction represent the predominant metabolisms during the biostimulation experiment.

The wastewater treatment literature has long recognized that SMP production can constitute a significant carbon sink in microbial systems. Aquino and Stuckey (2003, 2004a) reported as much as 37% of substrate being shuffled into SMP production under anaerobic

conditions based on the presence of toxic metals or nitrogen availability. SMPs have previously not been considered in the carbon cycle that affects the geochemistry of biostimulated aquifers even though organic carbon cycling is a primary driver of biogeochemical reactions that are harnessed to achieve bioremediation. During the Rifle IFRC biostimulation experiment, SMP concentrations more than doubled for wells CD04 and CD07, and increased five-fold for well CD01 on day 47, just as sulfate reduction become predominant. It should be noted that the amount of SMP produced still fails to account for all the acetate consumed in well CD01. Roughly 1.6 and 1.8 mM-C of SMP were produced in well CD01 on days 47 and 67. However, the carbon mass balance suggests a carbon deficit of over three times as much (~3.2 mM-C and 6.7 mM-C respectively) for the same days.

SMP continued to be present in measurable concentrations even after acetate injections were halted on day 72. On day 105 (23 days after acetate injections), SMP concentrations ranged from 1.3 mM-C to 3.2 mM-C, while on day 169 SMP were still between 0.79 mM-C and 1.5 mM-C among the three wells (Fig. 2.6). Microbes are known to shuffle carbon into storage polymers and EPS that may be released as substrate during starvation periods when either carbon or nitrogen are limited in supply (Krishna et al. 1999, Wang et al. 2007). In addition, EPS are produced to grow biofilms to support adhesion to sediment particles and protect against toxic compounds. We postulate that the excess carbon consumption observed during the biostimulation period may have been shuffled into a solid organic matter phase and that the degradation of this solid-phase organic matter lead to elevated DOC concentrations post-stimulation. Incidentally the peak SMP production in well CD07 on day 105 (Fig. 2.6) also coincided with a uranium spike observed during that same time period in well CD07 (Fig. 2.5). This post-stimulation release of uranium and DOC may be attributable to the re-oxidation and/or

complexation of uranium due to elevated organic matter (Ganesh et al. 1997, Gu et al. 2005(a)), or the degradation of biomass that incorporated non-uraninite U(IV) (Bernier-Latmani et al. 2010).

It was hypothesized that the bulk characteristics of the soluble SMP would be different during the stimulation and post-stimulation periods. Fluorescence and SUVA were used in this study to characterize SMP produced during the field experiment. Soluble SMP production was observable after 47 days, which coincided with the onset of sulfate reduction. A distinct protein-like signature also appeared on EEMs of the observation wells by day 47. EEMs show that the SMP produced during acetate addition contains protein-like material as well as humic and fulvic materials. EEMs of DOC in wells CD01 and CD04 showed the appearance of characteristic protein-like peaks at ex/em 280/340 on days 47 and 67 that were absent from background EEMs. Well CD07 also showed increased intensities region IV, though the signature was less distinct. In addition, overall fluorescence intensity increased in the SMP region (Region IV) for all wells on day 16 and remained high for wells CD01 and CD04 on day 67. The presences of these peaks are in agreement with other fluorescence literature and indicate SMP associated with microbial growth (or UAP) (Aquino and Stuckey 2008, Hur et al. 2009, Jarusutthiark et al. 2007, Wang et al. 2010, Xie et al. 2010, Zhao et al. 2009).

On day 105 protein-like peaks were greatly diminished in all wells, and vanished completely on day 167. Overall fluorescence intensity in the SMP region was also greatly reduced after biostimulation ceased. Undiluted, post-stimulation EEMs were essentially indistinguishable from samples in background wells, even though DOC concentrations were still elevated by a factor of 3 to 8 for all wells. Samples that were diluted to the 4 ppm-C of background DOC, for comparative purposes, showed virtually no fluorescence signals. The

reduction of fluorescent material in post stimulation EEMs would suggest that the produced SMP was composed of low molecular weight compounds or aliphatics.

We believe the SMP observed during acetate injection were most likely associated with UAP. This conjecture is based on the protein-like signatures in EEMs that have previously been linked to UAP formation Xie et al. (2010) found that the protein-like peak at ex/em 280/350 nm increased in intensity during the growth phase of denitrifying bacteria in batch tests. This observation was consistent with UAP formation and an increase in the protein fraction of SMP. Meanwhile, Zhao et al. (2009) observed the release of protein-like fluorophores during the growth and stationary phase of *P. donghaiense*, while EEMs shifted to more humic and fulvic like components during the death phase. Overall EEMs could identify the production of UAP in bioremediation systems, through the presence of protein-like and fulvic-like peaks during biostimulation. The produced SMP observed post-stimulation are postulated to be BAP. In the absence of added substrate, microbial growth and corresponding UAP formation would be limited and an insignificant contributor to SMP composition (Aquino and Stuckey 2008). These results support our conceptual model illustrated in figure 2.3.

Fluorescence EEM for well CD07 210 days post-stimulation showed significant differences in character from both background EEMs as well as EEMs found during biostimulation. A fivefold increase in intensity was observed in region IV that even surpassed values found during active stimulation. In a literature review on fluorescence in waste water treatment systems peaks in the <380 nm emission regions have been correlated to increased BOD loading (Carstea et al. 2016) and indicate high microbial activity common to waste water and landfill leachates (He et al. 2011). The increased microbial activity stands in contrast to the actual DOC values which returned to background values of ~0.3 mM-C in all wells at day 282.

However, a small but highly bioavailable amount of DOC would explain the continued production of Fe(II) observed in all three observation wells 210 days post-stimulation.

High SUVA values have been shown to correlate to increased aromaticity (Weishaar et al. 2003) in DOC and linked to more refractory DOC (Wang et al. 2009, Zhao et al. 2012). Batch tests on the microbial degradation of leaf litter noticed that the release of higher molecular weight compounds corresponded to a similar increase in SUVA (Hur et al. 2009). The higher molecular weight and high SUVA DOC was also determined to be more refractory based on rates of microbial utilization of DOC in these systems. Given the previous literature SUVA could be used to qualitatively assess the bioavailability of SMP in biostimulated systems. SUVA was difficult to quantify during the first 30 days of biostimulation. Acetate does not absorb UV light at 254 nm wavelengths, yet it was added at concentrations 50-100 times that of non-acetate DOC. Since instrumental errors for both the Shimadzu TOC analyzer and the HPLC were between 5%-10%, calculated concentrations of non-acetate DOC were essentially within the instrumental errors. In well CD04 non-acetate concentrations dipped to “zero” on day 67, most likely an artifact of the instrument errors. SUVA values 100 days post stimulation, however, dropped down to about a fourth of the observed background SUVA values, even though DOC was still elevated above background concentrations. Together with findings from previous literature (Hur et al. 2009, Wang et al. 2009) this data suggests that the reduction in SUVA values is mostly due to the addition of newly produced aliphatic, low molecular weight organic matter.

If a fraction of SMP were more bioavailable than the background DOC (as suggested by SUVA) then it could be used to prolong reducing conditions. EEMs suggest that more complex SMP are produced during biostimulation while both EEMs and SUVA show that aliphatic, low molecular-weight compounds predominate DOC up to 90 days post-stimulation. Post stimulation,

the soluble SMP measured on days 105 and 169 contained ample electron equivalents ( $> 2 \text{ mM}$ ) to provide the stoichiometric donor requirement of the observed iron and uranium reduction ( $< 0.1 \text{ mM e- equivalents}$ ). On day 282, soluble SMP was below the resolution of the DOC analysis. The concentration of SMP needed to provide sufficient electron equivalents for the observed iron and uranium reduction was  $< 0.2 \text{ mg/L as DOC}$ . These results suggest that the BAP portion of SMP could prolong reducing conditions for at least 90 days and possibly longer past biostimulation, by providing a more easily available carbon source than background DOC.

Our results indicate that a significant portion of carbon may have been shuffled into an unaccounted for carbon sink that is not related to metabolic activity or UAP production. In addition, elevated DOC levels persisted 90 days post-stimulation, which was accompanied by continued Fe(II) production and uranium removal. Fluorescence EEMs showed intensities associated with microbial growth during biostimulation in all observation wells, while SUVA analyses indicated that post-stimulation SMP were more bioavailable than background DOC. Based on our results we believe that acetate was utilized to produce solid phase organic matter during biostimulation that became available after acetate injections ceased and sustained microbial activity beyond the stimulation period. In addition, fluorescence spectroscopy and SUVA may offer unique insights into the organic matter dynamics that occur during biostimulation and may be used as indicators of microbial activity and the bioavailability of DOC during and post-stimulation.

## CHAPTER 3

### LABORATORY COLUMN EXPERIMENTS AND TRANSPORT MODELING TO EVALUATE RETARDATION OF URANIUM IN AN AQUIFER DOWNGRAIENT OF A URANIUM IN-SITU RECOVERY SITE

Article published in *Applied Geochemistry*<sup>1</sup>

Martin A. Dangelmayr<sup>2</sup>, Paul W. Reimus<sup>3</sup>, Naomi L. Wasserman<sup>4</sup>, Jesse J. Punsal<sup>3,6</sup>, Raymond H. Johnson<sup>5</sup>, James T. Clay<sup>6</sup>, James J. Stone<sup>7</sup>

<sup>1</sup> Reprinted with permission from  
Martin A. Dangelmayr<sup>2</sup>, Paul W. Reimus<sup>3</sup>, Naomi L. Wasserman<sup>4</sup>, Jesse J. Punsal<sup>3,6</sup>, Raymond  
H. Johnson<sup>5</sup>, James T. Clay<sup>6</sup>, James J. Stone<sup>7</sup>

<sup>2</sup> Department of Civil and Environmental Engineering, Colorado School of Mines, 1500 Illinois  
St, Golden, CO 80401, USA

<sup>3</sup> Los Alamos National Laboratory, Bikini Atoll Rd., SM 30 Los Alamos, NM 87545, USA

<sup>4</sup> Department of Geology, University of Illinois at Urbana-Champaign, Champaign, IL 61820,  
USA

<sup>5</sup> Navarro Research and Engineering, Inc., 2597 Legacy Way, Grand Junction, CO 81503, USA

<sup>6</sup> Power Resources Inc., Smith Ranch-Highland Operation, 762 Ross Road, Douglas, WY 82633,  
USA

<sup>7</sup> Department of Civil and Environmental Engineering, South Dakota School of Mines and  
Technology, 501 East Saint Joseph Str, Rapid City, SD 57701, USA

### 3.1 Introduction

*In-situ* recovery (ISR) now accounts for most of the uranium produced in the U.S., and about half of the uranium produced worldwide (Macfarlane and Miller 2007, Mudd 2014). ISR involves the injection of O<sub>2</sub>, CO<sub>2</sub>, and either NaHCO<sub>3</sub> or H<sub>2</sub>SO<sub>4</sub> fortified water (i.e., lixiviant) into a uranium-bearing ore zone to oxidize and solubilize the uranium (Pelizza 2008). The solubilized uranium is then pumped to the surface, extracted, and processed into uranium oxide.

This process avoids excavation or the processing of solid ores and does not leave behind open pits, shafts or tailing piles. However, ISR does significantly alter the geochemistry of ore zones, and leaves behind elevated concentrations of uranium, alkalinity, as well as other potential contaminants such as arsenic and selenium. The industry restoration practice to reduce contaminant concentrations can vary, but commonly involve a combination of groundwater withdrawal to replace the existing groundwater, treatment of the groundwater by reverse osmosis, and the use of chemical reductants to induce reducing conditions on aquifer waters and sediments (Catchpole and Kuchelka 1993), or biostimulation to precipitate contaminants. These practices work well to significantly reduce constituent concentrations, however, they typically do not succeed in lowering concentrations of all species to pre-mining ‘baseline’ levels. As a consequence, industry may be faced with applying for alternate concentration limits for contaminants of concern (Borch, et al. 2012, Hall 2009).

Prior studies of ISR restoration projects have reported several challenges to restoring groundwater contaminants to regulatory levels. Hall (2009) demonstrated that no well-fields to date managed to achieve pre-mining conditions of all constituents. Pump and treat as well as abiotic reduction via H<sub>2</sub>S injections were also shown to be insufficient (Abitz and Kooyoomjian 2011, Borch et al. 2012, Osiensky and Williams 1990), though some of the shortfall may have resulted from imperfect hydrologic sweep efficiency whereby some volumes of water were not treated. The industry and its regulators (Environmental Protection Agency (EPA), Nuclear Regulatory Committee (NRC), and state agencies) are currently working toward an ISR regulatory framework that considers best mining and restoration practices, the need to protect groundwater resources, the realities of geochemical changes resulting from ISR mining, and relative risks to the environment and the public. Reactive transport models have the potential to

inform stakeholders on the risk that mining operations pose to downgradient aquifers and could provide regulators and industries with a valuable tool to protect drinking water supplies and public health. This study evaluates the ability of an aquifer to attenuate the transport of uranium to downgradient groundwater supplies, and to provide a quantitative estimate of how well the model fits the data.

Several thermodynamic processes determine the mobility of uranium in the subsurface. Transport models commonly account for sorption to mineral phases, reduction and subsequent precipitation, and the aqueous chemistry of Uranium. U(VI) readily sorbs to Fe-containing minerals, (Barnett et al. 2002; Cheng et al. 2007; Ho and Miller, 1986) clays (Ames et al. 1983, Echevarria et al. 2001, Missana, et al. 2004), and natural organic matter (Evans et al. 2011, Lenhart and Honeyman, 1999, Mibus et al. 2007), which may slow down uranium transport to downgradient aquifers. Furthermore, U(VI) may be reduced to U(IV) through abiotic or microbial processes in the subsurface, if redox potentials are low enough (Anderson and Lovley 2002, Gorby and Lovley, 1992, Lovley and Phillips 1992). However, U(VI) mobility may become significantly enhanced in high alkalinity systems due to the preferential formation of carbonate-uranium complexes since the neutral and negatively charged ions of  $\text{UO}_2\text{CO}_3(\text{aq})$  and  $\text{UO}_2(\text{CO}_3)_2^{2-}$  are unlikely to adhere to the surfaces of negatively charged ferric hydroxide minerals (Geipel et al. 1998, Ho and Miller, 1986, Morrison et al. 1995). The presence of Ca and Mg further shifts uranium aqueous speciation toward highly stable neutral or negatively-charged calcium and magnesium uranyl-carbonate compounds (Dong and Brooks, 2008 Fox et al. 2006; Nair and Merkel 2011a, 2011b, Stewart et al. 2010). The interplay between enhancing and attenuating effects should be accurately portrayed in any predictive transport models that attempt to assess risks to downgradient aquifers. Thus, these processes need to be better estimated and

quantified to allow for post-mining ore zone restoration targets that ensure the safety of the environment and the public.

In this study, an assessment was made of site-specific attenuation mechanisms of a post-production aquifer downgradient of an ISR site through bench-scale column experiments using sediment from the post-mining, down-gradient zones. General surface complexation models were embedded in a transport model to determine whether this combined approach could predict uranium retardation in columns with chemistries that were varied between post-mining restoration and unaltered down-gradient conditions. The goal of this study is to provide a modeling framework for regulatory agencies and industry to better assess the potential for uranium contamination of aquifers downgradient of ISR mining zones.

## **3.2 Methods**

### **3.2.1 Site description**

The water and sediment cores used in this study were collected from the Smith Ranch-Highland (SRH) ISR facility near Douglas, WY U.S., operated by Cameco Resources. Figure 3.1 shows a map of the site, including the locations where water and core materials were collected. Further details on the geology of the region can be found in Hunter (1999). The site hosts multiple roll-front uranium deposits that are in various stages of exploration, ISR mining, or restoration. Until May of 2016, Smith Ranch-Highland was the largest uranium ISR operation in the U.S., accounting for approximately 1/3 of all domestic uranium production in recent years. As of May 2016, production is limited to currently developed areas with no further mining development planned, and operations are focused on restoration.

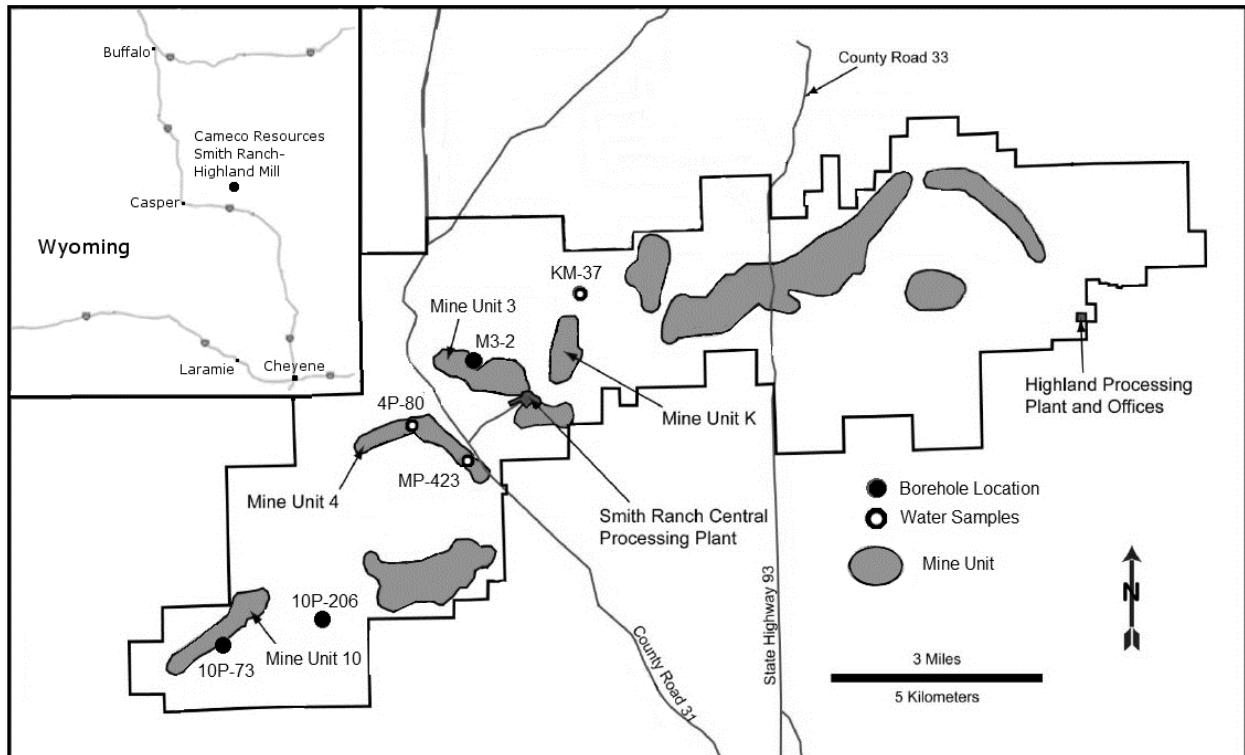


Figure 3.1. Map showing the location of Smith Ranch-Highland facility with water wells (hollow circles) and core sampling locations (solid circles) for this study. Irregular-shaped regions are mining units in various stages of exploration, operation, restoration, or stability.

### 3.2.2 Sediment core collection

Sediment cores were collected from the Fort Union formation of the highland property in the Powder River Basin. The core material used for MU10 A and MU10 B column experiments came from a depth of ~270 m below ground surface from borehole 10P-73 in Mining Unit 10 at SRH (see Fig. 3.1). This core was collected prior to the mining unit going into production and was recognized as consistent with material generally encountered downgradient of an ore-zone at SRH. sediment cores from this zone were not anaerobically preserved post-collection, and were shipped to Los Alamos National Laboratory (LANL) several months after collection.

The core material for MU3A, MU3B, and MU3C column experiments all came from the same borehole, M3-2, which was drilled downgradient of Mining Unit 3 at SRH before the mining unit went into production (Fig. 3.1). Material retrieved from the MU3-2 coring was

carefully preserved by vacuum sealing in airtight bags and freezing as soon as possible after it reached the surface. Three different intervals were selected for column experiments (191.2 – 191.5 m, 191.5 – 191.8 m, and 192.5 – 192.8 m). Although these samples were close together in depth, they exhibited significant visual differences in grain size, mineralogy, and visual organic carbon content. The materials were shipped to LANL after being carefully processed in an inert-atmosphere glovebox to remove the outer layer of core that could have been contaminated by organic additives during drilling operations.

### **3.2.3 Sediment core analysis**

The materials for the MU10 experiments were not characterized in detail. However, X-ray diffraction (XRD) and X-ray fluorescence (XRF) analyses (included in supporting information) were performed on sediment cores from a borehole downgradient of the MU10 ore-zone (location noted in Fig. 3.1) for mineralogy determination. For the MU3 experiments, XRD and XRF analyses were performed on sediment core section between 191.8 – 192.1 m. That section does not coincide exactly with the intervals used in the column experiments, however, it was considered representative of the mineralogy of that depth range.

Inorganic carbon was determined by acid digestion of the sediments with a UIC Inc. (Joliet, IL). acidification module, while total carbon content was measured through the thermal oxidation of sediment samples at 935 degrees F. Evolved CO<sub>2</sub> was then determined by coulometric titration using a UIC Inc. CO<sub>2</sub> coulometry module (Joliet, IL). Total organic carbon (TOC) was determined by subtracting inorganic from total carbon (Tiessen et al 1993). Surface area of sediment particles was quantified through the Brunauer-Emmet-Teller (BET) test (Brunauer 1938). A Micrometrics (Norcross, GA) FlowPrep 060 was used to purge roughly 0.3 g of sample

with nitrogen at 50° C for 90 minutes, before determining surface area with a Micrometrics Gemini III 2375 Surface Area Analyzer.

### 3.2.4 Ground water preparation

Three different influent chemistries were used for the experiment. A general “background” water that represents pre-mining conditions (low uranium and alkalinity) and two different types of ore-zone waters with increased levels of uranium and alkalinity (Table 1). The ‘background’ water (KM-37) used in all column experiments was collected from monitoring well KM-37 in Mining Unit K North at SRH (Figure 3.1). KM-37 chemistry is very typical of waters collected from both upgradient and downgradient monitoring wells at SRH. A distinct sulfide smell was observed during collection, and field measurements of the oxidation-reduction potential (YSI XLM 650 multiprobe system) gave very low Eh values at about 99 mV SHE (Table 3.1).

Table 3.1: Major ion chemistry of waters used in column experiments.

<b>Constituents</b>	<b>KM-37</b>	<b>4P-80</b>	<b>MP-423</b>
Ca <sup>2+</sup> (mg/l)	105	374	461
Na <sup>+</sup> (mg/l)	31	44	46
Mg <sup>2+</sup> (mg/l)	28	92	108
K <sup>+</sup> (mg/l)	11	18	20
Fe(total) (mg/l)	0.03	1.06	2.5
UO <sub>2</sub> <sup>2+</sup> (mg/l)	0.01	19.5	40.7
SO <sub>4</sub> <sup>2-</sup> (mg/l)	302	810	895
Cl <sup>-</sup> (mg/l)	2	133	131
Alk. (mg/l CaCO <sub>3</sub> )	160	360	540
Eh (mV SHE)	99	263	177
pH	7	6	6.2

Well waters from two different ore zones were used in the column experiments. One was collected from well 4P-80, a former production well in an area of Mining Unit 4. The other was collected from MP-423, a well that served as both a production well and a monitoring well in Mining Unit 4. The 4P-80 water was used for the MU10 material experiments, while MP-423 water was used for the columns with sediment cores from MU3-2. The chemistries of all waters are summarized in Table 3.1. Both of these wells had not yet undergone restoration at the time waters from them were collected for the column experiments

### **3.2.5 Column setup**

The core materials were dry-packed into 1-inch diameter by 12-inch long glass columns (Ace Glass, Columbia, SC.) in a glove bag under a 4% H<sub>2</sub>/96% N<sub>2</sub> atmosphere to minimize introduction of oxygen. The sources of the core materials (borehole and depth) used in each column are listed in Table 3.2. Material for the columns was extracted from the interior portions of the core to avoid potential contamination by the organic additives in the drilling fluids used during the coring operation. After packing, a vacuum was drawn on the columns, and then vacuum-degassed KM-37 water was slowly introduced to the columns while still under vacuum to saturate them. This procedure minimized entrapment of air bubbles in the column. Once the columns were saturated, they were moved back into the anaerobic glovebox.

For the MU10 experiments, influent waters were fed from a 2-liter reservoir that was kept under an atmosphere consisting of a mixture of the 4% H<sub>2</sub>/96% N<sub>2</sub> gas mixture and pure CO<sub>2</sub> after purging with the gas mixture to eliminate dissolved oxygen. CO<sub>2</sub> partial pressures were maintained at approximately the calculated pCO<sub>2</sub> of the water at its field-measured pH and alkalinity (Table 3.1). A syringe pump (KD Scientific) was used to push water through

Table 3.2: Summary table for all five columns, showing borehole depth, influent waters and their injection duration, and the alkalinity during the different time segments for each experiment.

Experiment	Depth (feet)	Flow Rate and Porosity	Duration (hours)	Influent Water	Alkalinity (mg/l CaCO <sub>3</sub> )	pH
MU3A	627-628	0.9 ml/h 0.45	0 - 848	MP-423	540	6.15
			848 - 1238	KM-37	540	6.15
MU3B	629-630	0.9 ml/h 0.45	0 - 240	MP-423	540	6.15
			240 - 964	KM-37	540	6.15
MU3C	631-632	0.9 ml/h 0.32	0 - 240	MP-423	540	6.15
			240 - 570	KM-37	540	6.15
MU10A	888	2.3 ml/h 0.48	0 - 521	4P-80	360	6
			521 - 715	KM-37	160	7
			715 - 1300	KM-37	360	6
MU10B	888	2.3 ml/h 0.48	0 - 307	4P-80	540	6
			307 - 589	KM-37	540	6

the MU3 columns at approximately 0.9 ml/hr, while a peristaltic pump (Masterflex) supplied water to the MU10 columns at a rate of 2.3 ml/h. When the syringe pumps were used, they were filled outside the glovebox using water taken directly from the reservoir after bubbling thoroughly with the gases, and then the pumps were moved into the glovebox. A fraction collector (Foxy 200) was used to collect samples of the effluent. The reservoir, peristaltic pumps, and fraction collector were all kept outside the glovebox. All columns were initially equilibrated with an inflow of KM-37 water until uranium concentrations in the effluent decreased to steady low levels. Uranium concentrations were measured by Kinetic Phosphorescence Analysis (KPA, ChemChek, Inc.)

### 3.2.6 Column operation

Once the uranium concentrations in the column effluent had stabilized, the injection water was switched to the post-mining water, either 4P-80 (for the MU10 columns) or MP-423 (for the MU3 columns). Sodium iodide was added to the 4P-80 water, and tritiated water ( $^3\text{HHO}$ ) was added to the MP-423 water to serve as nonreactive tracers. The iodide was analyzed by ion-selective electrode (Orion), and the tritium was analyzed by liquid scintillation counting (Perkin-Elmer Tri-Carb 2500). Column porosities were calculated from the 50% tracer breakthrough point and flow rates, summarized in table 3.2. An adjustment was made to the  $\text{pCO}_2$  of the 4P-80 water in the second MU10 experiment (MU10 B) to increase alkalinity from its field-measured value of 360 mg/l  $\text{CaCO}_3$  to 540 mg/L  $\text{CaCO}_3$  so that it was approximately the same as the MP-423 water. Alkalinity was checked in all solutions before injection by titrating with  $\text{H}_2\text{SO}_4$ , using a Bromo cresol green-methyl red indicator for the endpoint determination (Hach method 8203). The post-mining waters were continuously injected into the columns until the uranium concentrations stabilized at their inlet concentrations, indicating complete breakthrough of the uranium, and the injection of ore-zone water was then continued for at least one additional pore volume.

After uranium concentrations in the column effluents had been maintained at their inlet concentrations for some time, the column injection water was switched back to the KM-37 water to observe the elution of uranium from the columns. In one of the experiments (MU3 A), two extended flow interruptions were introduced after the uranium concentrations had reached inlet concentrations. A summary of which waters were injected into each column experiment as a function of time, including any changes to pH and alkalinity achieved through  $\text{pCO}_2$  adjustments and/or addition of  $\text{NaHCO}_3$ , is presented in table 3.2.

### 3.2.7 Column transport modeling

PHREEQC (Parkhurst and Appelo 2013) was used to model the breakthrough of uranium for all column experiments. Briefly, PHREEQC was used to perform reactive advective transport modeling by coupling sorption models to advective flow equations. The modeling procedures were adopted and modified for column experiments from Johnson and Tutu (2015) and Johnson and Tutu (2016) and are described below. The column length was divided into 30 cells, each 1 cm long. Equilibrium conditions were calculated as the solution shifts through each cell. The time steps for each shift were adjusted to simulate a mean residence time of about 84 hrs, 68 hrs and 31 hrs, to match the experimental residence times for MU3 A and B, MU3 C and MU10 derived from tracers, respectively. Influent solutions were allowed to equilibrate with the two specified equilibrium phases (calcite and gypsum) prior to transport. Solid uranium phases and uranium reduction were specifically excluded from the system, since abiotic system kinetics are considered too slow to occur to significantly impact uranium attenuation, and the primary focus of the modeling was adsorption.

PHREEQC's default database was updated to incorporate thermodynamic data for uranium as provided by Guillaumont et al. (2003) and data for calcium and magnesium carbonate uranyl ternary complexes were added as reported by Bernhard et al. (2001) and Dong and Brooks (2006). Adsorption reactions were incorporated via the general component surface complexation (GC) proposed by Davis et al. (2003). The GC SCM assumes that uranium sorption occurs primarily to the ferrinol and aluminol groups in mineral surfaces (Davis et al. 2004). While metal oxides represent only a small fraction of the sediment they have shown a significant affinity to uranyl sorption (Dong et al. 2011). Heterogeneity in mineralogy and surface composition was abstracted into generic surfaces with fixed equilibrium constants proposed by Davis et al. (2004).

Our models compartmentalized the surface area into three theoretical components with fixed equilibrium constant for the complexation of the uranyl ion: A super-strong site (>SSOH), a strong binding site (>SOH), and a weakly binding site (>WOH). The modeling of the column experiments were tested by using a combination of the three binding sites, as well as a model using only a single super-strong sorption site (>SSOH). Reactions for the thermodynamic equations added to PHREEQC are provided in Table 3.3. Corrections for electric double layers are not normally used in GC models (Davis and Curtis 2003, Davis et al., 2004) and were ignored for these simulations.

Table 3.3: Pertinent reactions added to the PHREEQC database for the model simulations and their formation constants ( $\log \beta$ )

<b>Reaction</b>	<b><math>\log \beta</math></b>
$\text{Ca}^{2+} + \text{UO}_2^{2+} + 3\text{CO}_3^{2-} \leftrightarrow \text{CaUO}_2(\text{CO}_3)_3^{2-}$	27.4 <sup>a</sup>
$2\text{Ca}^{2+} + \text{UO}_2^{2+} + 3\text{CO}_3^{2-} \leftrightarrow \text{Ca}_2\text{UO}_2(\text{CO}_3)_3(\text{aq})$	30.55 <sup>a</sup>
$>\text{WOH} + \text{UO}_2^{2+} \leftrightarrow >\text{WOUO}_2^+ + \text{H}^+$	2.57 <sup>b</sup>
$>\text{SOH} + \text{UO}_2^{2+} \leftrightarrow >\text{SOUO}_2^+ + \text{H}^+$	5.817 <sup>b</sup>
$>\text{SSOH} + \text{UO}_2^{2+} \leftrightarrow >\text{SSOUO}_2^+ + \text{H}^+$	6.798 <sup>b</sup>

<sup>a</sup> Dong and Brooks. (2006)

<sup>b</sup> Davis et al. (2004)

PEST (Doherty and Hunt 2010) is a parameter estimation and fitting program (Watermark Numerical Computing Inc.) that allows direct coupling with the PHREEQC code to automatically adjust specified parameters and evaluate goodness-of-fit by calculating the sum of weighted squares of the residuals (SWSR) between model outputs and experimental results. It also provides correlation coefficients (R) for model fits and sensitivity values for each estimated parameter. PEST was used with the nonreactive tracer curves to estimate dispersivity values for each column, which were then applied to the transport model. The experimental data for uranium

breakthrough was then used to derive sorption parameters for uranium transport in each column. The fitting parameters for the column experiments were primarily the density of sorption sites for each general surface component, although the effect of calcite equilibrium was also investigated for the MU10 column experiments. Prior batch studies utilizing a similar approach found that best fits are usually produced when equilibrium constants are fixed while allowing PEST to adjust site densities (Johnson et al. 2016). Introducing too many fitting parameters can produce multiple "best" solutions, thus no more than three fitting parameters were allowed to model adsorption in each experiment.

### **3.3 Results**

#### **3.3.1 Sediment analysis and estimation of site densities**

Data for TOC and surface areas are given in Table 3.4 (page 54) while results for XRF and XRD analyses for two representative sediment cores are included in Tables 3.5 (page 54) and 3.6 (page 56). Inorganic carbon was negligible or below the detection limit, and thus not included. A generic site density of  $1.92 \mu\text{mol}/\text{m}^2$  surface area (Davis and Kent 1990) was used to convert surface area to number of binding sites, providing an upper bound of  $25.2 \mu\text{mol}/\text{g}$ -sediment and  $18.1 \mu\text{mol}/\text{g}$ -sediment of sorption sites for column MU3 A and B respectively (with a bulk density of  $1.6 \text{ g}/\text{cm}^3$ ) assuming bidentate bonding as given in Table 3.3. Carboxyl functional groups in soil humic matter are normally considered the strong binding sites in complexation models (Zhou et al. 2005) and literature values commonly estimate them around  $4.0 \text{ mmol}$  per gram carbon (Janoš et al. 2008, Kurán et al. 2008, Tan 2010). Using these parameters resulted in  $3.8 \mu\text{mol}/\text{g}$ -sediment and  $2.1 \mu\text{mol}/\text{g}$ -sediment of strong binding sites for MU3 A and MU3 B, respectively. The number of binding sites in column MU3 C was determined to be  $9.1 \mu\text{mol}/\text{g}$ -

sediment. TOC content was 0.011% g/g-sediment, which would give 0.44  $\mu\text{mol/g}$ -sediment of carboxylic functional groups. BET and TOC results for the MU10 sediment gave 8.2  $\mu\text{mol/g}$ -sediment of binding sites and 1.4  $\mu\text{mol/g}$ -sediment of carboxyl functional groups respectively.

### 3.3.2 Column operation

Effluent measured uranium and modeled breakthrough curves for each column experiment are presented as a function of time in Figures 3.2 – 3.6 (pages 56 and 57). Within each figure, annotations are provided when significant events, such as changing injection water chemistries or extended flow interruptions occurred. Model outputs are also provided for all columns in Figures 3.2-3.6. SWSR and R results for each column is provided in Table 3.7 (page 33), with the model best fit (highest R) shown within each figure. Uranium recoveries for each column are listed in Table 3.8 (page 55). Over 90% of uranium was recovered for four of the five columns, with 87% recovery for Column MU3, which experienced flow interruptions.

All columns experienced uranium delayed breakthrough compared to their respective non-reactive tracers. For MU3 A, B, and C (Figs. 3.2 – 3.4) uranium appeared after 1.68, 1.69 and 1.47 as many pore volumes as the non-reactive tracer tritium. MU10 sediment (Figs. 3.5 and 3.6) exhibited an almost threefold greater uranium retardation than any of the MU3 columns, while MU10 B exhibited a lower capacity for uranium attenuation than MU10 A (a retardation factor of 2.80 compared to 4.26), most likely due to the elevated alkalinity associated with the influent water (540 mg/l as  $\text{CaCO}_3$  compared to 360 mg/l as  $\text{CaCO}_3$ ) (Figure 3.6). The results are consistent with literature findings, which predict a higher uranium mobility in the presence of elevated alkalinity (at a given pH) due to the formation of poorly sorbing calcium-carbonate-uranyl ternary complexes (Davis et al., 2004; Fox et al., 2006; Hyun et al., 2009).

Table 3.4: Total organic carbon as percent of sediment dry weight and BET results as surface area for each column.

Column	% TOC	Surface Area (m <sup>2</sup> /g)
MU3 A	0.095	13.1
MU3 B	0.053	9.44
MU3 C	0.011	4.74
MU10	0.035	4.26

Table 3.5. X-ray fluorescence (XRF) elemental data for core samples collected near samples used in this study (considered reasonably representative of the study samples). Note that the XRF results for the M3-2 samples were provided by Colorado State University.

Element	Sample <sup>a</sup>							
	P 967	P 967.5	P 968	P 968.5	P 969	M 629	M 634	M 638
Na <sub>2</sub> O %	1.95	1.15	1.99	0.33	1.57	NR	NR	NR
MgO %	0.20	0.56	0.17	1.14	0.30	NR	NR	NR
Al <sub>2</sub> O <sub>3</sub> %	9.86	10.47	10.45	13.21	9.81	NR	NR	NR
SiO <sub>2</sub> %	81.38	78.90	80.72	71.84	81.41	92.5	92.8	94.8
P <sub>2</sub> O <sub>5</sub> %	0.048	0.053	0.041	0.047	0.023	NR	NR	NR
K <sub>2</sub> O %	3.98	3.12	4.50	2.26	3.50	NR	NR	NR
CaO %	0.48	0.50	0.37	0.69	0.43	0.89	1.14	1.33
TiO <sub>2</sub> %	0.09	0.23	0.06	0.59	0.13	0.588	0.541	0.157
MnO %	0.008	0.009	0.007	0.014	0.001	0.027	0.022	0.015
Fe <sub>2</sub> O <sub>3</sub> %	0.596	1.515	0.537	3.44	0.888	5.46	4.91	3.32
V ppm	18	52	12	91	23	59	59	59
U ppm	617.4	184.9	7.6	10.2	<5.4	109	268	399
Mo ppm	NR	NR	NR	NR	NR	128	136	44
LOI <sup>b</sup> %	1.3	3.39	1.04	6.32	1.83	NR	NR	NR
Total %	100.09	100.06	100.03	100.06	100.01	NR	NR	NR

<sup>a</sup> P – indicates 10P-206 and M indicates M3-2; numbers are depths in ft. below ground surface

<sup>b</sup> LOI = Loss on Ignition

Table 3.6. X-ray diffraction (XRD) mineralogy data for core samples collected near samples used in this study (considered reasonably representative of the study samples). Note that the XRD results for the M3-2 samples were provided by Colorado State University.

Borehole	P-206	P-206	P-206	P-206	P-206	M3-2	M3-2	M3-2
Depth (ft.)	967	967.5	968	968.5	969	629	634	638
quartz	68.8	55.7	44.0	52.7	52.4	91.1	73.1	54.4
albite	7.2	13.3	30.5	4.3	16.7	2.5	14.4	15.2
K-feldspar	13.8	18.1	16.4	12.5	21.0	6.2	8.8	23.6
muscovite	3.2	4.7	3.7	7.0	2.9	NR	NR	NR
kaolinite	2.1	5.1	3.3	8.1	3.7	b.d.	0.9	0.6
calcite	b.d.	0.7	1.1	0.7	0.9	0.2	2.7	6.2
smectite	4.8	1.6	0.7	14.4	2.3	b.d.	b.d.	b.d.
pyrite	b.d.	0.7	+	+	b.d.	NR	NR	NR
coffinite	b.d.	b.d.	b.d.	b.d.	b.d.	NR	NR	NR
<b>Total</b>	<b>100</b>	<b>100</b>	<b>100</b>	<b>100</b>	<b>100</b>	<b>100</b>	<b>99.9</b>	<b>100</b>

Table 3.7: R values and sum-of-weighted-square residuals (SORS) for each system of surface sites in each column. All models in figures 3.2 – 3.6 use a system with 2 surface sites (results used in the models are highlighted in bold).

Column	1 surface site		2 surface sites		3 surface sites	
	R	SWSR	R	SWSR	R	SWSR
MU3 A	0.904	2.150	<b>0.926</b>	1.290	0.924	1.170
MU3 B	0.968	1.080	<b>0.989</b>	0.267	0.996	0.134
MU3 C	0.978	0.435	<b>0.983</b>	0.234	0.996	0.070
MU10 B	0.865	3.020	<b>0.990</b>	0.302	0.982	0.632

Table 3.8. Calculated uranium fractional recoveries in the column experiments.

Experiment	U(VI) Recovery
MU3 A	0.87
MU3 B	0.90
MU3 C	0.98
MU10 A	0.98
MU10 B	0.93*

\* Uranium was still eluting from this column when experiment was terminated, so recovery is not considered representative.

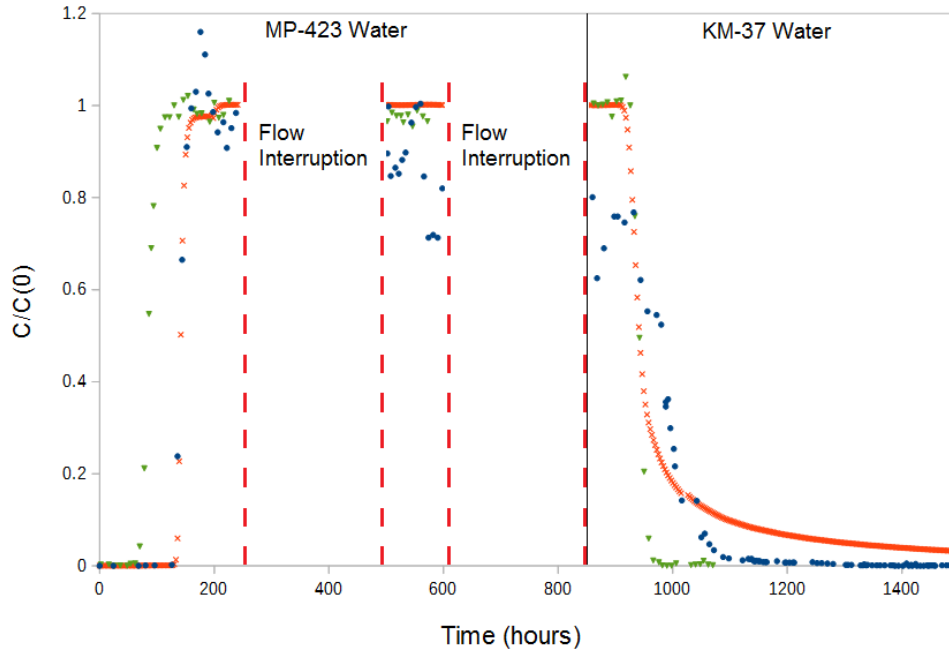


Figure 3.2. Measured (●, blue) and modeled (x, red) uranium concentrations together with the experimental tritium tracer (▼, green) breakthrough for column MU3 A at 540 mg/L alkalinity. The solid line indicates a switch from post-mining water to background water chemistry while dashed lines delineate periods of flow interruptions. The model uses a 2-pK surface system.

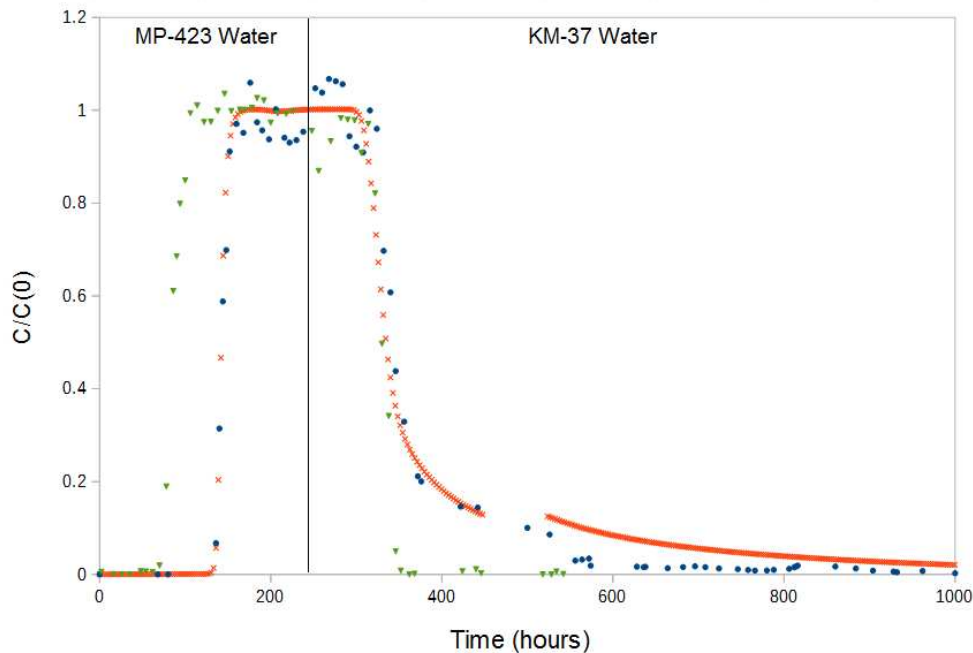


Figure 3.3. Measured (●, blue) and modeled (x, red) uranium concentrations together with the experimental tritium tracer (▼, green) breakthrough for column MU3 B at 540 mg/L alkalinity. The solid line indicates a switch from post-mining water to background water chemistry.

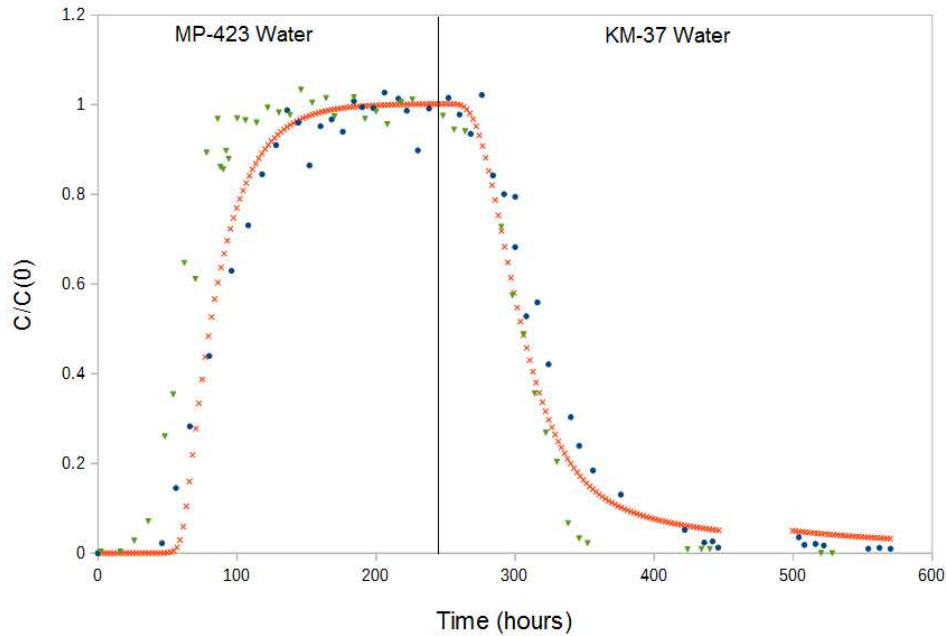


Figure 3.4. Measured (●, blue) and modeled (x, red) uranium concentrations together with the experimental tritium tracer (▼, green) breakthrough for column MU3 C at 540 mg/L alkalinity. The solid line indicates a switch from post-mining water to background water chemistry.

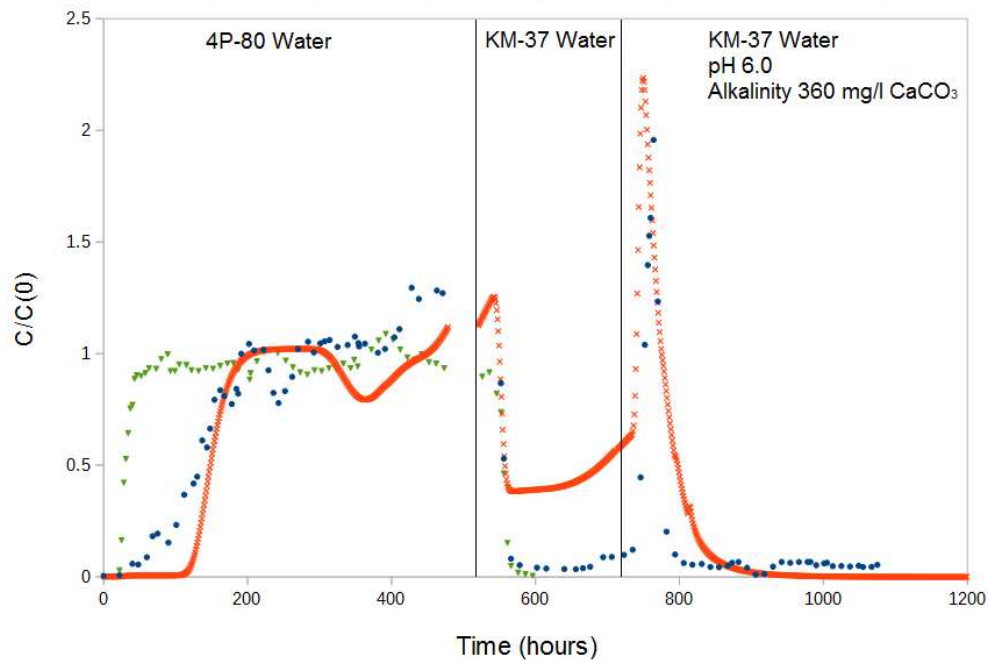


Figure 3.5. Measured (●, blue) and modeled (x, red) uranium concentrations together with the experimental tritium tracer (▼, green) breakthrough for column MU10 A at 360 mg/L alkalinity. The first solid line indicates a switch from post-mining water to background water chemistry at its natural alkalinity and pH while the second line represents a switch to background water at a higher alkalinity and lower pH.

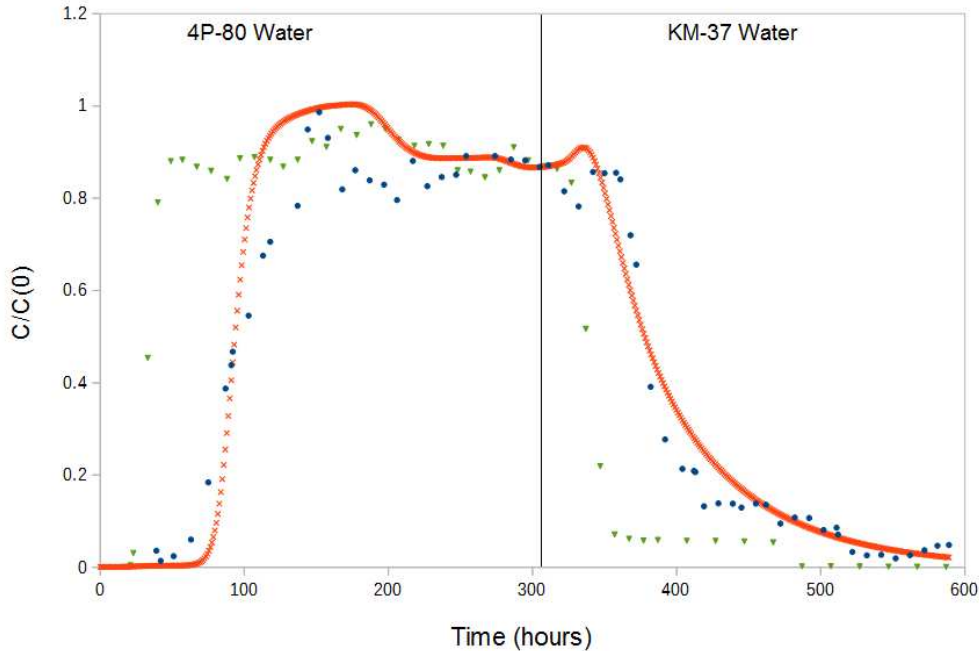


Figure 3.6. Measured (●, blue) and modeled (x, red) uranium concentrations together with the experimental tritium tracer (▼, green) breakthrough for column MU10 B at 540 mg/L alkalinity. The solid line indicates a switch from post-mining water to background water chemistry.

These findings explain why bicarbonate is favored as an additive for uranium in situ recovery mining. Flushing MU10 A with 360 mg/L  $\text{CaCO}_3$  after the initial flushing of the column with low alkalinity (160 mg/L) background water (KM-37) resulted in a late spike in uranium concentrations due to uranium desorption induced by the higher alkalinity solution (Fig. 3.5).

### 3.3.3 Column modeling

Reactive transport models were able to accurately model the initial breakthrough of uranium in all 5 column experiments. Figures 3.2 - 3.6 depict experimental measurements together with the results for the 2 surface site models (2-pK) while Table 3.9 provides PEST results for the binding sites of the strong (>SOH) and super-strong sites (>SSOH) for the 2-pK models of the 4 columns. In general, all fitting models produced R values above 0.85 and SWSR

values below 2 (Table 3.7). Improvements over a single, super-strong surface site model using only >SSOH sites (1-pK) was consistently obtained by including a second strongly binding surface >SOH and >SSOH. Adding a third surface site (3-pK) with weak formation constants (>WOH) gave modest improvements for MU3 B and MU3 C, while fits for MU3 A and MU10 B showed no significant differences between the 2-pK and 3-pK systems. The model for MU3 A provided a good match to the early breakthrough behavior; however once flow interruptions were introduced, actual uranium concentrations were consistently 60-90% below the predicted values.

Table 3.9: Number of >SOH and >SSOH binding sites for columns MU3 A-C and MU10 B derived from PEST, using the 2-pK surface complexation model.

<b>Column</b>	<b>&gt;SOH (<math>\mu\text{mol/kg-soil}</math>)</b>	<b>&gt;SSOH (<math>\mu\text{mol/kg-soil}</math>)</b>
MU3 A	70.2	$5.91 \times 10^{-3}$
MU3 B	73.7	$40.0 \times 10^{-3}$
MU3 C	17.4	$4.43 \times 10^{-3}$
MU10	97.6	16.3

Sorption parameters estimated in the MU10 B column were applied to model MU10 A, since both experiments were completed using the same sediment material. The parameters from MU10 B were able to accurately predict the initial uranium breakthrough for MU10 A experiment (R of 0.974) despite the difference in alkalinity between those two systems (Figures 3.5 – 3.6). However, during the second phase of the experiment for MU10 A when KM-37 water with low alkalinity (160 mg/l as CaCO<sub>3</sub>) and pH 7 was introduced, the model overestimated uranium concentrations by 10-20 times the measured values. The last stage of the experiment (starting at 715 hours with the introduction of KM-37 water at 360 mg/l CaCO<sub>3</sub>) required the

addition of 1% initial calcite in the model to produce the second uranium peak occurring at 750 hours (Figure 3.5). This effect has been previously observed (Dong et al. 2005, Johnson and Tutu 2013), when influent water with a lower pH solubilizes  $\text{CaCO}_3$  and increases the alkalinity in the system, subsequently remobilizing sorbed uranium. The addition of calcite also affected the variability of uranium concentrations during elution for MU10 B (Fig. 3.6) while the removal of calcite from the system steadied uranium concentrations after the initial breakthrough. The addition or removal of calcite phases had no visible effect on the MU3 columns.

### **3.4 Discussion**

#### **3.4.1 Effect of sediment heterogeneity on uranium breakthrough**

All three columns in the MU3 experiments (Figs. 3.2 – 3.4) showed a delayed uranium breakthrough compared to their corresponding tracers. MU3 A and MU3 B gave a retardation factor of 1.68 and 1.69 respectively. Visual inspections of the material for MU3 A and B suggests that sediments interactions with uranium were similar for both columns. This was confirmed through both BET and TOC analyses (Table 3.4), which showed values that were within 33% and 50% of each other. The total number of binding sites for MU3 A and B were calculated at  $25.1 \mu\text{mol/g-sediment}$  and  $18.1 \mu\text{mol/g-sediment}$ . The sediment with coarser and more oxidized core material from MU3 C exhibited the least amount of uranium retardation (Fig. 3.4). BET results (Table 3.4) as well as visual inspections indicated that the specific surface area of the MU3 C sediments was significantly less than that for the other two MU3 samples (Fig. 3.7 – 3.9) and site densities were estimated at  $9.1 \mu\text{mol/g-sediment}$ . Sediment characteristics from MU3 coincided well with the expected retardation of uranium across the three experiments with higher sediment surface area and TOC values leading to increased uranium retardation.

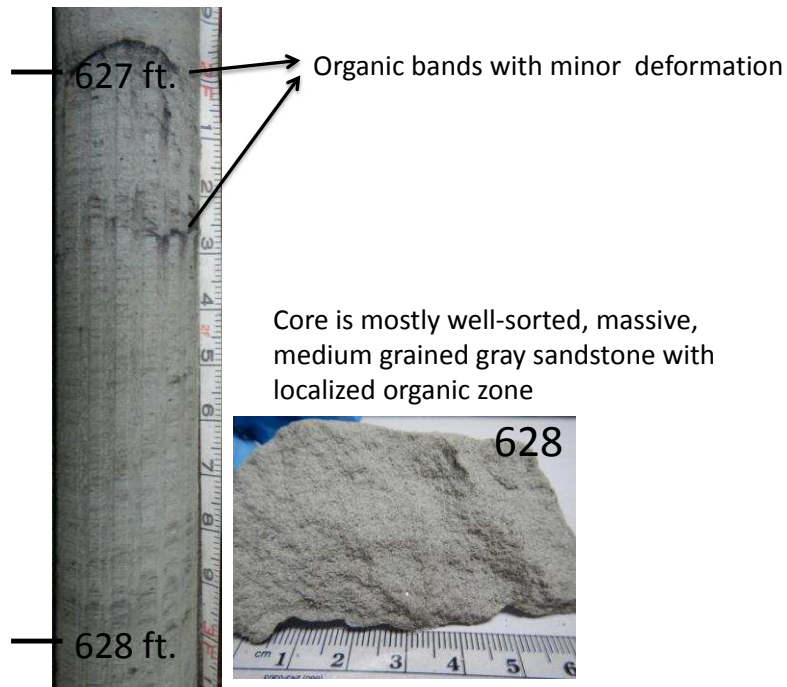


Figure 3.7: Photos of core material from 191.2-191.5 m below ground surface in borehole M3-2.



Figure 3.8: Photos of core material from 191.5 – 192.1 m below ground surface in borehole M3-2. Note that the interval used in column studies was 191.8 – 192.1 m, shown in the two plastic bags.

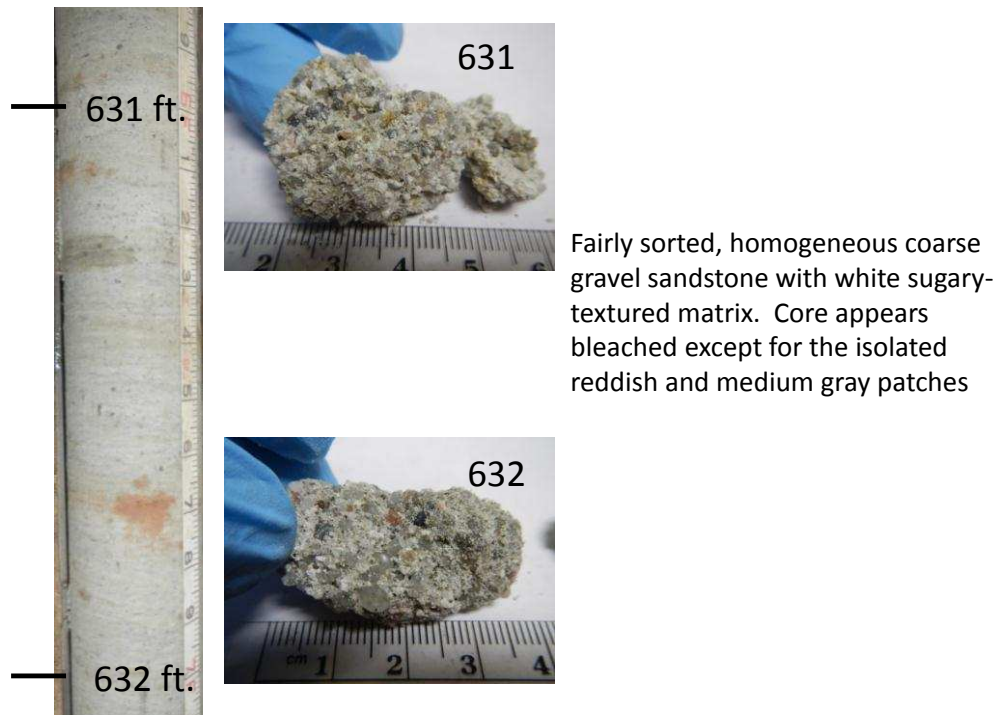


Figure 3.9: Photos of core material from 192.4 – 192.7 m below ground surface in borehole M3-2.

The modeling results generally resulted in robust simulations for all MU3 systems through the use of the 2-pK general complexation model (Davis et al. 2004, Davis et al. 2009). Correlation coefficients for the 2 pK models of all three MU3 experiments all exceeded 0.9 while SWSR values were below 2.0 (Table 3.7). Fitting site densities to a 2 pK GC model with fixed sorption coefficients provided a good correlation between PEST results and the site density estimates from the BET analysis. PEST results for the number of >SOH sites for the 2-pK models were 0.28%, 0.40% and 0.19% of the total number of binding sites derived from BET analyses, for columns MU3 A, B, and C respectively. Only a small amount of >>SSOH sites were required to fit the data accurately for the MU3 columns ( $2.35 \times 10^{-5}$  %,  $2.21 \times 10^{-4}$  %, and  $4.87 \times 10^{-5}$  % for MU3 A,B, and C).

The GC SCM approach generally assumes only a fraction of sorption sites participate in uranyl binding composing 0.1% and 0.01% of the total number of sorption sites for >SOH

and >SSOH respectively (Davis et al. 2004). The assumption behind the small number of participating sorption sites is based on the observation that uranium forms strong complexes with aluminol and ferrinol sites of mineral grains (Bargar et al. 2000) which represent only a fraction of all negatively charged sorption sites available on mineral surfaces (Davis et al. 2004). Another sorption study by Johnson and Tut (2016), however, observed site densities of 370  $\mu\text{mol/kg}$ -sediment in sediments taken from the Dewey Burdock ISR site (near Edgemont, SD) which would compare to ~1% of the available site densities, if a similar surface area of ~10  $\text{m}^2/\text{g}$ -sediment is used. Overall our modeling results indicate that BET analyses could provide a rough estimate of the range of >SOH sites applicable for GC SCM models (Table 3.9) when sediments are composed of a fairly homogenous mineralogy. Figures 3.2 – 3.6 show only fits for the 2-pK models, since the 3-pK simulations improved R values only marginally for two columns (MU3 B and MU3 C), while showing no difference in the other two (MU3 A and MU10 B).

The MU10 B column experiment (Fig. 3.6), which was run at the same alkalinity as the MU3 experiments at 540  $\text{mg/l}$   $\text{CaCO}_3$ , did not exhibit similar behavior as the MU3 columns. There was higher uranium retention (a threefold uranium delay over tracers) than the MU 3 sediments despite a lower TOC (0.035 %) and surface area (4.26  $\text{m}^2/\text{g}$ ). Further, the breakthrough curve for uranium exhibited significant spreading that was not apparent for the iodide tracer. Attempts to simulate MU10 B with either 1, 2, or 3 pK GC models resulted in poor correlations when the number of >SOH sites were constrained to less than 0.2% of the total number of binding sites derived from BET results. To produce a good model fit ( $R = 0.990$ ) PEST required the number of >SOH sites to be 1.19% of the BET derived values, while the number of required >SSOH sites in MU10 exceeded those in the MU3 by 3 to 4 orders of magnitude (Table 3.9), and composed 0.20% of the BET derived values.

The MU10 column differed from the MU3 sediments in several regards that could explain the discrepancy in sorption behavior between the two systems. XRD results (Table 3.6) from boreholes similar to the MU10 well, revealed a notable presence of smectite (4% - 14% across several depths) and kaolinite (2% - 8%) clays. sediment samples from the MU3 borehole were predominantly (95% or more) composed of albite, K-feldspar, and quartz while clay content was generally below 1%. The higher clay content in the MU10 substitutes was corroborated by XRF analyses (Table 3.5) showing about 10% aluminum oxides, which were absent in the MU3 samples. While clays composed only ~10% of the MU10 sediments, the specific surface area for systems composed of kaolinite and/or smectite have shown to vary greatly. Specific surface area for kaolinite was measured at 16.2 m<sup>2</sup>/g – 20.6 m<sup>2</sup>/g (Dong 2012) while the surface area of smectites has been reported to range from 56.7 m<sup>2</sup>/g (Koirichi et al. 2009) up to 335 m<sup>2</sup>/g (Yuang et al. 2005). In addition, BET analyses have been shown to consistently underestimate surface area measurements by a factor of 3.7 to 6.4 in sediments containing mixtures of kaolinite and montmorillonite when compared to results from the methylene blue spot test or the soil water characteristic curve method (Maček et al. 2013). Together with metal oxides, clays would represent the majority of the available surface area of the MU10 sediments compared to the MU3 sediments where quartz and ferric oxides dominated the mineralogy. As a consequence, the surface area for MU10 may be higher than estimated by our BET results.

Prior efforts to model uranyl sorption to kaolinite clays has been shown to depend on the presence of three types of binding sites: silanol, aluminol, and titanol impurities (Payne et al. 2004, Bachmaf et al. 2011). Of the three different sites titanol has shown the greatest affinity towards uranium sorption with pK values of 9.57 – 10 (Bachmaf et al. 2011). Aluminol sites bind uranium less effectively with pK values reported between 4.17 (Payne et al. 2004) and 6.0

(Bachmaf et al 2011), depending on the reaction used to describe sorption. Uranium adsorption to the aluminol and titanol sites in clays is generally assumed to occur through the formation of inner-sphere ternary uranyl-carbonate-surface complexes (Korichi 2009, Payne 2004). This mechanism increases in importance at the near-neutral pH range of the experiments (Payne 2004, Korichi 2009). Previous parameter estimation attempts observed better fits after carbonate species were included when modeling sorption to titanol sites (Bachmaf et al. 2011). Our own models assumed that uranyl primarily sorbs to negatively charged surfaces directly through a simple ion-exchange mechanism as proposed by Dzombak and Morel (1990) and Davis et al. (2004). These assumptions provided reasonable parameters for the simpler MU3 systems, but the fitting results for MU10 show that a more mechanistic approach may be needed to provide good model fits for systems composed of more heterogeneous sediments.

MU3 sediments and the MU10 surrogates also showed a difference in  $\text{Fe}_2\text{O}_3$  content. XRF results showed the presence of 3.3% - 5.5% ferric oxides in MU3 sediments, compared to 0.5% to 3.4% in the MU10 representative sediment. Since sediment cores from the MU10 surrogates were not preserved anaerobically it is possible reduced iron phases may have been oxidized into ferric oxyhydroxides during transport and storage. Amorphous ferrihydrites generally have a high surface area ( $600 \text{ m}^2/\text{g}$ ) (Dzombak and Morel 1990). In addition, uranyl di-carbonate species have shown a strong affinity to form inner sphere complexes on ferrihydrites with log K values reported at 15.3 (Mahoney et al. 2009). The mineralogy data suggest that sorption in the MU3 systems was dominated by a single mineral surface, most likely composed of iron oxides, while sorption in MU10 was influenced by multiple types of binding sites from clays and ferrihydrites. This could explain the increased sorption in the MU10 systems compared to MU3 despite the lower specific surface area of the MU10 sediment measured by BET analyses. An

increase in complexity of modeling uranium sorption to sediments consisting of a mix of iron-containing minerals and clays has also been observed by Korichi et al. (2009). Our results confirm the difficulty in using generalized surface complexation models with empirically derived parameters for heterogeneous sediments with a wide range of binding affinities and mechanisms.

### **3.4.2 effect of reductive processes on uranium breakthrough**

Column MU3 A and MU3 B exhibited fairly similar behavior for uranium breakthrough, which appeared at 150 hours after start up (Figure 3.2 and 3.3). After that time, flow interruptions were introduced into column MU3 A to allow for a qualitative assessment of possible kinetic influences on uranium attenuation. As illustrated in Figures 3.2 and 3.3, the flow interruptions had a significant impact on the effluent concentrations of uranium. The additional residence time in MU3 A resulted in a 10-30% reduction in uranium concentrations relative to the model predictions after the first flow interruption (Fig. 3.2). The second flow interruption at ~ 600 hours enhanced this effect, reducing uranium concentrations even further to between 20-40% of the modeled values. The MU3 B column, however, showed no significant reduction in uranium effluent concentrations as long as the ore-zone water was injected (Fig. 3.3). While the reduction of  $\text{UO}_2^{2+}$  to  $\text{U}^{4+}$  can occur at an Eh of 0.273 V under acidic conditions (Bratsch 1989), uranyl-carbonate and calcium-uranyl-carbonate species at environmentally relevant concentrations and conditions continue to dominate at an Eh range of -0.05 to -0.15 V (Ginder-Vogel et al. 2006) inhibiting the reduction of aqueous  $\text{UO}_2^{2+}$ . Field values for Eh (0.177 V) were therefore considered too high and uranium concentrations too low for reductive processes to occur and were excluded from the transport models.

Since our equilibrium model for MU3 A failed to predict the tailing effect caused by the

flow interruptions, it could suggest that there may be rate-limited processes controlling the breakthrough characteristics observed. Diffusion of contaminant into immobile pore space has been shown to create a similar tailing effect in other experiments ( Brouyère 2006). However, we dismissed dual-porosity as an explanation for this behavior, since our tracer data did not exhibit similar behavior as the uranium concentrations, and prior studies indicated tritium to be more affected by interstitial pore space than heavier molecules (Black and Kipp 1983). Another potential kinetic mechanism could be the catalytic reduction of uranium at mineral surfaces and subsequent precipitation as uraninite, which has been shown to proceed at a slower rate than adsorption in abiotic systems (Liger et al. 1999). Reductive precipitation has been well studied for microbial systems *in-situ* and *in-vitro* (Anderson and Lovley 2002, Gorby and Lovley 1992, Lovley and Phillips 1992), however literature on abiotic uranium reduction is comparatively sparse. Abiotic U(VI) reduction by pyrite minerals was first demonstrated by Wersin et al. (1994). Liger et al. (1999) observed that sorbed uranium in hematite suspensions can be reduced within a matter of hours at neutral pH; the surfaces of hematite nanoparticles provided a catalyst for adsorbed uranium to react with ferrous iron according to pseudo-first order reaction kinetics. A different study investigated the effect of carbonate addition on the abiotic reduction of uranium by dissolved Fe(II) and found that even in systems with about 40 mM bicarbonate, colloidal hematite catalyzed the reduction of ~20% of the uranium in solution (Behrends and Van Cappellen 2005).

Our study suggest that the reduction occurred at a significantly lower rate than observed in batch experiments by others (Behrends and Van Cappellen 2005, Liger et al. 1999, Wersin et al. 1994), and only became predominant when flow was stopped entirely as observed for MU3 A. If it is assumed that the reaction occurs at a rate that is greater than the water residence time, but

less than the sum of the residence time and the flow interruption times, an upper bound of 0.0007 hr<sup>-1</sup> can be placed on the rate constant for this reduction mechanism assuming pseudo first-order kinetics (Liger et al., 1999). The possibility of abiotic uranium reduction at low flow conditions could result in underestimation of attenuation capacity when using models that do not account for such processes. Accurate incorporation of such processes into models will require more detailed studies.

### **3.4.3 Effect of alkalinity on uranium breakthrough**

Data from the MU10 columns provided several noteworthy observations. In MU10 B, where alkalinity was adjusted to a higher concentration (540 mg/L), the uranium breakthrough occurred earlier compared to MU10 A where influent was kept at its natural alkalinity (360 mg/L) (Figures 3.5 and 3.6). The 50% increase in alkalinity resulted in a ~35% faster breakthrough in the MU10 B column, compared to the iodide tracer which showed no difference in breakthrough characteristics. This result is consistent with the expectation that higher carbonate concentration at neutral pH reduces sorption capacity through the formation of highly stable aqueous calcium-carbonate-uranyl ternary complexes ( $\text{Ca}_2\text{UO}_2(\text{CO}_3)_3^{2-}$  and  $2\text{Ca}_2\text{UO}_2(\text{CO}_3)_{3(\text{aq})}$ ) (Bernhard et al. 2001, Dong and Brooks 2006, Kalmykov and Choppin 2000, Kelly et al. 2007). The ternary uranium species (Table 3.3) were generally assumed to adsorb poorly to the negatively charged surfaces of ferric hydroxides or clays due to their neutral and negative charge. Subsequent studies investigated and confirmed the inhibition of uranyl sorption in the presence of calcium and high alkalinity (Davis et al. 2004, Nair and Merkel, 2011a, 2011b, Stewart et al. 2010). Fox et al. (2007) reported that uranium sorption to quartz in the presence of 8.9 mM Ca decreased from 66% to 10% while only 1.8 mM of Ca<sup>2+</sup> were sufficient to reduce sorption to ferrihydrites

by one third. Increasing pH causes uranyl carbonate species to desorb more readily. Stewart et al. (2010) observed that a pH of 8.5 would keep 97% of uranium in solution in the presence of goethite compared to only 6.4 % at a pH of 6.5. The results from the current study confirm that alkalinity and pH are controlling factors of uranium mobility during groundwater transport, and that uranyl ternary species need to be incorporated into transport models of column studies and field sites.

The MU10 A and MU10 B experiments used the same sediment material. Therefore, sorption parameters for MU10 A (Fig. 5) were not fitted with PEST. Instead PEST results for the site densities of MU10 B (Fig. 3.6) were applied to the MU10 A model (Fig. 3.5), to test whether sorption parameter would accurately predict uranium behavior for differing alkalinities (360 mg/l versus 540 mg/l). The sorption parameters from MU10 B, were able to predict the initial breakthrough curve for MU10 A even though it was run at a lower alkalinity (Figs. 3.5 and 3.6). This would indicate that experimentally derived parameters for GC SCM models could be employed to predict uranium transport over a wide range of geochemical conditions. Batch experiments have confirmed the applicability of common sorption parameters to experiments with varying calcium concentrations (Fox et al. 2006) as long as the thermodynamic data for calcium-carbonate-uranyl ternary complexes were included.

It should be noted that the MU10 models over-predicted desorption during 500-750 hours (Figure 3.5) while under-predicting desorption during the second flushing event, unless the model allowed calcite to dissolve and precipitate. The carbonate concentrations were fourfold higher during the first flush at pH 7 and alkalinity 160 mg/l compared to the higher alkalinity flush at pH 6 and 360 mg/l alkalinity. These results suggest that uranium desorption may be more dependent on total alkalinity than the concentration of carbonate ions. It is possible that the

failure to predict the observed uranium desorption between 500-750 hours, was simply because the model did not incorporate strongly sorbing titanol or ferrihydrite sites. Previous studies, however, have shown that the formation of uranyl-surface complexes can be dependent upon pH. Monodentate uranyl sorption to exchange sites on clays become predominant at  $\text{pH} < 5$  (Koirichi 2009) while uranyl at near neutral pH prefers ternary carbonate-uranyl-surface site species (Payne 2004, Koirichi 2009, Dong 2012). A pH change from 6 to 7 during the first background flush between 500-750 hours could have shifted sorption dynamics from lower affinity exchange sites to strongly binding uranyl-carbonate surface complexes. Future modeling attempts may have to incorporate uranyl-carbonate-surface species if pH changes in influent water chemistries are suspected to occur during uranium transport.

#### **3.4.4 Effect of calcite on uranium sorption**

The MU10 A experiment provided further noteworthy observations. After the initial uranium slug eluted from the column and water was switched to the background KM-37 water, a second background flush was introduced at 715 hours with an alkalinity of 360 mg/l and a pH of 6 (Table 3.2). This second flush produced a spike of uranium in the effluent that was almost twice the injected concentrations (Fig. 3.5). Models failed to show this latter spike entirely, unless approximately 1% weight calcite was introduced as an initial mineral phase. XRD results showed actual calcite concentration in the MU10 surrogates between 0 and 1.1% weight (Table 3.6). Influent water during the first KM-37 flush was oversaturated with respect to calcite and PHREEQC results showed calcite precipitation between 521 and 715 hours. The second flush after 715 hours at pH 6, on the other hand was undersaturated with respect to calcite and model results predicted an alkalinity in excess of 800 mg/l once carbonate equilibrium had been

achieved between calcite and the influent water chemistry. Previous modeling attempts to simulate ISR-uranium transport reported similar effects even at fairly low calcite concentrations (0.15 weight %) (Johnson and Tutu 2013). It was assumed that lower pH with increased bicarbonate concentrations dissolved calcite and subsequently increased the pH, calcium, and carbonate concentrations. A batch study of uranium sorption in calcite and calcite free systems also indicated that the presence of calcite may increase aqueous uranium concentrations at neutral or higher pH (Dong et al. 2005). Calcite generally had no effect on the initial uranium breakthrough and none of the MU3 models were affected by the presence or absence of any calcite phases, since the restoration waters were generally slightly oversaturated with respect to calcite.

It should be noted that the alkalinity, calcium, and pH in the MU10 experiments were not as carefully controlled as those for the MU3 experiments, since the influent water was drawn from a 2 liter reservoir. Equilibration of the influent water in the reservoir could have changed influent chemistries and may explain difficulties in producing good model fits for the MU10 experiments. The model also understated uranium sorption during the first flush between 521 and 715 hours by about 90%. While this mismatch could be explained by inaccurate alkalinity and pH measurements, uranium has been shown to co-precipitate with calcite as well (Curti 1999, Kitano et al. 1971, Reeder et al. 2001). If uranium precipitated together with calcite during the first KM-37 flush, and dissolved again during the second KM-37 flush that was undersaturated with respect to calcite, it could also explain the differences observed between the model and experimental results, since co-precipitation would be a kinetic effect not modeled by our simulations. The results show that uranium retardation is not only dependent upon pH and alkalinity, but calcium concentrations and calcite saturation as well.

### 3.5 Conclusions

This study attempted to model the retardation of uranium transport due to adsorption in 5 column experiments using sediments taken from the Smith Ranch-Highland *in-situ* recovery field site in Wyoming. A strong correlation between BET results and uranium adsorption behavior was observed in three column experiments using sediments from with high (3-5%) content of Fe<sub>2</sub>O<sub>3</sub> phases and low clay content (<1%). GC SCM using 2 surface sites were able to accurately predict uranium breakthrough when the number of binding sites was fitted using PHREEQC with parameter estimation automated by PEST. The number of >SOH binding sites estimated by PEST were generally between 0.1% and 0.5% of the number of binding sites derived from BET measurements. This indicates that, surface complexation modeling using empirically derived parameters constrained by BET surface area, can explain transport behavior when uranium sorption is dominated by a single mineral. Experimentally derived parameters for SCM could potentially be applied to field conditions when the site has a fairly homogeneous mineral composition. The presence of kaolinite and smectite clay complicated parameter estimation in another column experiment. In this case, a generic surface complexation model consistently underestimated retardation when modeling parameters were constrained by BET results. More mechanistic models may be needed in systems with high clay content and heterogeneous mineral composition.

While this study only addresses uranium retardation via sorption, one experiment (MU3 A) suggested potential reductive processes acting on uranium when flow interruptions were introduced, even though Eh values were prohibitive to uranium reduction. Naturally occurring uranium reduction in our column experiments, suggests that long-term reductive attenuation processes at the SRH site may be active as well. The potential of abiotic uranium reduction in

environments with slow groundwater velocities would need further investigations in long-term studies.

Another set of column experiments showed that a 50% increase in alkalinity can decrease uranium retardation by 35% in the same column. The same model parameters were able to predict uranium breakthrough in both experiments in this column, suggesting that experimentally derived sorption constants from systems of different alkalinities and aqueous geochemistries can be used to model ISR sites provided that surface area, mineralogy, iron content and organic carbon content of the solids are similar. However, the same set of experiment also showed that uranium transport was dependent on calcite saturation and indicated that calcite dissolution may have a detrimental effect on uranium retardation. Our experiments highlight a need for further research regarding the effects of calcite equilibrium on uranium transport and demonstrate that uranium transport predictions are likely highly site-specific due to their dependency on mineralogy and geochemistry.

This research highlights the importance of transport models for sustainable groundwater restoration processes at uranium ISR facilities. By providing insight as to what parameters are of greatest importance for minimizing the mobility of uranium and other species, restoration processes can be tailored using models to the geochemistry of a specific site. As an example, the role of calcium in mobilizing uranium has been clearly identified as an important issue in this study. Furthermore, the removal of carbon dioxide added during mining is also likely to be important since that would raise the pH of the restoration zone and allow more rapid desorption of uranium species before water treatment ends. Thus, the model results have highlighted the importance of these two parameters in the restoration zone studied at the Smith Ranch mine. At other mine sites, other parameters may be more important. The methods outlined in this paper

offer a road map as to how data can be obtained to construct robust, reliable models for many of the geochemical environments likely to be encountered in uranium ISR mining.

## CHAPTER 4

### UNCERTAINTY AND VARIABILITY IN LABORATORY DERIVED SORPTION PARAMETERS FROM A URANIUM IN-SITU RECOVERY SITE

Submitted to Journal of Contaminant Hydrology July 2017<sup>1</sup>

Martin A. Dangelmayr<sup>2</sup>, Paul W. Reimus<sup>3</sup>, Raymond H. Johnson<sup>4</sup>, James T. Clay<sup>5</sup>, James J.  
Stone<sup>6</sup>

<sup>1</sup> Reprinted with Permission from:

Martin A. Dangelmayr<sup>2</sup>, Paul W. Reimus<sup>3</sup>, Raymond H. Johnson<sup>4</sup>, James T. Clay<sup>5</sup>, James J.  
Stone<sup>6</sup>

<sup>2</sup> Department of Civil and Environmental Engineering, Colorado School of Mines, 1500 Illinois  
St, Golden, CO 80401, USA

<sup>3</sup> Los Alamos National Laboratory, Bikini Atoll Rd., SM 30 Los Alamos, NM 87545, USA

<sup>4</sup> Navarro Research and Engineering, Inc., 2597 Legacy Way, Grand Junction, CO 81503, USA

<sup>5</sup> Power Resources Inc., Smith Ranch-Highland Operation, 762 Ross Road, Douglas, WY 82633,  
USA

<sup>6</sup> Department of Civil and Environmental Engineering, South Dakota School of Mines and  
Technology, 501 East Saint Joseph St., Rapid City, SD 57701, USA

#### **4.1. Introduction**

In-situ recovery (ISR) of uranium is a non-intrusive method to extract uranium from the subsurface, and accounts for most of uranium produced worldwide (Mudd 2014). ISR alters the geochemistry of the ore zone significantly during operation and mobilizes contaminants such as arsenic, radon, and uranium (Hall 2009). While industry restoration practices manage to significantly reduce contaminant concentrations, they rarely bring groundwater chemistry back to pre-mining conditions (Borch et al. 2012, Hall 2009). Consequently, industry may be faced with applying for alternate concentration limits (ACLs) for contaminants of concern by assessing

the risk of residual contaminants to human health and environment (Borch, et al. 2012, Hall 2009). Risk assessments normally employ reactive fate and transport models to approximate uranium movement through the aquifer. A plethora of geochemical and hydrological processes can affect uranium transport. Sorption to mineral surfaces remains an important mechanism that can lead to a significant retardation of uranium in groundwater (Davis et al. 2004) and is an important focus of reactive-transport models (Davis et al. 2007). However, currently neither the U.S. Environmental Protection Agency (EPA) nor the Nuclear Regulatory Commission (NRC) provide any guidelines to assess and model aquifer's sorption capacity. The lack of accepted modeling assumptions and practices, such as which thermodynamic databases to include, what kind of sorption models to apply, and what methods to use to determine important parameters, can produce significant variability with computational errors and uncertainties for final model predictions. In addition, inherent variability in experimental designs and scale dependent uncertainty can introduce further errors when transferring bench-scale experiments to the field scale (Miller et al. 2011). These challenges pose liability issues for regulators, industry, and the public if or when models fail to predict observed plume behavior at a later time.

Research literature has demonstrated that the speciation of aqueous uranium is highly dependent on alkalinity and pH due to the preferred formation of stable ternary uranyl-carbonate complexes with calcium and magnesium (Bargar et al. 2000, Bernhard et al. 2001, Dong et al. 2006, Fox et al. 2006, Guillaumont and Mompean 2003). The effect of these species on sorption have been investigated by others (Nair et al. 2011(a), Nair et al. 2011(b) Stewart et al. (2010)) and indicate that uranyl-calcium-carbonate species can reduce total sorption by as much as 90% while increasing the reaction time by a factor of two (Nair et al. 2011(b)). Calcite and calcite saturation also have emerged as a component that affects uranium mobility (Dangelmayr et al.

2017, Dong et al 2005, Hyun et al. 2009). Influent waters under saturated with regards to calcite may cause mineral dissolution and increase pH, alkalinity, and calcium concentrations, thereby favoring aqueous uranium species over sorbed complexes. As a consequence, assessing the variability of alkalinity, carbonate systems, and pH, while concurrently addressing the presence of mineral calcite phases within field restoration sites, appear to be critical for accurate uranium predictive behavior, and thus should be accounted for during the derivation of modeling parameters. Moreover, a standardized thermodynamic database that accounts for these critical parameters that influence aqueous uranium speciation will be crucial for providing more robust risk assessments at former ISR sites.

A range of theoretical models of varying complexity and accuracy have been proposed to simulate metal sorption onto mineral surfaces. Generalized surface complexation models (GC SCM) have become favored by many researchers due to their semi-empirical nature and the relative ease with which they can be incorporated into transport calculations (Davis and Curtis 2003, Davis et al. 2004, Kohler et al. 1996, Zhang et al. 2009). GC SCM models rely on experimental data to estimate important sorption parameters such as sorption site density and equilibrium constants. This approach has the advantage of incorporating experimental verifications of the model from the beginning, compared to component additive surface complexation models (CA SCM) that rely on assumed sorption mechanisms based on the observed mineralogy of soil cores (Davis et al. 2004, Davis et al. 2009, Payne et al. 2006). However, experimentally derived sorption parameters are highly dependent on experimental designs and methods of parameterization (Miller et al. 2011, Payne et al. 2013), which can make them difficult to transfer between systems of different mineralogy or geochemistry and introduce experimental uncertainties.

This work attempts to determine variability in experimentally derived sorption parameters, and investigates the sensitivity of parameters to experimental conditions, by comparing the results of several column and batch studies completed on cores collected from the Smith-Ranch Highland (SRH) ISR facility near Douglas, Wyoming US. Our research focuses on three key aspects: 1) determining whether our conceptual model can accurately simulate uranium transport behavior due to changes in alkalinity and pH; 2) assessing the sensitivity of model outputs to changes in pH, alkalinity and derived sorption parameters; and 3) investigating the inherent variability that may exist between sorption parameters obtained in different experiments on the same soil materials. Data from column experiments conducted on soil cores taken from the Smith-Ranch Highland ISR facility were compared with two other studies (column and batch experiments) (Dangelmayr et al. 2017, Truax 2016) to address these questions.

## **4.2 Methods**

### **4.2.1 Sediment collection and characterization**

A full description of the Smith-Ranch Highland site and its geology can be found in Hunter (1999), while a map of the relevant core location are shown in Figure 4.1. Sediments were obtained from an observation well at the SRH ISR site located downgradient from Mine Unit 3 in the Fort Union formation. The location from which the core was taken, ensured that no mining activity had altered the sediments. The collection and preservation of relevant sediment samples for depths 192 and 193 m below ground are described elsewhere (Dangelmayr et al. 2017). Briefly, sediment cores were partitioned and sealed anaerobically (98% N<sub>2</sub> 2%H<sub>2</sub>) and preserved at -4° C during transport and storage. The core sections used came from a depth of 192.3 to 192.6 meters (referred to 192 herein) and 193.2 to 193.5 meters below ground (referred to as 193). Size

fractionation was carried out by sequentially sieving ~450 g of each section through a 2 mm, a 1 mm, and 0.6 mm mesh size sieve. X-Ray Diffraction (Rigaku's Ultimate-Plus, Scottsdale, AZ) and X-Ray Fluorescence (Bruker's Tracer IV, Billerica, MA) analyses were conducted on sediment depths to determine dominant mineralogy. The sediment samples were fractionated using a Humboldt riffle splitter and mixed and pulverized in a shaker mill using ball bearings, prior to X-ray analysis. Sediment characterization also included Brunauer-Emmet-Teller (BET) analysis using a Micrometrics Gemini III 2375 Surface Area Analyzer (Norcross, GA) to determine surface area as well as total organic carbon (TOC) and inorganic carbon analysis (IC) by coulometric titration with a UIC Inc. CO<sub>2</sub> coulometry module (Joliet, IL). A detailed description of results for of pertinent sediment characteristics for three core sections (depths 191 m, 192 m and 193 m below ground) are presented in Tables 4.1 and 4.2. All characterization was performed on the fine fractions (< 2 mm dia.) of the sediments.

Table 4.1. Sediment characterization by XRF, BET, and TOC analyses.

<b>Depth</b>	<b>BET</b>	<b>% TOC</b>	<b>Fe<sub>2</sub>O<sub>3</sub></b>	<b>SiO<sub>2</sub></b>	<b>CaO</b>	<b>TiO<sub>2</sub></b>
191	9.44	0.054	5.46	92.5	0.89	0.59
192	4.74	0.011	2.9	88.4	1.00	0.30
193	9.34	0.053	3.15	87.4	1.05	0.30

Table 4.2. Sediment mineralogy by XRD analysis.

<b>Depth</b>	<b>Quartz</b>	<b>Microcline</b>	<b>Albite</b>	<b>Illite/Muscovite</b>	<b>Montmorillonite</b>
191	91.1	6.2	2.5	NR	NR
192	71.3	17.4	7.9	1.7	5.7
193	74.2	14.5	8.6	2.7	NR

#### 4.2.2 Column preparation

Four columns were run simultaneously using two different sediments and two different influent chemistries. Two columns were filled with material from a depth of 192 m, while the other two columns were filled with sediment from depth 193 m. Previous sorption experiments reported in Truax (2016) and Dangelmayr et al. (2017) and conducted at Los Alamos National Laboratory (LANL) and South Dakota School of Mines and Technology (SDSM&T), were used as a comparison to our experiments. Data from those studies were further analyzed in this project to determine whether sorption parameters can be transferred between experiments with variable geochemical conditions. Prior to column filling sediment sections were homogenized by mixing and stirring with a spatula to break up pieces. Sediments were then wet-packed with synthesized background water according to methods adopted from Lewis and Sjöstrom (2010) compacting the slurry at one cm intervals during filling. Based on dry weight measurements and column volumes, porosities for the four columns were between 0.24 and 0.29 assuming an average solids bulk density of 2.65 g/cm<sup>3</sup>. Influent solutions were delivered to the columns by four programmable NE-1000 Single Syringe Pumps (New Era Pump Systems, Farmingdale, NY) at a rate of 1 ml per hour. Syringes were filled every 46-49 hours with new influent solutions prepared on the same day. Prior to the actual experiments, sediment columns were flushed with synthesized background water (shown in Table 4.3) with an alkalinity adjusted to 360 mg/l CaCO<sub>3</sub> over the course of 25 days, to elute any remaining uranium from the sediments and equilibrate the sediment with the influent solutions. The columns, pumps, and fraction collector were kept in a glovebox at 2% H<sub>2</sub> 98% N<sub>2</sub> atmosphere to maintain anoxic conditions in the columns and influent.

### 4.2.3 Column operation and water analysis

Columns were fed a solution of synthesized restoration water at a rate of 1 ml/h for 143 hours after which influent was switched to simulated background water. Water chemistries for both influent solutions are presented in Table 4.3. The column tracer consisted of 640 mg/l bromide added to the restoration water as  $\text{CaBr}_2$ . The two columns at replicate depths were run at different alkalinities to determine the replicability of column tests between different geochemical conditions and investigate the effect alkalinity has on uranium breakthrough. One set of columns received restoration water at an alkalinity of 320-380 mg/l  $\text{CaCO}_3$  with an average of 360 mg/l  $\text{CaCO}_3$ . The other set of columns was fed restoration water with an alkalinity of 160-180 mg/l  $\text{CaCO}_3$  that is the typical range for post-treatment water at the Smith-Ranch Highland site. The high and low alkalinity solutions are referred to as HAW and LAW from here on.

Table 4.3. Chemical constituents of synthetic restoration and background groundwater. All concentrations are shown in mg/l unless shown otherwise.

<b>Constituent</b>	<b>Restoration</b>	<b>Background</b>
$\text{Ca}^{2+}$	400	120
$\text{Mg}^{2+}$	96	24
$\text{Na}^+$	2	69
$\text{Cl}^-$	144	71
$\text{SO}_4^{2-}$	768	288
$\text{UO}_2^{2+}$	19	0
Alkalinity (as mg/l $\text{CaCO}_3$ )	320-380	140-200
pH	6.3-6.8	7.3-7.8

The alkalinity of the influent waters was prepared by sparging 250 mL of synthetic groundwater with a mixture of 100%  $\text{N}_2$  and 80%  $\text{N}_2$ / 20%  $\text{CO}_2$  gases in a sealed container for 6 or more hours. Flow rates of  $\text{CO}_2$  and  $\text{N}_2$  into the container were controlled by rotameters to

achieve an approximate headspace  $p\text{CO}_2$  of 10% and 5% for the HAW and LAW waters respectively. The feed solution was measured at 30 minute intervals for alkalinity (Hach method 8203) and pH, and was adjusted with 106 a mg/l  $\text{Na}_2\text{CO}_3$  solution (prepared anew each day) to produce the desired water chemistry. Two hundred microliters of 0.5 M MES buffer were added to the restoration water after the sparging period to stabilize the pH at approximately 6.5 and to maintain over-saturation with respect to calcite. After the feed solutions were prepared, 48 mL of solution was transferred to 60 mL syringes and loaded onto the syringe pumps. All columns received the same background water (Table 4.3) after 143 hours of operation. Background waters were prepared in the same fashion as restoration water with a target pH of 7.2 - 7.8 and an alkalinity that ranged from 140-200 mg/l  $\text{CaCO}_3$ . MES buffer was not added to the background water since the feed solutions were already oversaturated with regard to calcite (Calcite S.I. of 0.49 – 0.88). A summary graph for the pH and alkalinity of the influent waters over the duration of the experiments is shown in Figure 4.1. Effluent samples were collected with a Teledyne ISCO, Foxy 200 Fraction Collector (Lincoln, NE) over 12 hour intervals and tested for pH, bromide, and alkalinity immediately upon collection. Bromide was measured with a Cole-Parmer combination ion-selective electrode (Vernon Hill, IL) while alkalinity was determined via the Hach method 8023. Cations were analyzed for iron, calcium, uranium and magnesium by ICP-MS Agilent 7800 (Santa Clara, CA) to assess recoveries for uranium and calcium.

#### **4.2.4 Modeling and parameter fitting**

A transport model was developed in PHREEQC to simulate uranium transport through the column. Details on transport modeling used by PHREEQC can be found in Parkhurst and Appelo (2013), while the modeling process is described as well in Dangelmayr et al. (2017) and

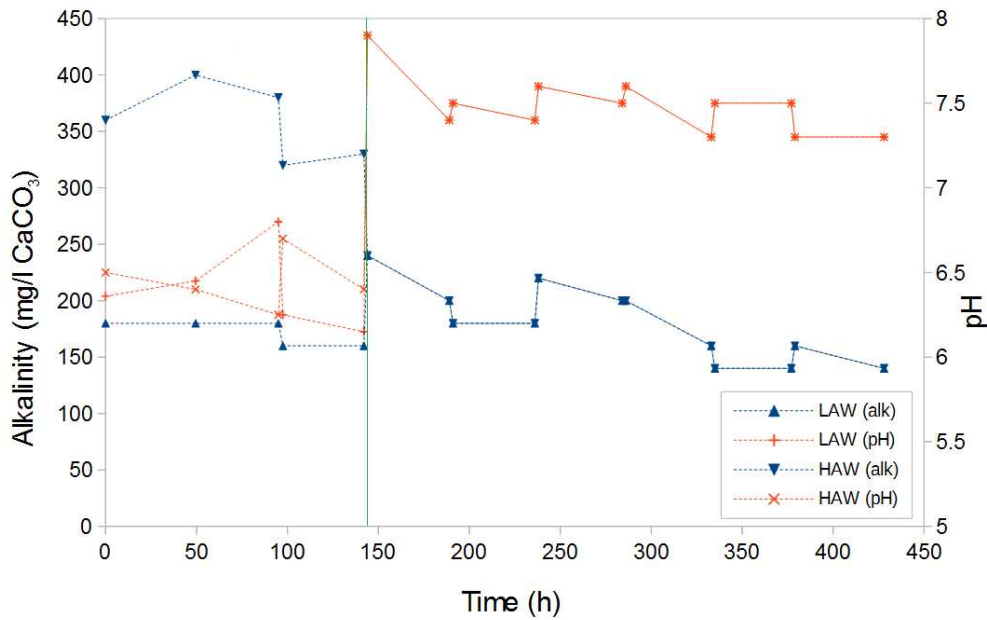


Figure 4.1. Alkalinity (triangles) and pH (cross) of influent restoration (0-143 hours) and background water (144-428 hours) for high alkalinity restoration water (HAW) and low alkalinity restoration water (LAW). Green line indicates the time when all columns were switched to background water.

Johnson et al. (2016). An example PHREEQC input file is provided in Appendix B). A parameter estimation software (PEST) produced by Doherty and Hunt (2010) was coupled to PHREEQC to derive the best-fits for transport and sorption parameters based on the lowest sum of squared residuals (SORS) and R values. Prior to applying uranium sorption, the dispersivities and grid sizes for each column were fitted to the breakthrough curves of the tracers using PHREEQC's 1-D advection-dispersion function. In order to describe the complex aqueous chemistry of uranium PHREEQC's default database was updated with the uranium speciation reactions from Guillaumont and Mompean (2003). Equilibrium constants for calcium-carbonate-uranyl ternary complexes (Dong and Brooks 2006) are shown in Table 4.4. The MES buffer was added manually into PHREEQC as a master species using a  $pK_a$  value of 6.15. Interactions between MES and uranium were considered negligible based on the review of metal-buffer complexes by Ferreira et al. (2015).

Table 4.4. Pertinent reactions added to the PHREEQC database for the model simulations and their formation constants (log  $\beta$ ).

Reaction	log $\beta$
$\text{Ca}^{2+} + \text{UO}_2^{2+} + 3\text{CO}_3^{2-} \leftrightarrow \text{CaUO}_2(\text{CO}_3)_3^{2-}$	27.4 <sup>a</sup>
$2\text{Ca}^{2+} + \text{UO}_2^{2+} + 3\text{CO}_3^{2-} \leftrightarrow \text{Ca}_2\text{UO}_2(\text{CO}_3)_3(\text{aq})$	30.7 <sup>a</sup>
$\text{Mg}^{2+} + \text{UO}_2^{2+} + 3\text{CO}_3^{2-} \leftrightarrow \text{MgUO}_2(\text{CO}_3)_3^{2-}$	26.1 <sup>a</sup>
$>\text{SOH} + \text{UO}_2^{2+} \leftrightarrow >\text{SOUO}_2^+ + \text{H}^+$	5.817 <sup>b</sup>
$>\text{SSOH} + \text{UO}_2^{2+} \leftrightarrow >\text{SSOUO}_2^+ + \text{H}^+$	6.798 <sup>b</sup>

<sup>a</sup> Dong and Brooks. (2006)

<sup>b</sup> Davis et al. (2004)

A non-electrostatic, generic composite surface complexation model (GC SCM) was used to simulate sorption of uranium to sediment surfaces. Surface complexation models have been examined extensively in the literature and details on fundamental concepts can be found in Dzombak and Morel (1990), Waite et al. (1994), and Davis et al. (1998). SCMs incorporate adsorption through mass action equations, wherein cations form surface species with negatively charged sorption sites on the surface of minerals. The formation of these surface species is governed by equilibrium constants similar to aqueous speciation reactions. Equations 1 and 2 depict how the formation of uranium surface complexes is dependent on both the equilibrium constant of the surface species and the number of sorption sites available for the strong and very strong sites respectively.

$$K_{SOH} = \frac{[=SOUO_2^+][H^+]}{[=SOH][UO_2^{2+}]}$$

Equation 4.1

$$K_{SSOH} = \frac{[=SSOUO_2^+][H^+]}{[=SSOH][UO_2^{2+}]}$$

Equation 4.2

In complex mineral assemblages found in natural sediments, determining the number of reactive sorption sites can be difficult if not impossible (Davis et al. 2004). If both the number of sorption sites and the K values are not available then solutions to surface complexation equations are inherently non-unique.

The GC SCM does not accurately represent stoichiometries and interactions occurring at the molecular scale and ignores electrostatic effects of mineral surfaces. Nor does it tie sorption reactions to a specific surface type. Instead it takes a semi-empirical approach to surface complexation where many molecular-scale processes are combined into a few experimentally derived parameters. Goodness of fit and simplicity are suggested criteria when applying the GC SCM approach to risk assessment (Waite et al. 2000, Payne et al. 2013). Previous studies (Johnson et al. 2016, Dangelmayr et al. 2017) showed that best fits for soils were achieved with a 2 pK model. Including a weak site did not improve the model fits significantly, while adding another degree of non-uniqueness to the fitting process. Our model used two generic metal oxide surfaces, a strong sorption site (=SOH) and a very strong sorption site (=SSOH). The pK values for those two theoretical sites were based on Davis et al. (2004) and are provided in Table 4.4 while the number of sorption sites for the =SOH and =SSOH sites were used as a fitting parameter to model uranium breakthrough. Fixing pK to literature values not only reduced the number of optimal solutions, but it also allowed us to compare fitted parameters between the different columns and previous experiments since the goal of this project was to understand inherent variability in this process, rather than finding the best solution to an individual data set. Both parameters were constrained to no more than 5% and 0.5% of the total number of sorption sites available, to maintain an approximate 10:1 ratio between =SOH and SSOH sites as suggested by Davis et al. 2004. No weights were applied to the objective function.

Experimental data from prior column experiments (Dangelmayr et al. 2017) on sediments 191.4 m and 192.3 m below ground (referred to as 191 and 192 respectively) were used to compare fitted parameters from different column experiments on similar sediment sections. Experiments in Dangelmayr et al. (2017) were conducted with different influent chemistries and column preparation procedures, but employed the same modeling procedures as described herein. Additional results of batch experiments completed at SDSMT on sediments 191 m and 193 m (Truax 2015) were refitted with the same procedure outlined in this section to derive site densities. The experimental methods and results of Truax (2015) are provided in Appendix A. The fitted site densities of those three data sets were compared to each other to determine the variability of fitted parameters between the different methodologies employed.

A sensitivity analysis was performed on our models by varying input pH, alkalinity, and site densities to determine shifts in uranium breakthrough time ( $t_{-50\%}$ ) versus variability in input parameters. Variables were changed one at a time at percentile increments and plotted versus the percentile change in  $t_{-50\%}$ . The increments were compared to a baseline alkalinity of 320, a pH of 6.5, and 0.1% by weight calcite content similar to the 192 HAW experimental setup. A second sensitivity analysis was performed on pH and alkalinity, with calcite precipitation and dissolution excluded. The purpose of the sensitivity analyses were to simulate how uncertainties in actual influent chemistries, as compared to model input, could affect uranium transport after the aqueous chemistry was allowed to equilibrate with the aquifer geochemistry. As a consequence pH and alkalinity were not fixed during the sensitivity analyses even though they are dependent parameters, to provide a more realistic estimation.

## 4.3 Results

### 4.3.1 Experimental results

BET analysis on sediments from depth 192 m and 193 m showed surface areas of  $4.7 \pm 0.58 \text{ m}^2/\text{g}$  and  $9.4 \pm 0.38 \text{ m}^2/\text{g}$  respectively, consistent with the observation that 192 contained coarser material. Sediment size fractions were relatively similar for both depths with 95.4% and 87.9 % of sediment mass being composed of the <2 mm fraction for 192 m and 193 m respectively. Sediment from depth 192 had a higher fine fraction (<0.6 mm) than 193 m (Table 4.5). XRF results (Table 4.1) indicated the presence of 0.74 and 0.275 mol/kg-soil of iron for depths 193 and 192 m respectively, which according to XRD analyses may have been present as impurities in feldspar. Sediment characterization revealed a generally similar mineralogy between 192 and 193, except for TOC content and the presence of montmorillonite in sediment 192. Porosities calculated from tracer breakthroughs and flow rates were between 0.204 and 0.27. The lower effective porosity of tracer breakthrough compared to porosities derived from soil weights used (represented in Table 4.6), can be attributed to the presence of trapped air that was introduced during packing. Subsequent unit conversions and calculations all use the effective porosity derived from tracer data.

Breakthrough curves for the bromide tracer and uranium effluent are provided in Figures 4.2 – 4.5. Models using best fit parameters are shown over the uranium breakthrough curve. Uranium breakthrough experienced significant retardation in all columns by a factor of 2-3 over tracer breakthrough. Changing the alkalinity of restoration waters from approximately 160 to 320 mg/l  $\text{CaCO}_3$  increased breakthrough times for uranium by 25% and 30% for the 193 and 192 set respectively. Retardation factors and pore volumes for each experiment are shown in Table 4.6 while effluent alkalinity for all four columns are provided in Figure 4.7a. Calcite saturation

indexes together with influent alkalinities and column porosities are listed in Table 4.8 while total recoveries for uranium and calcium are provided in Table 4.7. Recoveries were above 90% for uranium in all columns and between 94% and 103% for calcium. Sediments from depth 192 m below ground, provided slightly lower uranium recoveries than sediments from depth 193 m. The discrepancy can be attributed to minute (less than 1 mg/l) but persistent residual uranium that was still eluting from those columns after the experiment was terminated, compared to the 193 columns. Sediment from depth 192 was finer grained than sediment from 193 and had a higher porosity as well. Hence, the residual tail observed post-injection could be explained by the diffusion of uranium into dead end pores and interstitial spaces.

Table 4.5. Sediment size fractionation for depths 192 m and 193 m as percent of total mass.

<b>Mesh Size</b>	<b>&gt; 2 mm</b>	<b>1 – 2 mm</b>	<b>0.6 – 1 mm</b>	<b>&lt; 0.6 mm</b>
192	4.4 %	19.0 %	15.7 %	40.4 %
193	12.1 %	28.3 %	18.7 %	61.0 %

Table 4.6. Pore volumes ( $V_p$ ), uranium retardation as a multiple of tracer breakthrough time, fitted site densities for strong and very strong sites ( $\mu\text{mol/kg-soil}$ ),  $R^2$  and SORS values for the best model fits.

<b>Experiment</b>	<b><math>V_p</math> (ml)</b>	<b>Retardation Factor (<math>t_u/t_r</math>)</b>	<b>SOH sites <math>\mu\text{mol/kg-soil}</math></b>	<b>SSOH sites <math>\mu\text{mol/kg-soil}</math></b>	<b><math>R^2</math></b>	<b>SORS</b>
192 LAW	39	2.79	177	15.5	0.96	0.236
192 HAW	40	2.15	138	14.8	0.98	0.148
193 LAW	30	3	135	9.6	0.95	0.243
193 HAW	35	2.4	157	19	0.98	0.113

Table 4.7. Uranium and calcium recoveries for all 4 column experiments as a percentage of expected influent total.

<b>Experiment</b>	<b>192 LAW</b>	<b>192 HAW</b>	<b>193 LAW</b>	<b>193 HAW</b>
Uranium	95%	98%	90%	93%
Calcium	94%	103%	98%	102%

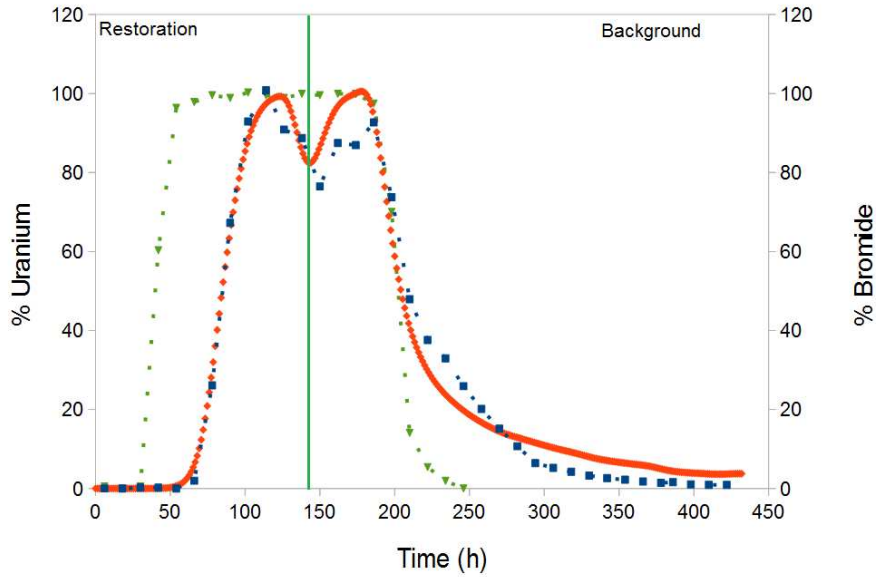


Figure 4.2. Bromide tracer (▼, green) and uranium (■, blue) as a percentage of influent concentrations plotted together with best model fits (◆, red) for experiment on depth 192 at an influent alkalinity of 360 mg/l CaCO<sub>3</sub>. The line at 143 hours indicates the switch from restoration water to background water.

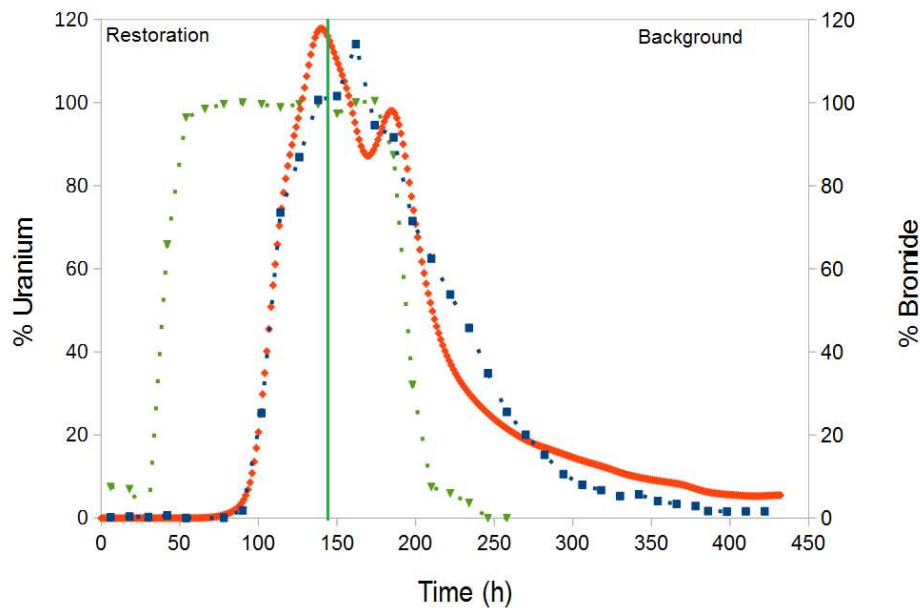


Figure 4.3. Bromide tracer (▼, green) and uranium (■, blue) as a percentage of influent concentrations plotted together with best model fits (◆, red) for experiment on depth 192 at an influent alkalinity of 160 mg/l CaCO<sub>3</sub>. The line at 143 hours indicates the switch from restoration water to background water.

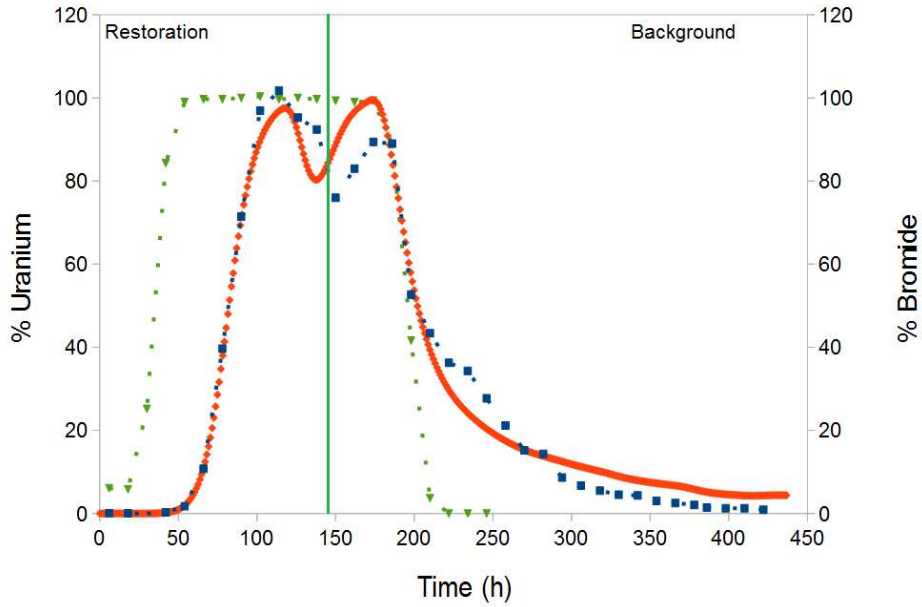


Figure 4.4. Bromide tracer ( $\blacktriangledown$ , green) and uranium ( $\blacksquare$ , blue) as a percentage of influent concentrations plotted together with best model fits ( $\blacklozenge$ , red) for experiment on depth 193 at an influent alkalinity of 360 mg/l  $\text{CaCO}_3$ .

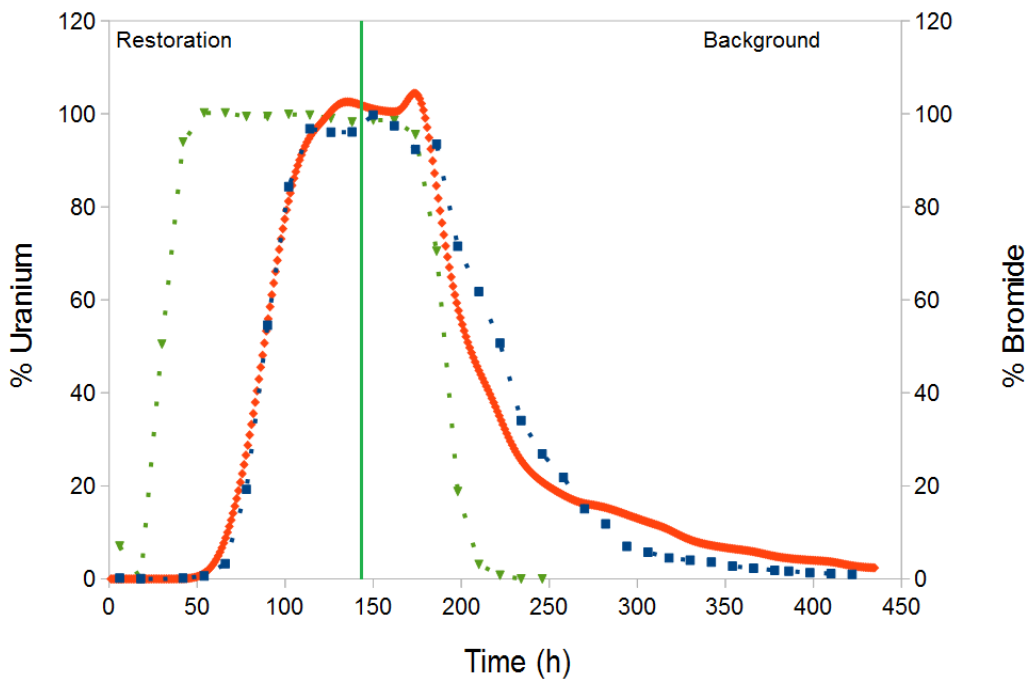


Figure 4.5. Bromide tracer ( $\blacktriangledown$ , green) and uranium ( $\blacksquare$ , blue) as a percentage of influent concentrations plotted together with best model fits ( $\blacklozenge$ , red) for experiment on depth 193 at an influent alkalinity of 160 mg/l  $\text{CaCO}_3$ .

Table 4.8. Sediment depths, alkalinity, calcite saturation, and porosities for all column experiments.

Experiment	Soil Depth (m)	Restoration Alk. (mg/l CaCO <sub>3</sub> )	Calcite S.I.	Porosity	Effective Porosity
192 LAW	192.3 - 192.6	160	-0.14 - 0.56	0.29	0.26
192 HAW	192.3 - 192.6	360	0.31 - 0.69	0.33	0.27
193 LAW	193.2 - 193.5	160	-0.14 - 0.56	0.28	0.204
193 HAW	193.2 - 193.5	360	0.31 - 0.69	0.31	0.24

Influent waters were almost continuously over-saturated with respect to calcite with a saturation index (SI) varying between -0.14 and 1.24 with a median of 0.64 (Table 4.8). Only the 160 mg/l alkalinity experiments were slightly under saturated with a saturation index (SI) of -0.14 to -0.04 during the uranium injection period for a total of 48 out of 143 hours. As a result, very little calcite dissolution would be expected during the column experiment. Effluent SI based on measured effluent pH and alkalinity were significantly higher than influent SI due to the increase in pH that all columns experienced during the experiment duration. Alkalinity and calcium concentrations remained relatively stable between influent and effluent. The pH increase would likely indicate micromolar amounts of CO<sub>2</sub> evolution for the high alkalinity column experiments, since the influent waters were oversaturated with respect to CO<sub>2</sub>. Visual inspection of influent in the syringes did not reveal any significant calcite precipitation, but small amounts of air bubbles did form in the syringes over the 48 hours injection period.

#### 4.3.2 Modeling and fitting results

PHREEQC produced generally good model fits with coefficients of determination ( $R^2$ ) of 0.98 and 0.96 for the high and low alkalinity experiments using sediment depth 192, and 0.95 and 0.98 for high and low alkalinity influent for sediments from depth 193, respectively (Table

4.8). Fitting parameters for strong and very strong binding sites are shown in Table 4.6 together with the experiment's  $R^2$  and SORS (normalized to influent uranium). The number of fitted sites involved in uranium sorption were between 135 to 177  $\mu\text{mol}/\text{kg}\text{-soil}$  for  $=\text{SOH}$  and 9.60 and 19.0  $\mu\text{mol}/\text{kg}\text{-soil}$  for  $=\text{SSOH}$ . Sediment from depth 193 m below ground had a slightly reduced sorption capacity with a mean of 146  $\mu\text{mol}\text{-sites}/\text{kg}\text{-soil}$  compared to 158  $\mu\text{mol}\text{-sites}/\text{kg}\text{-soil}$  for sediment from depth 192. However, fitted site densities were generally similar between the two sediments. The higher delay in observed breakthrough for the 193 sediments can be attributed to a higher surface area to solution ratio (Table 4.6) rather than inherent differences in sorption capacity due to mineralogy. This would suggest that geochemical heterogeneity at the SRH site plays a less significant role in uranium retention than variability in aquifer porosities and sediment surface area.

The fitted number of sorption sites represents only between 0.75% and 1.94 % of total sorption sites based on a generic site density of  $3.84 \mu\text{mol}/\text{nm}^2$ , bidentate bonds (Dzombak and Morel 1990), and BET results. Figures 2-5 show experimental uranium breakthrough together with models using the best-fit values derived through PEST. The pH of the model outputs varied between 6.8 and 7.5, which was consistently lower by about 1 pH unit compared to measured effluent pH (7.5 - 8.3). Modeled alkalinity varied by +/- 25% of measured alkalinity and predicted calcite precipitation/dissolution was consistently below 100 nM. With the exception of pH, modeled carbonate dynamics corresponded generally well to measured data. Modeled pH and alkalinity are shown alongside measured pH and alkalinity in figures 4.6-4.9 (pages 94 and 95) for all four column experiments. Results for sensitivity analyzes are shown in Figure 4.10 and 4.11 (page 97). Site density and alkalinity had a linear relationship between parameter increments and t-50%. The sensitivity of pH showed lowest retardation at a pH of 6.5 in the

presence of calcite while increasing or decreasing the pH by one unit increased breakthrough time by up to 15%. Modeling the system without allowing calcite to precipitate produced characteristic sorption behavior with a significant drop in uranium retardation past pH 6.5. Of the three parameters investigated, changes in site density had the greatest effect on uranium retardation when calcite was allowed to regulate alkalinity and pH.

#### **4.4. Discussion**

##### **4.4.1 Modeling effects of carbonate dynamics on uranium transport**

As shown in Figures 4.2 -4.5 and Table 4.6, doubling the influent alkalinity increased uranium breakthrough time ( $t_{-50\%}$ ) by 25-30% compared to the tracer. This trend has been observed in prior literature as well (Kohler et al 1996, Curtis et al. 2006, Dangelmayr et al. 2017). Model fits were generally accurate and close in all four columns ( $R^2 > 0.9$ ) despite variability in both influent pH ( $\pm 0.3$  pH units) and alkalinity ( $\pm 40$  mg/l  $\text{CaCO}_3$ ) between syringe replacements (Figure 4.1). LAW experiments show two uranium peaks; one during the slug injection and the other shortly after switching to background water. The second uranium peak was likely caused by the restoration water having a slightly higher alkalinity during the first injection (240 mg/l  $\text{CaCO}_3$ ) than the subsequent influent water (160 mg/l  $\text{CaCO}_3$ ) in addition to a higher pH ( $\sim 7.5$  versus  $\sim 6.5$ ). Our results demonstrate that the GC SCM approach can effectively model the behavior of uranium induced by shifts in geochemistry typically encountered at ISR restoration sites. The close model fits indicate that similar de-/sorption events due to changes in alkalinity and pH can be predicted in field systems, provided carbonate dynamics in the field are well described in the model.

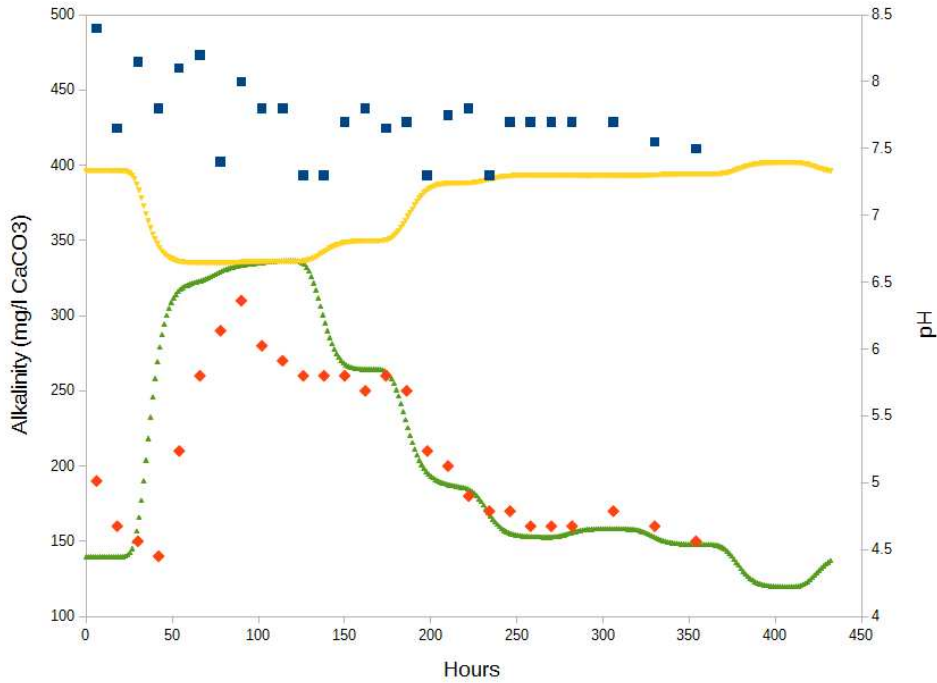


Figure 4.6: Modeled alkalinity ( $\blacktriangle$ , green) and pH ( $\blacktriangledown$ , yellow) versus measured alkalinity ( $\blacksquare$ , blue) and pH ( $\blacklozenge$ , red) for column experiment 192 HAW.

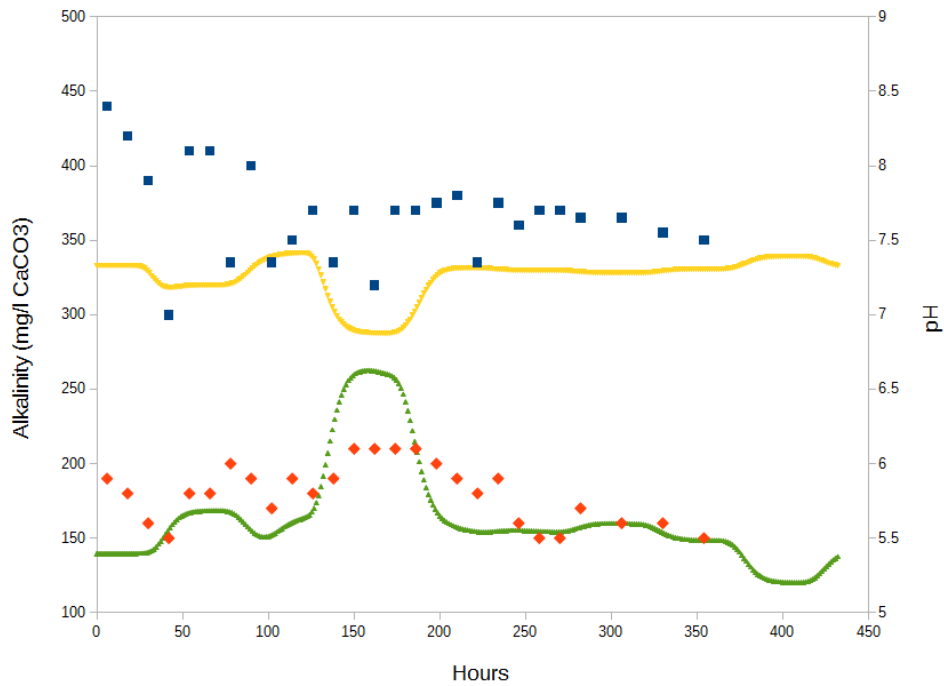


Figure 4.7: Modeled alkalinity ( $\blacktriangle$ , green) and pH ( $\blacktriangledown$ , yellow) versus measured alkalinity ( $\blacksquare$ , blue) and pH ( $\blacklozenge$ , red) for column experiment 192 LAW.

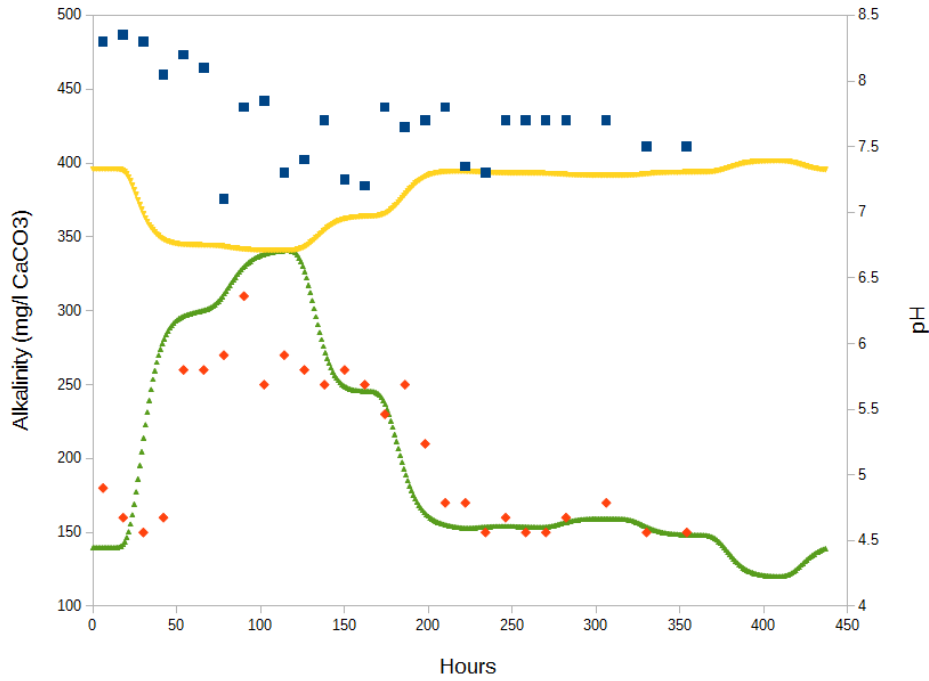


Figure 4.8: Modeled alkalinity ( $\blacktriangle$ , green) and pH ( $\blacktriangledown$ , yellow) versus measured alkalinity ( $\blacksquare$ , blue) and pH ( $\blacklozenge$ , red) for column experiment 193 HAW.

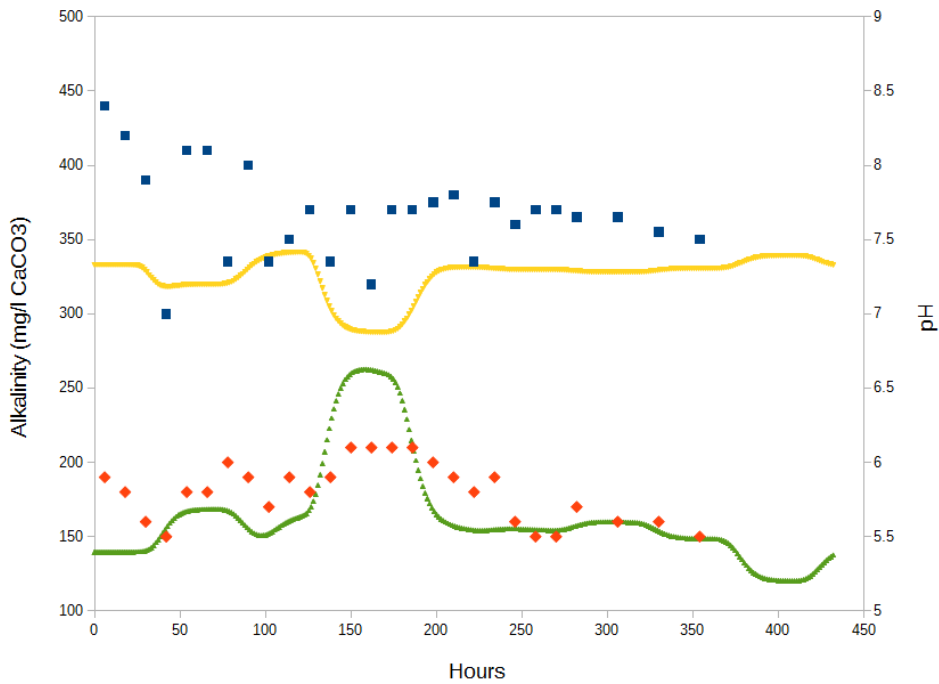


Figure 4.9: Modeled alkalinity ( $\blacktriangle$ , green) and pH ( $\blacktriangledown$ , yellow) versus measured alkalinity ( $\blacksquare$ , blue) and pH ( $\blacklozenge$ , red) for column experiment 193 LAW.

Effluent alkalinity experienced slight deviations from model predictions (+/-20%) during all column runs. We considered this deviation negligible, since the Hach titration method can only measure alkalinity in steps of +/- 20 mg/l that would represent a 5% - 17% instrumental error. However, PHREEQC consistently underestimated effluent pH from measured values by approximately 1.2 pH units. The discrepancy could be explained by the kinetics of calcite precipitation in the experiments. PHREEQC assumed equilibrium conditions with respect to calcite, which would decrease the pH in the model output, while calcite precipitation may have been kinetically limited in the columns. The fact that the effluent was consistently over-saturated with regards to calcite (S.I. of 0.51 to 1.88) further supports this idea. It should be noted that the lack of calcite kinetics in our models could have overestimated actual sorption capacity of the columns. If calcite precipitates slowly in the columns, then the pH and  $\text{CO}_3^{2-}$  in the model would be lower than observed in experimental conditions. As a consequence, PEST would require a lower site density to fit the observed data. It is advisable to assess the potential impact calcite dissolution/ precipitation and kinetics could have on GC SCM parameters, when designing sorption tests on actual sediments.

#### **4.4.2 Model sensitivity to carbonate dynamics**

A sensitivity analysis on pH and alkalinity was performed on the 192-column run with high alkalinity influent, and results are presented in Figures 4.10 and 4.11. Despite the significant impact of alkalinity on uranium transport observed in the column experiment, the model showed linear but low sensitivity to alkalinity. Relative change in t-50% only increased by 7.5% after reducing influent alkalinity to 160 mg/l from 360 mg/l, while a 25% - 30% earlier uranium breakthrough in the HAW columns occurred. PHREEQC corrected this discrepancy by fitting a

higher number of sorption sites to the LAW columns (1.4  $\mu\text{mol/L}$ -solution and 1.3  $\mu\text{mol/L}$ -solution compared to 1.33  $\mu\text{mol/L}$ -solution and 0.98  $\mu\text{mol/L}$ -solution for the 192 and 193 sediments respectively). The discrepancy can be explained by the difference between model and experimental pH as well. Uranyl ternary species are assumed to form from carbonate ions, which would be present in insufficient quantities at the lower pH observed in the model.

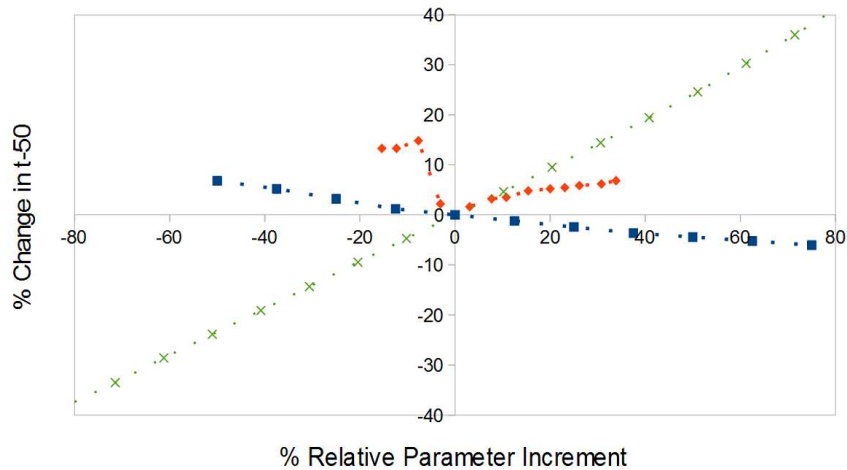


Figure 4.10: Sensitivity analysis for alkalinity (■, blue), pH (◆, red), and site densities (x, green) on column model 192 HAW. Relative increments in alkalinity are calculated with respect to 320 mg/l  $\text{CaCO}_3$ , while pH is calculated with respect to a pH of 6.5.

The impact of influent pH was more significant, but also showed more variability. Reducing the pH by half a unit from 6.5 increased t-50% by more than 10%, while increasing the pH also increased t-50% by 5%. Lowest retardation was observed in the pH range of 6.5 – 6.7. The effect of pH on the sorptive behavior of uranium has been well studied (Waite et al 1994, Kohler et al. 1996, Echevarria et al. 2001, Davis et al. 2004, Curtis et al. 2006) and generally show uranyl sorption to be maximum between pH 6 and 7 in batch experiments, contrary to our simulations. This discrepancy can be explained by the addition of calcite in the simulations.

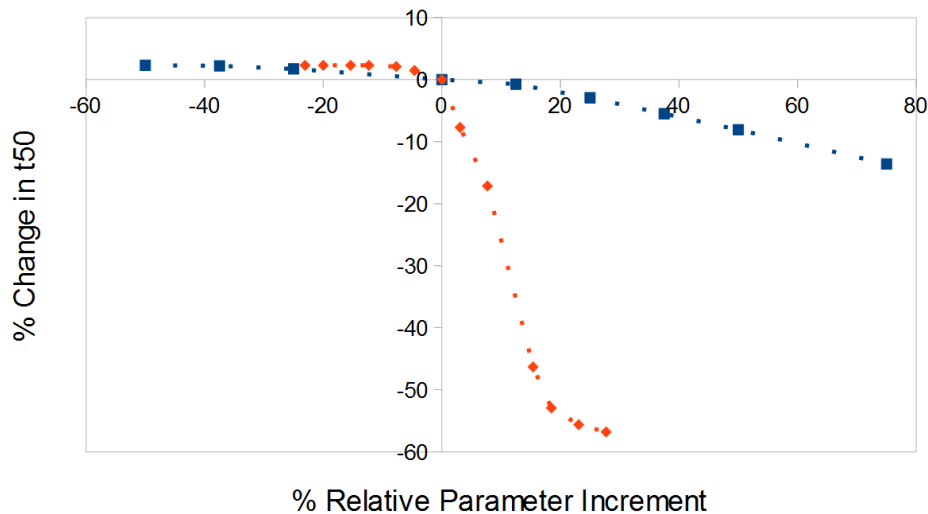


Figure 4.11: Sensitivity Analysis for alkalinity (■, blue) and pH (◆, red) on column model 192 HAW with calcite precipitation and dissolution disabled. Relative increments in alkalinity are calculated with respect to 320 mg/l CaCO<sub>3</sub>, while pH is calculated with respect to a pH of 6.5.

In our case, waters were close to calcite saturation at pH 6.5 and alkalinity 320 mg/l CaCO<sub>3</sub>. Reducing the pH below 6 in the simulation caused significant calcite dissolution, which equilibrated at a pH of 6.0 according to PHREEQC. Even though alkalinity doubled from the baseline after equilibration, the resulting pH of around 6.0 produced insufficient carbonate to form ternary uranium complexes necessary to reduce sorption. Meanwhile, a higher pH induced calcite precipitation and subsequently lowered total alkalinity and dissolved calcium, increasing retardation. Excluding calcite in the sensitivity analysis produced characteristic sorption behavior with a sharp drop in uranium retention past pH 6.5 due to the preference of uranium to form calcium-carbonate-uranyl complexes (Figure 4.8). Our model simulations indicate that the effect of alkalinity and pH on uranium breakthrough is regulated by calcite saturation and precipitation kinetics. Groundwater velocities at the SRH site are significantly lower than those used in our experiments, (2-3 m per year). As a consequence, purely thermodynamic models may be inappropriate for column studies where calcite kinetics would produce additional uncertainty.

However, they might be sufficient for ISR sites and batch experiments that are completed over a longer equilibration time span.

#### **4.4.3 Significance of calcium carbonate dynamics for ISR restoration**

The alkalinity of post-mining groundwater at ISR sites can reach up to 800 mg/l CaCO<sub>3</sub> while background waters may drop to 120 mg/l CaCO<sub>3</sub>. Typical post-mining pH values are 6.5 to 6.8 before groundwater restoration is completed while background waters range in pH from 7.5 to 8.2. This variability in groundwater geochemistry can produce challenges when trying to conduct risk assessments and apply remediation technologies. The necessity of reducing pCO<sub>2</sub> during ISR restoration has been well documented (Davis and Curtis 2007). Proven methods for removing dissolved carbon dioxide as a part of the restoration process are available and commonly used such as air stripping or vacuum degassing, and their use can significantly raise pH in the restoration zone and thus decrease dissolved uranium mobility. The results discussed here underscore the importance of including one or more of these removal methods during restoration. Our research indicates that restoration practices also need to account for calcium concentrations. Calcium hardness at the SHR site can reach 400 mg/l and background calcite is approximately 0.1 % – 1.0 % by weight. Significant amounts of dissolved calcium is removed during the reverse osmosis process typically employed during restoration. Removing CO<sub>2</sub> must therefore be done with respect to calcite S.I. as well as pH, since under saturated restoration water may dissolve sediment calcite and increase uranium mobility outside of the restoration zone. Blending treated effluent with background water may alleviate this effect and bring restoration water into equilibrium with sediment mineralogy.

#### 4.4.4 Modeling desorption hysteresis

Uranium breakthrough and uranium behavior during the slug injection were accurately captured by the GC SCM model. However, a significant discrepancy in uranium desorption was observed between models and experimental results (Figures 4.2 – 4.5). Hysteresis between sorption and desorption has been observed in prior literature (Dangelmayr et al. 2017, Dittrich and Reimus 2015, Kohler et al. 1996, Liu et al. 2013, Liu et al. 2015, Miller et al. 2013) and is a common phenomenon of uranium transport. The tailing behavior has been ascribed to mass transfer limitations at the pore-scale and differences in sorption/desorption kinetics (Liu et al. 2013, Liu et al. 2015) as well as heterogeneity in sediment hydraulic conductivity (Miller et al. 2013). Prior attempts to predict the tailing behavior of uranium also found that the model fits depend highly on the number of sorption sites used. Dittrich and Reimus (2015) noted that a 3-site model with an additional weak sorption site performed better than a 2-site or 1 site model, even though all three models were able to capture initial uranium breakthrough. The presence of a small number of very strong sorption sites was found to be responsible for the tailing behavior. For our experiments, desorption was actually overestimated by the model past ~280 hours while the model under-predicted uranium retention during the early stages of the elution phase (~200-280 hours). This discrepancy was more pronounced in the LAW experiments where SORS were about twice that of the HAW columns. This behavior could be indicative of a higher =SOH to =SSOH ratio, since long-term uranium elution is reduced in the experimental data. Our fitting procedures did not assign weights to different parts of the breakthrough curves and restricted SSOH sites to no less than 0.05% of the SOH sites. As a consequence, PEST prioritized the initial breakthrough curve and behavior of the uranium slug over the desorption tailing, since those would produce higher residuals. The sensitivity of the model to the number of =SSOH sites

would also be lower, since their influence on uranium desorption appeared during the latter stages of the experiment. Furthermore, our design applied a simple model with few fitting parameters to the experimental data to reduce the non-uniqueness of our solution space and simplify the application to field systems. However, the effect of =SOH to =SSOH ratios and the possible need for a third site in the fitting process calls for further investigations, as their effect on the long-term behavior of uranium at actual ISR sites could be significant when compared to short-term, laboratory experiments.

#### **4.4.5 Cross-comparison between different sorption experiments**

One goal of our study was to assess the variability in sorption parameters obtained from the GC SCM fitting process between different experimental set-ups. To this end, select data from prior experiments on the same sediment cores were analyzed and their parameters re-fitted, if necessary, to the model developed for in this research. The previous column and batch experiments are described in detail in Dangelmayr (2017) and Truax (2016). Site densities from prior experiments were recalculated with updated porosity values. Table 4.9 summarizes site densities obtained for each experimental setup for the strong binding sites (=SOH) and sorts them according to sediment depth and alkalinity. Fitted parameters completed on the same sediment section within the same experiment group varied by a factor 15%-33%, providing replicable results given the inherent uncertainty in experimental data.

Parameter comparisons on the same sediments between experimental setups yielded significantly higher variability in site densities. Column experiments produced site densities that were higher by a factor of ~1.5 for sediment depth 193 to ~3.9 for sediment depth 191 compared to the corresponding batch experiments. It should be noted that the presence of calcite in the

Table 4.9. Comparison of strong site densities (=SOH) in  $\mu\text{mol/kg}$ -sediment between different experiments, sorted by alkalinity, solid-solution ratios ( $V_s/V_w$ ) and sediment depth.

Experiment	Alkalinity (mg/l $\text{CaCO}_3$ )	$V_s/V_w$	Site Density of =SOH ( $\mu\text{mol/kg}$ -soil) for Sediment Depths		
			191	192	193
Batch	0	0.047	9.8 <sup>1</sup>	–	45 <sup>1</sup>
Batch	110	0.047	24.5 <sup>1</sup>	–	115 <sup>1</sup>
Batch	169	0.047	32.7 <sup>1</sup>	–	100 <sup>1</sup>
Column 1	540	0.95	96 <sup>2</sup>	–	–
Column 2	540	0.95	89.7 <sup>2</sup>	–	–
Column 3	540	1.82	–	20.5 <sup>2</sup>	–
Column 4	160	2.78	–	177 <sup>3</sup>	–
Column 5	360	2.68	–	138 <sup>3</sup>	–
Column 6	160	3.91	–	–	135 <sup>3</sup>
Column 7	360	3.21	–	–	157 <sup>3</sup>

<sup>1</sup> Batch experiments completed at SDSM&T (Truax 2015)

<sup>2</sup> Column experiments completed at LANL (Dangelmayr et al. 2017)

<sup>3</sup> Column experiments completed at SDSM&T

batch experiment completed at 0%  $p\text{CO}_2$  could be responsible for the low site densities produced during the fitting process. The complete dissolution of an uncertain amount of calcite would have raised the alkalinity and pH to a higher value than predicted in the model, and as a result, under predict actual sorption capacity. Variability in batch to column scaling has been reported in several other studies and consensus on the causes as well as extent for these observations is in dispute (Kohler et al. 1996, Porro et al. 2000, Phillippi et al. 2007, Miller et al. 2011, Huber et al. 2016). One study showed that sorption capacity derived from column experiments deviated by a factor of 2-6 times from that of batch experiments (Huber et al. 2016). Dispersion as well as diffusion into immobile phases are processes that occur exclusively in flow through systems and have been implicated in increasing apparent sorption capacity (Huber et al. 2016, Miller et al 2011, Porro et al. 2000). In addition, Phillippi et al (2007) and Porro et al. (2000) postulated that

a solid concentration effect could impact and underestimate sorption in batch experiments compared to column studies. Specifically, errors in solution to sediment ratios in the batch experiments can produce high variability in resulting site densities (Miller et al. 2011, Porro et al. 2000). At a solid-solution ratio of 0.047, a 5% error in porosity (sediment volume to total volume) can change the total number of sorption sites available for batch experiments by a factor of 2. On the other hand, column experiments are conducted at solid-solution ratios where errors in porosity produce equivalent errors in total number of sorption sites. Uncertainties in alkalinity, pH, and calcite S.I. would compound the observed discrepancies, and thus could explain the variability between batch and column experiments.

The highest variability (by a factor of 8.6), however, was observed between two column experiments completed on sediment 192 (Table 4.9). Our sensitivity analyses show that uncertainties in alkalinity, pH, or sediment calcite cannot fully account for the differences in the estimated parameters. In addition, errors in porosity cannot explain the significantly lower sorption site density in the LANL column experiment. Partial oxidation of pyrite into oxidized Fe phases could account for the higher sorption capacity in the SDSM&T experiments, despite best efforts to preserve sediments anaerobically during transport and experimental set-up. More importantly, the two different column studies used different methods of packing sediment and mounting the column. The SDSM&T study employed wet packing with compaction to produce saturated conditions, while the LANL columns were dry packed, saturated with CO<sub>2</sub>, and flushed with background to dissolve CO<sub>2</sub> out of the columns (Dangelmayr et al. 2017). The effect of packing methods on flow properties has been reviewed in Lewis and Sjöström (2010). Different propensities for creating preferential flow paths and immobile pore spaces in the two packing methods could impact apparent retardation between the two columns. In addition, the SDSMT

columns utilized a bottom to top flow while the LANL columns were placed sideways, which could have produced different flow paths during sediment settling. Our study demonstrates the need for guidelines for conducting and assessing sorption experiments that employ either column or batch studies. Methodology with regards to packing, mineral phases present, chemistry, and sediment-solution ratios can produce fitted sorption parameters that vary by a factor of almost an order of magnitude. The uncertainty associated with methodology outweighs any uncertainty in sediment mineralogy at the SRH site. The industry and regulators would benefit from a better development of best practices when designing sorption studies that intend to utilize the GC SCM approach.

#### **4.4.6 Uncertainty in upscaling parameters to field sites**

The GC SCM does not assume modeled sorption sites to be specific to any one mineral phase or metal oxide (Davis 2004). However, when applying the GC SCM approach to field systems, a scaling factor needs to be used. Common scaling factors that have been suggested in the literature include Fe content (Gustafsson et al. 2009, Johnson et al 2015, Papynov et al. 2016, Waite et al. 1994) and surface area (Bertetti et al 1998, Jang et al 2007, Johnson et al. 2015, Loganathan et al. 2009, Papynov et al. 2016, Prikryl et al. 2001). XRF results showed around 3% iron for the two sediment depths studied. Fe at the SRH site is also predominantly found in reduced forms downgradient of the mining zone. While partial oxidation of Fe-minerals may have occurred when sediments were prepared for laboratory experiments, if we assume uranium binding to ferrinol sites as the primary surface complexation mechanism, then only 0.035% to 0.049% of iron actually participated in uranium sorption. XRD did not detect any crystalline iron bearing minerals and BET results are relatively low for the presence of significant amounts of

amorphous Fe. If the measured 3% of Fe content was really in the form of amorphous ferric oxides, then one would expect an almost 5-fold higher surface area for our sediments assuming a surface area of 600 m<sup>2</sup>/g for ferrihydrite (Dzombak and Morel 1990). The lack of definite Fe mineral phases makes it uncertain to what degree Fe occurs as amorphous material or as substitutions in Feldspar, which would be unavailable for surface complexation. As a consequence, sediment Fe represents a problematic scaling factor that could potentially add significant uncertainty into the model, if an unknown fraction of Fe actually participates in uranium sorption. Two other studies pointed out that total or extractable Fe produce poor scaling parameters for predicting uranium sorption to mineral phases (Johnson et al. 2015, Loganathan et al 2009).

Prior studies have suggested that metal sorption to aluminosilicates can be scaled to field systems through surface area estimates. (Bertetti et al 1998, Prikryl et al. 2001). SRH sediments were primarily composed of quartz (73-74%), K-Feldspar (8.8-19.4%) and albite (6.6-14%), suggesting that aluminol and silanol sites could dominate uranium sorption. Despite a measurable amount of clay content (5.7% montmorillonite) and more TOC (Table 5) found in the 192 material, both sediments showed similar uranium sorption behavior. BET results provided a surface area of 4.7 and 9.4 m<sup>2</sup>/g for both sediments 192 and 193 respectively (Table 6). Together with an assumed site density of 3.84 μmol/m<sup>2</sup> (Dzombak and Morel 1990) and bidentate uranyl complexation, the total percentage of sites involved in uranyl sorption constitutes only 0.75% to 1.94% of the total sites available. In five prior column experiments completed on materials from wells at the SRH site, the fitted site densities represented only between 0.23% and 1.19% of the total BET derived surface sites (Dangelmayr et al. 2017). The variability in reactive surface sites as a percentage of total surface sites observed in our two

laboratory studies presents a challenge when trying upscale GC SCM results to the field scale. Based on these two studies on the same sediments, upscaling the GC SCM to the field would require a factor of safety of almost an order of magnitude between the upper and lower sorption density estimates.

#### **4.5. Conclusion**

Uranium sorption plays a key role in inhibiting uranium mobility at the SRH ISR facility, reducing uranium breakthrough by a factor of 2-3 compared to tracer velocities. Alkalinity and pH have shown to impact uranium mobility, increasing uranium breakthrough by 25-30% when average influent alkalinity was doubled. This study demonstrates the applicability of GC SCM to model uranium behavior under shifting geochemical conditions. Representable fits were produced for all columns when using a 2-surface site, non-electrostatic GC SCM. Sensitivity analyses showed that influent alkalinity or pH have a moderate effect on uranium transport, while calcite saturation may have an indirect effect on uranium transport by regulating pH and alkalinity. Calcite kinetics may also be a source of error in observed sorption parameters in flow conditions when effluent pH is underestimated in the model outputs. These results highlight the inherent need of ISR restoration procedures to remove dissolved CO<sub>2</sub> and blend restored effluent with background water. In addition, site risk assessment should incorporate calcite saturation and kinetics within appropriate transport models.

A comparison of fitted site densities between three experimental studies showed a 1.5 to 3.9 fold difference between parameters derived from batch experiments and column experiments. These discrepancies cannot be explained by uncertainties in experiment pH and alkalinity, and demonstrates the importance of porosity and solid-solution ratios when upscaling laboratory

parameters to field scale models. Separate column studies completed on the same sediments produced almost an order of magnitude difference in fitted sorption site densities. Methodology in column packing was found to have a greater impact on fitted parameters than heterogeneity in sediment mineralogy. Addressing the uncertainties associated with GC SCM models can inform both regulators and industry as to the number of cores that should be collected for laboratory testing, the importance of parameters such as porosity, and the degree to which a standard model construction procedure can be transferred to other hydrological and geochemical environments. This research shows the potential of GC SCM in fate and transport modeling under variable geochemical conditions, but also highlights the need for standardized guidelines for regulators and industry when applying the GC SCM to ISR sites.

## CHAPTER 5

### SUMMARY REMARKS AND FUTURE RESEARCH NEEDS

This thesis contributes to a growing body of knowledge on the subsurface fate and transport of uranium at former and future mining and milling sites and highlights the importance of uranium biogeochemistry in remediation designs and risk assessments. The work herein informs future subsurface biostimulation projects on the importance of microbial transformation of injected organic carbon. Our research shows that the microbial utilization of acetate does produce SMP that may influence the efficacy of uranium removal at those sites. SMP production during the Rifle biostimulation experiment increased DOC concentrations in the groundwater by a factor of four over measured background values. Elevated SMP concentrations persisted 90 days past active substrate injections. In addition, post-stimulation SMP were shown to be more bioavailable than background DOC possibly prolonging observed reducing in the remediation zone. Utilizing SMP production could enhance longevity of engineered bioremediation systems by optimizing substrate injections schemes. Our research also indicates that carbon sinks need to be monitored more closely during biostimulation. A significant carbon sink was observed in the field experiment that consumed ~20% of available carbon over the stimulation period. As a consequence carbon mass balance assessments should be part of remediation design due to their potential impact in maintaining reducing conditions. Furthermore, the work illustrates the potential of spectroscopic techniques to provide unique insights into the biogeochemical cycling of organic carbon in biostimulated systems. Fluorescence measurements detected unique microbial signatures in DOC sampled during biostimulation that are indicative of UAP

production. EEMs and SUVA of DOC revealed significant differences between stimulation and post-stimulation DOC and their application could provide information on the bioavailability and origin of SMP.

However, the research herein is mostly exploratory and qualitative in nature. Subsurface systems at the field scale are complex and difficult to assess and investigate. For example, our electron mass balance assumed that Br tracers would correlate to acetate influent in the wells and that incoming sulfate concentrations were steady. These assumption, however, could have introduced significant sources of errors and under or overestimated the magnitude of the missing carbon sink observed. Furthermore, the story of solid phase organic matter is neglected in this study due to the fact that solid phase characterizations cannot be easily performed at the field scale. Laboratory studies are needed to replicate our findings in more controlled settings. Bench scale experiments that examine the appearance of microbial signatures in EEMs, conduct a more careful accounting of the carbon mass balance, and characterize both microbial communities and solid phase organic matter are needed to elucidate the story of organic matter cycling in biostimulated systems.

General component surface complexation models present powerful tools to assess risk to human health at sites with uranium contaminated groundwater. Our results demonstrate that the complex geochemistry of uranium can be simulated with a GC SCM thermodynamic model, if the aqueous chemistry is well characterized. While alkalinity and pH are key chemical components that control uranium mobility our models generally succeed at representing uranium sorption and desorption in conditions even when those parameters were varied during the experiment. Model fits reproduced experimental data in the column systems with R values of > 0.9 using only a two surface site model. This illustrates the potential of thermodynamic models

to predict uranium behavior at ISR restoration sites for regulatory purposes even when the site mineralogy is complex and groundwater conditions may shift during the restoration process.

Furthermore, our results highlight important geochemical parameters that can inform industry and regulators on how to best mitigate the potential impacts of uranium contamination on human health and the environment. Both alkalinity and pH were shown to influence uranium mobility. Doubling influent alkalinity increased uranium breakthrough by 25-50% in column experiments run with the same sediments. As a consequence, the removal of excess CO<sub>2</sub> introduced during the mining operation should be included in restoration designs. Our experiments also demonstrate the significance of calcite dynamics and its impact on the remobilization of uranium. In one column study calcite dissolution enhanced uranium transport by inducing the desorption of previously immobilized contaminants, when influent waters were undersaturated with respect to calcite. As a consequence, bringing restoration waters into chemical equilibrium with sediment mineralogy by blending with background water might prove a necessary step for the closure of some ISR sites.

While the GC SCM approach shows great potential in simulating uranium behavior when parameters are fitted to existing data, the research herein, demonstrates that significant challenges remain when trying to apply parameterized results from one study to another. While fitted parameters were consistent within the same experimental designs (such as the column experiments described in chapter 4) replicability between different experimental set-up varied by almost an order of magnitude even when conducted on similar sediments. A nine fold difference between fitted parameters was observed between two column studies performed on sediments from a depth of 192 m. A more than threefold difference between fitted parameters was also shown to exist between batch studies and column experiments done on sediment depth 191 m

and 193 m. Uncertainties in alkalinity and pH measurements, were not able to explain the differences observed. Instead, the variability in fitted sorption parameters is likely due to differences in column design and operation, such as packing methods and vertical versus horizontal flow. Further research needs to be conducted on the general replicability of the GC SCM approach between different experimental designs. Chapter 3 and Chapter 4 illustrate the need for standardized guidelines and/or methodology when deriving sorption parameters for field scale models from laboratory studies.

## APPENDIX A

### BATCH SORPTION STUDY AND RESULTS

#### **A.1 Sediment collection**

Two sediment sections 0.3 m in length were collected from the MU3 downgradient core at depths 191.4 m and 193.2 m below ground (referred to as 191 m and 193 m respectively). The sediments were kept in an anaerobic chamber in a 97.5:2.5 N<sub>2</sub>:H<sub>2</sub> atmosphere while being lightly disaggregated with a pestle and mortar and sorted with a 2mm sieve. Samples were allowed to dry before being shipped to SDSMT in glass serum bottles. Once received, the serum bottles were stored within an anaerobic chamber (100% N<sub>2</sub>) before being used for batch sorption experiments.

#### **A.2 Batch experiment methods**

Batch experiments were prepared by combining 4 grams of sediment (depth 191 and 193) with 20 mL background water in 30 ml serum bottles. Experiments were done at three different uranium concentrations and three different pCO<sub>2</sub>. A uranyl nitrate stock solution (5 g /l) was used to produce concentrations of 0.5 mg/l, 1 mg/l, and 2 mg/l of uranium to each bottle. A gassing station was used to deliver pCO<sub>2</sub> concentrations of either 0%, 6.5% and 10% to the headspace of each serum bottle. The gassing station consisted of an 80:20 N<sub>2</sub>:CO<sub>2</sub> gas tank hooked to a manometer and a three-way valve, which was used to pressurize a syringe with a measured volume and pressure of gas. Next, a needle was injected through the rubber septum of the batch vial and the three-way valve was opened. The syringe was pressed to deliver the gas to

the serum bottle at the target concentrations. A duplicate was prepared for each uranium-pCO<sub>2</sub> combination. In addition, three uranium blanks were prepared for each sediment. The serum bottles were allowed to equilibrate for 7 days on a mechanical rotator (moving at 10 rpm) before measurements were taken. After equilibration, 7-8 mL of solution were extracted by a syringe, and filtered through a 1 µm glass-fiber filter. The final pH was measured, and the filtrates were stored in high-density polyethylene scintillation vials with a polypropylene screw cap. The filtrates were preserved with 3-4 drops of 15.3 N nitric acid and analyzed for total metals (Al, As, Ba, Ca, Cd, Cu, Fe, K, Li, Mg, Mn, Na, P, Pb, Se, Si, S, Sr, U, V and Zn) using an Inductively Coupled Plasma-Optical Emission Spectrometer (ICP-OES).

### A.3 Batch experiments results

Final uranium concentrations in the serum bottles sorted by initial concentrations and headspace pCO<sub>2</sub> are shown in tables A.1 and A.2 for sediment 191 and 193 respectively.

Sorption isotherms (Initial uranium plotted against final uranium concentrations) for the different sediment sections at pCO<sub>2</sub> 0%, 6.5% and 10% are provided in figures A.1 and A.2.

Table A.1: Uranium concentration in solution after 7 day equilibration sorted by initial uranium spike and partial pressure of CO<sub>2</sub> for experiments on sediment section 191 m.

<b>Initial [U] mg/l</b>	<b>pCO<sub>2</sub> 0%</b>	<b>pCO<sub>2</sub> 6.5%</b>	<b>pCO<sub>2</sub> 10%</b>
0	0.05	0.05	0.06
0.5	0.45	0.44	0.44
0.5	0.44	0.46	0.46
1	0.78	0.83	0.82
1	0.8	0.81	0.80
2	1.56	1.62	1.58
2	1.55	1.58	1.52

Table A.2: Uranium concentration in solution after 7 day equilibration sorted by initial uranium spike and partial pressure of CO<sub>2</sub> for experiments on sediment section 193 m.

Initial [U] mg/l	pCO <sub>2</sub> 0%	pCO <sub>2</sub> 6.5%	pCO <sub>2</sub> 10%
0	0.03	0.01	0.02
0.5	0.06	0.15	0.22
0.5	0.05	0.15	0.21
1	0.09	0.31	0.45
1	0.12	0.33	0.43
2	0.13	0.49	0.77
2	0.14	0.51	0.77

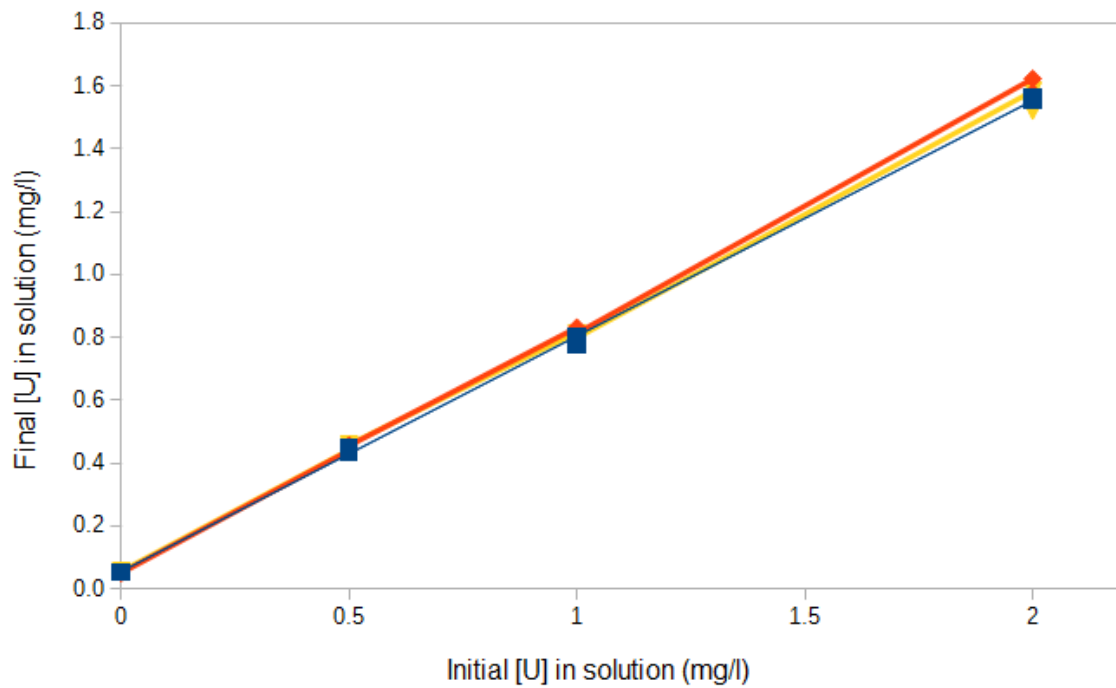


Figure A.1: Sorption isotherm for sediment 191 for pCO<sub>2</sub> at 0% (■, blue) 6.5% (◆, red) and 10% (▼, yellow) plotted as initial uranium concentration versus final uranium concentrations in solution.

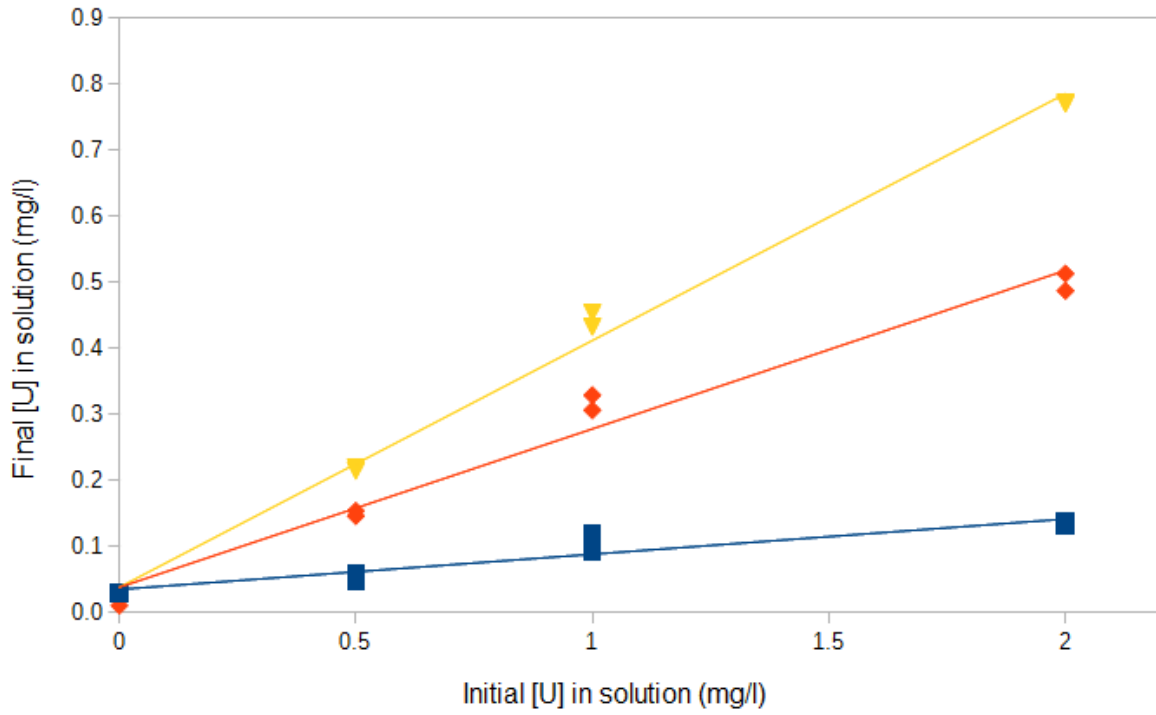


Figure A.2: Sorption isotherm for sediment 193 for pCO<sub>2</sub> at 0% (■, blue) 6.5% (◆, red) and 10% (▼, yellow) plotted as initial uranium concentration versus final uranium concentrations in solution..

## APPENDIX B

### PHREEQC INPUT FILES FOR COLUMN MODELING

DATABASE C:\Users\mdangelm\Desktop\Martin\Blue\phr\_base.dat

USER\_PUNCH 1

-headings Total\_U\_C/C0 Total\_Br\_C/C0 Total\_U

-start

10 PUNCH (TOT("U")\*238000)

20 PUNCH (((TOT("Br")\*79900.0)-2)/640)

30 PUNCH (SYS("U"))

-end

TITLE 192 HAW (Blue)

SOLUTION\_MASTER\_SPECIES

Mes Mes- 1.0 Mes 195.2

SOLUTION\_SPECIES

Mes- = Mes-

log\_k 0

Mes- + H+ = MesH

log\_k 6.15

delta\_h0.0 kJ

-gamma 0.0 0.0

SOLUTION\_SPREAD

units mg/l

temp 22

Number	Alkalinity mg/l as HCO3	pH	Ca	Mg	Na	Cl	S(6) mg/l as SO4	U mg/l	Br	Mes mmol/l
0	560	6.5	400	96	0	142	768	19	640	1.0
1-30	180	7.5	120	24	69	71	288	0	0	0

#measured 360 mg/l alk

SURFACE\_MASTER\_SPECIES

Gc\_ss Gc\_ssOH

Gc\_s Gc\_sOH

# Gc\_w Gc\_wOH

SURFACE\_SPECIES

Gc\_ssOH = Gc\_ssOH

log\_k 0

Gc\_ssOH + UO2+2 = Gc\_ssOUO2+ + H+

```

log_k 6.798
Gc_sOH = Gc_sOH
log_k 0
Gc_sOH + UO2+2 = Gc_sOUO2+ + H+
log_k 5.81
#Gc_wOH = Gc_wOH
# log_k 0
#Gc_wOH + UO2+2 = Gc_wOUO2+ + H+
# log_k 2.57

```

```

SURFACE 1-3 Equilibrate the column
# fix log ks and estimate site densities
-equilibrate with solution 1
# Gc_w 5.00e-3
Gc_s 1.3383706E-03
Gc_ss 1.0000000E-05
-no_edl

```

```

EQUILIBRIUM_PHASES 1-61
Calcite 0.0 0.022
Gypsum 0.0 0.0
# Uraninite 0.0 0

```

```

SELECTED_OUTPUT 1
-file Blue.txt
-high_precision true
-reset false
-distance false
-time true
-step false
-pH false
-alkalinity false
# -totals Br
# -equilibrium_phases Calcite

```

```

TRANSPORT # 0-49 hours
-cells 30
-shifts 37
-time_step 4800 # seconds
-lengths 30*0.01
-dispersivities 30*0.005
-thermal_diffusion 2 3e-10
-print_cells 30
-punch_cells 30
-multi_d false

```

END

SOLUTION\_SPREAD

units mg/l

temp 22

Number	Alkalinity mg/l as HCO3	pH	Ca	Mg	Na	Cl	S(6) mg/l as SO4	U mg/l	Br	Mes mmol/l
0	390	6.5	400	96	0	142	768	19	640	1

#measured alk 380-400

TRANSPORT # 49-97 hours

-cells 30  
-shifts 37  
-time\_step 4800 # seconds  
-lengths 30\*0.01  
-dispersivities 30\*0.005  
-thermal\_diffusion 2 3e-10  
-print\_cells 30  
-punch\_cells 30  
-multi\_d false

END

SOLUTION\_SPREAD

units mg/l

temp 22

Number	Alkalinity mg/l as HCO3	pH	Ca	Mg	Na	Cl	S(6) mg/l as SO4	U mg/l	Br	Mes mmol/l
0	320	6.8	400	96	0	142	768	19	640	1

#measured Alk 320

TRANSPORT # 97-144 hours

-cells 30  
-shifts 36  
-time\_step 4800 # seconds  
-lengths 30\*0.01  
-dispersivities 30\*0.005  
-thermal\_diffusion 2 3e-10  
-print\_cells 30  
-punch\_cells 30  
-multi\_d false

END

SOLUTION\_SPREAD

units mg/l

temp 22

Number	Alkalinity mg/l as HCO3	pH	Ca	Mg	Na	Cl	S(6) mg/l as SO4	U mg/l	Br
0	240	7.5	120	24	69	71	288	0	0

#Alkalinity observed 240, pH changed to 7.5 from 7.9 to prevent convergence failure

TRANSPORT # 144-191 hours

-cells 30  
 -shifts 36  
 -time\_step 4800 # seconds  
 -lengths 30\*0.01  
 -dispersivities 30\*0.005  
 -thermal\_diffusion 2 3e-10  
 -print\_cells 30  
 -punch\_cells 30  
 -multi\_d false

END

SOLUTION\_SPREAD

units mg/l

temp 22

Number	Alkalinity mg/l as HCO3	pH	Ca	Mg	Na	Cl	S(6) mg/l as SO4	U mg/l	Br
0	180	7.4	120	24	69	71	288	0	0

TRANSPORT # 191-239 hours

-cells 30  
 -shifts 36  
 -time\_step 4800 # seconds  
 -lengths 30\*0.01  
 -dispersivities 30\*0.005  
 -thermal\_diffusion 2 3e-10  
 -print\_cells 30  
 -punch\_cells 30  
 -multi\_d false

END

SOLUTION\_SPREAD

units mg/l

temp 22

Number	Alkalinity mg/l as HCO3	pH	Ca	Mg	Na	Cl	S(6) mg/l as SO4	U mg/l	Br
0	210	7.6	120	24	69	71	288	0	0

#alkalinity 200-220 mg/l and pH 7.6

TRANSPORT # 239-287 hours

-cells 30

```

-shifts          36
-time_step       4800 # seconds
-lengths         30*0.01
-dispersivities  30*0.005
-thermal_diffusion 2 3e-10
-print_cells     30
-punch_cells    30
-multi_d        false

```

END

SOLUTION\_SPREAD

units mg/l

temp 22

Number	Alkalinity mg/l as HCO <sub>3</sub>	pH	Ca	Mg	Na	Cl	S(6) mg/l as SO <sub>4</sub>	U	Br
0	190	7.4	120	24	69	71	288	0	0

#Used middle values for pH and alkalinity

TRANSPORT # 287-336 hours

```

-cells          30
-shifts         37
-time_step       4800 # seconds
-lengths         30*0.01
-dispersivities  30*0.005
-thermal_diffusion 2 3e-10
-print_cells     30
-punch_cells    30
-multi_d        false

```

END

SOLUTION\_SPREAD

units mg/l

temp 22

Number	Alkalinity mg/l as HCO <sub>3</sub>	pH	Ca	Mg	Na	Cl	S(6) mg/l as SO <sub>4</sub>	U	Br
0	150	7.5	120	24	69	71	288	0	0

TRANSPORT # 336-380 hours

```

-cells          30
-shifts         35
-time_step       4800 # seconds
-lengths         30*0.01
-dispersivities  30*0.005
-thermal_diffusion 2 3e-10
-print_cells     30
-punch_cells    30

```

-multi\_d false  
END

SOLUTION\_SPREAD

units mg/l

temp 22

Number	Alkalinity mg/l as HCO <sub>3</sub>	pH	Ca	Mg	Na	Cl	S(6) mg/l as SO <sub>4</sub>	U	Br
0	170	7.3	120	24	69	71	288	0	0

TRANSPORT # 380-423 hours

-cells 30

-shifts 34

-time\_step 4800 # seconds

-lengths 30\*0.01

-dispersivities 30\*0.005

-thermal\_diffusion 2 3e-10

-print\_cells 30

-punch\_cells 30

-multi\_d false

END

## APPENDIX C

### COPYRIGHT PERMISSION TO REPRINT



RightsLink®

Home

Create Account

Help



**Title:** Laboratory column experiments and transport modeling to evaluate retardation of uranium in an aquifer downgradient of a uranium in-situ recovery site

**Author:** Martin A. Dangelmayr, Paul W. Reimus, Naomi L. Wasserman, Jesse J. Punsal, Raymond H. Johnson, James T. Clay, James J. Stone

**Publication:** Applied Geochemistry

**Publisher:** Elsevier

**Date:** May 2017

© 2017 Elsevier Ltd. All rights reserved.

**LOGIN**

If you're a **copyright.com** user, you can login to RightsLink using your copyright.com credentials. Already a **RightsLink** user or want to [learn more?](#)

Please note that, as the author of this Elsevier article, you retain the right to include it in a thesis or dissertation, provided it is not published commercially. Permission is not required, but please ensure that you reference the journal as the original source. For more information on this and on your other retained rights, please visit: <https://www.elsevier.com/about/our-business/policies/copyright#Author-rights>

BACK

CLOSE WINDOW

Copyright © 2017 Copyright Clearance Center, Inc. All Rights Reserved. [Privacy statement](#). [Terms and Conditions](#). Comments? We would like to hear from you. E-mail us at [customer@copyright.com](mailto:customer@copyright.com)

## LITERATURE CITED

- Abitz, Richard, and Jack Kooyoomjian. "Considerations Related to Post-Closure Monitoring of Uranium in-Situ Recovery Sites.", 2011.
- Ames, Lloyd L, Jefferey E McGarrah, and Becky A Walker. "Sorption of Uranium and Radium by Biotite, Muscovite, and Phlogopite." *Clays Clay Miner* 31, no. 5 (1983): 343-51.
- Anderson, Robert T, and Derek R Lovley. "Microbial Redox Interactions with Uranium: An Environmental Perspective." *Interactions of microorganisms with radionuclides* 2 (2002): 205-23.
- Aquino, Sérgio F, and David C Stuckey. "Integrated Model of the Production of Soluble Microbial Products (Smp) and Extracellular Polymeric Substances (Eps) in Anaerobic Chemostats During Transient Conditions." *Biochemical Engineering Journal* 38, no. 2 (2008): 138-46.
- Aquino, Sérgio F, and David C Stuckey. "Production of Soluble Microbial Products (Smp) in Anaerobic Chemostats under Nutrient Deficiency." *Journal of environmental engineering* 129, no. 11 (2003): 1007-14.
- Aquino, Sérgio F, and David C Stuckey. "Soluble Microbial Products Formation in Anaerobic Chemostats in the Presence of Toxic Compounds." *Water research* 38, no. 2 (2004): 255-66.
- Artinger, R, TH Rabung, JI Kim, S Sachs, K Schmeide, KH Heise, G Bernhard, and H Nitsche. "Humic Colloid-Borne Migration of Uranium in Sand Columns." *Journal of contaminant hydrology* 58, no. 1 (2002): 1-12.
- Bachmaf, Samer, and Broder J. Merkel. "Sorption of Uranium(VI) at the Clay Mineral–Water Interface." *Environmental Earth Sciences* 63, no. 5 (2011): 925-34.
- Bao, Chen, Hongfei Wu, Li Li, Darrell Newcomer, Philip E Long, and Kenneth H Williams. "Uranium Bioreduction Rates across Scales: Biogeochemical Hot Moments and Hot Spots During a Biostimulation Experiment at Rifle, Colorado." *Environmental science & technology* 48, no. 17 (2014): 10116-27.
- Bargar, John R, Rebecca Reitmeyer, John J Lenhart, and James A Davis. "Characterization of U (Vi)-Carbonato Ternary Complexes on Hematite: Exafs and Electrophoretic Mobility Measurements." *Geochimica et Cosmochimica Acta* 64, no. 16 (2000): 2737-49.
- Barker, Duncan J, and David C Stuckey. "A Review of Soluble Microbial Products (Smp) in Wastewater Treatment Systems." *Water Research* 33, no. 14 (1999): 3063-82.
- Barnett, Mark O, Philip M Jardine, and Scott C Brooks. "U (Vi) Adsorption to Heterogeneous Subsurface Media: Application of a Surface Complexation Model." *Environmental*

- science & technology* 36, no. 5 (2002): 937-42.
- Behrends, Thilo, and Philippe Van Cappellen. "Competition between Enzymatic and Abiotic Reduction of Uranium(Vi) under Iron Reducing Conditions." *Chemical Geology* 220, no. 3-4 (2005): 315-27.
- Bernhard, G, G Geipel, T Reich, V Brendler, S Amayri, and Heino Nitsche. "Uranyl (Vi) Carbonate Complex Formation: Validation of the  $\text{Ca}_2\text{UO}_2^+(\text{CO}_3)_3$  (Aq.) Species." *Radiochimica Acta International journal for chemical aspects of nuclear science and technology* 89, no. 8 (2001): 511.
- Bernier-Latmani, Rizlan, Harish Veeramani, Elena Dalla Vecchia, Pilar Junier, Juan S Lezama-Pacheco, Elena I Suvorova, Jonathan O Sharp, Nicholas S Wigginton, and John R Bargar. "Non-Uraninite Products of Microbial U (Vi) Reduction." *Environmental science & technology* 44, no. 24 (2010): 9456-62.
- Bertetti, F Paul, Roberto T Pabalan, and Michael G Almendarez. *Studies of Neptunium (V), Sorption on Quartz, Clinoptilolite, Montmorillonite and Alumina*. Adsorption of Metals by Geomedia. San Diego, CA: Academic Press, 1998.
- Black, JH., and KL. Kipp Jr. "Movement of Tracers through Dual-Porosity Media — Experiments and Modelling in the Cretaceous Chalk, England." *Journal of Hydrology* 62, no. 1-4 (1983): 287-312.
- Borch, Thomas, Nicholas Roche, and Thomas E Johnson. "Determination of Contaminant Levels and Remediation Efficacy in Groundwater at a Former In Situ Recovery Uranium Mine." *Journal of Environmental Monitoring* 14, no. 7 (2012): 1814-23.
- Bratsch, Steven G. "Standard Electrode Potentials and Temperature Coefficients in Water at 298.15 K." *Journal of Physical and Chemical Reference Data* 18, no. 1 (1989): 1-21.
- Brouyère, Serge. "Modelling the Migration of Contaminants through Variably Saturated Dual-Porosity, Dual-Permeability Chalk." *Journal of Contaminant Hydrology* 82, no. 3-4 (2006): 195-219.
- Carstea, Elfrida M., John Bridgeman, Andy Baker, and Darren M. Reynolds. "Fluorescence Spectroscopy for Wastewater Monitoring: A Review." *Water Research* 95 (2016): 205-19.
- Catalano, Jeffrey G., and Gordon E. Brown Jr. "Uranyl Adsorption onto Montmorillonite: Evaluation of Binding Sites and Carbonate Complexation." *Geochimica et Cosmochimica Acta* 69, no. 12 (2005): 2995-3005.
- Catchpole, Mr G, and R Kuchelka. "Groundwater Restoration of Uranium Isl Mines in the United States." (1993).
- Chen, Wen, Paul Westerhoff, Jerry A Leenheer, and Karl Booksh. "Fluorescence Excitation-

- Emission Matrix Regional Integration to Quantify Spectra for Dissolved Organic Matter." *Environmental science & technology* 37, no. 24 (2003): 5701-10.
- Cheng, Tao, Mark O Barnett, Eric E Roden, and Jinling Zhuang. "Reactive Transport of Uranium (Vi) and Phosphate in a Goethite-Coated Sand Column: An Experimental Study." *Chemosphere* 68, no. 7 (2007): 1218-23.
- Curti, Enzo. "Coprecipitation of Radionuclides with Calcite: Estimation of Partition Coefficients Based on a Review of Laboratory Investigations and Geochemical Data." *Applied Geochemistry* 14, no. 4 (6// 1999): 433-45.
- Curtis, Gary P, James A Davis, and David L Naftz. "Simulation of Reactive Transport of Uranium (Vi) in Groundwater with Variable Chemical Conditions." *Water Resources Research* 42, no. 4 (2006).
- Dangelmayr, Martin A, Paul W Reimus, Naomi L Wasserman, Jesse J Punsal, Raymond H Johnson, James T Clay, and James J Stone. "Laboratory Column Experiments and Transport Modeling to Evaluate Retardation of Uranium in an Aquifer Downgradient of a Uranium in-Situ Recovery Site." *Applied Geochemistry* 80 (2017): 1-13.
- Davis, JA, JA Coston, DB Kent, and CC Fuller. "Application of the Surface Complexation Concept to Complex Mineral Assemblages." *Environmental Science & Technology* 32, no. 19 (1998): 2820-28.
- Davis, James A, and Gary P Curtis. *Application of Surface Complexation Modeling to Describe Uranium (Vi) Adsorption and Retardation at the Uranium Mill Tailings Site at Naturita, Colorado*. Division of Systems Analysis and Regulatory Effectiveness, Office of Nuclear Regulatory Research, US Nuclear Regulatory Commission, 2003.
- Davis, James A, and Gary P Curtis. *Consideration of Geochemical Issues in Groundwater Restoration at Uranium in-Situ Leach Mining Facilities*. Division of Fuel, Engineering, and Radiological Research, Office of Nuclear Regulatory Research, US Nuclear Regulatory Commission, 2007.
- Davis, JA, SP Hyun, PM Fox, and KF Hayes. "A Surface Complexation Modeling Approach for Uranium (VI) Transport in Groundwater." In *International Mine Water Conference*. Pretoria, South Africa, 2009.
- Davis, JA, and DB Kent. "Surface Complexation Modeling in Aqueous Geochemistry." *Reviews in Mineralogy and Geochemistry* 23, no. 1 (1990): 177-260.
- Davis, James A, David E Meece, Matthias Kohler, and Gary P Curtis. "Approaches to Surface Complexation Modeling of Uranium (VI) Adsorption on Aquifer Sediments." *Geochimica et Cosmochimica Acta* 68, no. 18 (2004): 3621-41.
- Dittrich, Timothy. M., and Paul W. Reimus. "Uranium Transport in a Crushed Granodiorite:

- Experiments and Reactive Transport Modeling." *Journal of Contaminant Hydrology* 175–176 (2015): 44-59.
- Doherty, John E, and Randall J Hunt. *Approaches to Highly Parameterized Inversion: A Guide to Using Pest for Groundwater-Model Calibration*. US Department of the Interior, US Geological Survey, 2010.
- Dong, Wenming, William P Ball, Chongxuan Liu, Zheming Wang, Alan T Stone, Jing Bai, and John M Zachara. "Influence of Calcite and Dissolved Calcium on Uranium (VI) Sorption to a Hanford Subsurface Sediment." *Environmental science & technology* 39, no. 20 (2005): 7949-55.
- Dong, Wenming, and Scott C Brooks. "Determination of the Formation Constants of Ternary Complexes of Uranyl and Carbonate with Alkaline Earth Metals (Mg<sup>2+</sup>, Ca<sup>2+</sup>, Sr<sup>2+</sup>, and Ba<sup>2+</sup>) Using Anion Exchange Method." *Environmental science & technology* 40, no. 15 (2006): 4689-95.
- Dong, Wenming, and Scott C Brooks. "Formation of Aqueous MgUO<sub>2</sub> (CO<sub>3</sub>)<sub>3</sub><sup>2-</sup> Complex and Uranium Anion Exchange Mechanism onto an Exchange Resin." *Environmental science & technology* 42, no. 6 (2008): 1979-83.
- Dong, Wenming, Tetsu K Tokunaga, James A Davis, and Jiamin Wan. "Uranium (VI) Adsorption and Surface Complexation Modeling onto Background Sediments from the F-Area Savannah River Site." *Environmental science & technology* 46, no. 3 (2012): 1565-71.
- Dzombak, David A, and Francois MM Morel. *Surface Complexation Modeling: Hydrous Ferric Oxide*. John Wiley & Sons, 1990.
- Echevarria, Guillaume, Marsha I Sheppard, and JeanLouis Morel. "Effect of Ph on the Sorption of Uranium in Soils." *Journal of Environmental Radioactivity* 53, no. 2 (2001): 257-64.
- Englert, A., SS. Hubbard, KH. Williams, L Li, and CI. Steefel. "Feedbacks between Hydrological Heterogeneity and Bioremediation Induced Biogeochemical Transformations." *Environmental Science & Technology* 43, no. 14 (2009): 5197-204.
- Evans, Nick, Peter Warwick, Tara Lewis, and Nick Bryan. "Influence of Humic Acid on the Sorption of Uranium (IV) to Kaolin." *Environmental Chemistry Letters* 9, no. 1 (2011): 25-30.
- Fellman, Jason B, Eran Hood, and Robert GM Spencer. "Fluorescence Spectroscopy Opens New Windows into Dissolved Organic Matter Dynamics in Freshwater Ecosystems: A Review." *Limnology and Oceanography* 55, no. 6 (2010): 2452-62.
- Ferreira, Carlos MH, Isabel SS Pinto, Eduardo V Soares, and Helena MVM Soares. "(Un) Suitability of the Use of Ph Buffers in Biological, Biochemical and Environmental

- Studies and Their Interaction with Metal Ions—a Review." *RSC Advances* 5, no. 39 (2015): 30989-1003.
- Fox, Patricia M, James A Davis, and John M Zachara. "The Effect of Calcium on Aqueous Uranium (VI) Speciation and Adsorption to Ferrihydrite and Quartz." *Geochimica et Cosmochimica Acta* 70, no. 6 (2006): 1379-87.
- Freguia, Stefano, Korneel Rabaey, Zhiguo Yuan, and Jürg Keller. "Electron and Carbon Balances in Microbial Fuel Cells Reveal Temporary Bacterial Storage Behavior During Electricity Generation." *Environmental Science & Technology* 41, no. 8 (2007): 2915-21.
- Ganesh, Rajagopalan, Kevin G Robinson, Gregory D Reed, and Gary S Saylor. "Reduction of Hexavalent Uranium from Organic Complexes by Sulfate- and Iron-Reducing Bacteria." *Applied and Environmental Microbiology* 63, no. 11 (1997): 4385-91.
- Geipel, G, G Bernhard, V Brendler, and H Nitsche. "Complex Formation between  $UO_2^{2+}$  and  $CO_3^{2-}$ : Studied by Laser-Induced Photoacoustic Spectroscopy (LIPAS)." *Radiochimica Acta* 82, no. s1 (1998): 59-62.
- Ginder-Vogel, Matthew, Craig S Criddle, and Scott Fendorf. "Thermodynamic Constraints on the Oxidation of Biogenic  $UO_2$  by Fe (III)(Hydr) Oxides." *Environmental science & technology* 40, no. 11 (2006): 3544-50.
- Gorby, Yuri A, and Derek R Lovley. "Enzymic Uranium Precipitation." *Environmental Science & Technology* 26, no. 1 (1992): 205-07.
- Gu, Baohua, Wei-Min Wu, Matthew A Ginder-Vogel, Hui Yan, Matthew W Fields, Jizhong Zhou, Scott Fendorf, Craig S Criddle, and Philip M Jardine. "Bioreduction of Uranium in a Contaminated Soil Column." *Environmental science & technology* 39, no. 13 (2005): 4841-47.
- Gu, Baohua, Hui Yan, Ping Zhou, David B Watson, Melora Park, and Jonathan Istok. "Natural Humics Impact Uranium Bioreduction and Oxidation." *Environmental science & technology* 39, no. 14 (2005): 5268-75.
- Guillaumont, Robert, and Federico J Mompean. "Update on the Chemical Thermodynamics of Uranium, Neptunium, Plutonium, Americium and Technetium." Netherlands: NEA, 2003.
- Gustafsson, Jon Petter, Ellinor Dässman, and Mattias Bäckström. "Towards a Consistent Geochemical Model for Prediction of Uranium (VI) Removal from Groundwater by Ferrihydrite." *Applied Geochemistry* 24, no. 3 (2009): 454-62.
- Hall, Susan. "Groundwater Restoration at Uranium in-Situ Recovery Mines, South Texas Coastal Plain." US Geological Survey, 2009.
- He, Xiao-Song, Bei-Dou Xi, Zi-Min Wei, Yong-Hai Jiang, Yu Yang, Da An, Jin-Ling Cao, and

- Hong-Liang Liu. "Fluorescence Excitation–Emission Matrix Spectroscopy with Regional Integration Analysis for Characterizing Composition and Transformation of Dissolved Organic Matter in Landfill Leachates." *Journal of Hazardous Materials* 190, no. 1–3 (2011): 293-99.
- Henderson, RK., ABaker, KR. Murphy, A Hambly, RM. Stuetz, and SJ. Khan. "Fluorescence as a Potential Monitoring Tool for Recycled Water Systems: A Review." *Water Research* 43, no. 4 (2009): 863-81.
- Ho, CH., and NH. Miller. "Adsorption of Uranyl Species from Bicarbonate Solution onto Hematite Particles." *Journal of Colloid and Interface Science* 110, no. 1 (1986): 165-71.
- Huber, Maximilian, Sophia C Badenberg, Moritz Wulff, Jörg E Drewes, and Brigitte Helmreich. "Evaluation of Factors Influencing Lab-Scale Studies to Determine Heavy Metal Removal by Six Sorbents for Stormwater Treatment." *Water* 8, no. 2 (2016): 62.
- Hunter, John. "Fluvial Architecture and Paleo-Ground Water Infiltration of the Fort Union Formation near the Highland Uranium Mine, Southern Powder River Basin, Wyoming." 119-39: Wyoming Geological Association, 1999.
- Hur, Jin, Min-Hye Park, and Mark A Schlautman. "Microbial Transformation of Dissolved Leaf Litter Organic Matter and Its Effects on Selected Organic Matter Operational Descriptors." *Environmental science & technology* 43, no. 7 (2009): 2315-21.
- Hyun, Sung Pil, Patricia M Fox, James A Davis, Kate M Campbell, Kim F Hayes, and Philip E Long. "Surface Complexation Modeling of U (VI) Adsorption by Aquifer Sediments from a Former Mill Tailings Site at Rifle, Colorado." *Environmental science & technology* 43, no. 24 (2009): 9368-73.
- Jang, Je-Hun, Brian A Dempsey, and William D Burgos. "A Model-Based Evaluation of Sorptive Reactivities of Hydrous Ferric Oxide and Hematite for U (VI)." *Environmental science & technology* 41, no. 12 (2007): 4305-10.
- Janoš, Pavel, Sylvie Kříženecká, and Libuše Madronová. "Acid–Base Titration Curves of Solid Humic Acids." *Reactive and Functional Polymers* 68, no. 1 (2008): 242-47.
- Jarusutthirak, Chalor, and Gary Amy. "Understanding Soluble Microbial Products (Smp) as a Component of Effluent Organic Matter (Efom)." *Water Research* 41, no. 12 (2007): 2787-93.
- Johnson, Raymond H, Ryan A Truax, David A Lankford, and James J Stone. "Sorption Testing and Generalized Composite Surface Complexation Models for Determining Uranium Sorption Parameters at a Proposed in-Situ Recovery Site." *Mine Water and the Environment* (2016): 1-12.
- Johnson, Raymond H, and Hlanganani Tutu. "Predictive Reactive Transport Modeling at a

- Proposed Uranium in Situ Recovery Site with a General Data Collection Guide." *Mine Water and the Environment* (2015): 1-12.
- Johnson, Raymond H, and Hlanganani Tutu. "Reactive Transport Modeling at Uranium in Situ Recovery Sites: Uncertainties in Uranium Sorption on Iron Hydroxides." *Reliable mine water technology* 1 (2013): 377-83.
- Kalmykov, Stepan N, and Gregory R Choppin. "Mixed  $\text{Ca}^{2+}/\text{UO}_2^{2+}/\text{CO}_3^{2-}$ -Complex Formation at Different Ionic Strengths." *Radiochimica Acta International journal for chemical aspects of nuclear science and technology* 88, no. 9-11/2000 (2000): 603.
- Kang, Phil-Goo, and Myron J. Mitchell. "Bioavailability and Size-Fraction of Dissolved Organic Carbon, Nitrogen, and Sulfur at the Arbutus Lake Watershed, Adirondack Mountains, Ny." *Biogeochemistry* 115, no. 1 (2013): 213-34.
- Kelly, Shelly D, Kenneth M Kemner, and Scott C Brooks. "X-Ray Absorption Spectroscopy Identifies Calcium-Uranyl-Carbonate Complexes at Environmental Concentrations." *Geochimica et cosmochimica acta* 71, no. 4 (2007): 821-34.
- Kitano, Yasushi, and Tamotsu Oomori. "The Coprecipitation of Uranium with Calcium Carbonate." *Journal of the Oceanographical Society of Japan* 27, no. 1 (1971): 34-42.
- Kohler, M, GP Curtis, DB Kent, and JA Davis. "Experimental Investigation and Modeling of Uranium (VI) Transport under Variable Chemical Conditions." *Water Resources Research* 32, no. 12 (1996): 3539-51.
- Komlos, John, Aaron Peacock, Ravi K Kukkadapu, and Peter R Jaffé. "Long-Term Dynamics of Uranium Reduction/Reoxidation under Low Sulfate Conditions." *Geochimica et Cosmochimica Acta* 72, no. 15 (2008): 3603-15.
- Korichi, Smain, and Aicha Bensmaili. "Sorption of Uranium (VI) on Homoionic Sodium Smectite Experimental Study and Surface Complexation Modeling." *Journal of hazardous materials* 169, no. 1 (2009): 780-93.
- Krishna, Chundakkadu, and Mark CM Van Loosdrecht. "Effect of Temperature on Storage Polymers and Settleability of Activated Sludge." *Water Research* 33, no. 10 (1999): 2374-82.
- Kuráň, Pavel, Pavel Janoš, Libuše Madronová, Jaromír Novák, and Josef Kozler. "Determination of OH Groups in Humic Acids Using Methylation with Dimethylsulfate." *Talanta* 76, no. 4 (2008): 960-63.
- Laspidou, Chrysi S, and Bruce E Rittmann. "A Unified Theory for Extracellular Polymeric Substances, Soluble Microbial Products, and Active and Inert Biomass." *Water Research* 36, no. 11 (2002): 2711-20.

- Lenhart, John J., and Bruce D. Honeyman. "Uranium(VI) Sorption to Hematite in the Presence of Humic Acid." *Geochimica et Cosmochimica Acta* 63, no. 19–20 (1999): 2891-901.
- Lewis, Jeffrey, and Jan Sjöström. "Optimizing the Experimental Design of Soil Columns in Saturated and Unsaturated Transport Experiments." *Journal of contaminant hydrology* 115, no. 1 (2010): 1-13.
- Li, Li, Carl I Steefel, Kenneth H Williams, Michael J Wilkins, and Susan S Hubbard. "Mineral Transformation and Biomass Accumulation Associated with Uranium Bioremediation at Rifle, Colorado." *Environmental science & technology* 43, no. 14 (2009): 5429-35.
- Liger, Emmanuelle, Laurent Charlet, and Philippe Van Cappellen. "Surface Catalysis of Uranium(Vi) Reduction by Iron(Ii)." *Geochimica et Cosmochimica Acta* 63, no. 19–20 (1999): 2939-55.
- Liu, Chongxuan, Yuanyuan Liu, Sebastien Kerisit, and John Zachara. "Pore-Scale Process Coupling and Effective Surface Reaction Rates in Heterogeneous Subsurface Materials." *Reviews in Mineralogy and Geochemistry* 80, no. 1 (2015): 191.
- Liu, Chongxuan, Jianying Shang, Sebastien Kerisit, John M. Zachara, and Weihuang Zhu. "Scale-Dependent Rates of Uranyl Surface Complexation Reaction in Sediments." *Geochimica et Cosmochimica Acta* 105 (2013): 326-41.
- Loganathan, Vijay A., Mark O. Barnett, T. Prabhakar Clement, and Sushil R. Kanel. "Scaling of Adsorption Reactions: U(Vi) Experiments and Modeling." *Applied Geochemistry* 24, no. 11 (2009): 2051-60.
- Lovley, Derek R, and Elizabeth J Phillips. "Reduction of Uranium by Desulfovibrio Desulfuricans." *Applied and Environmental Microbiology* 58, no. 3 (1992): 850-56.
- Maček, Matej, Alenka Mauko, Ana Mladenovič, Bojan Majes, and Ana Petkovšek. "A Comparison of Methods Used to Characterize the Soil Specific Surface Area of Clays." *Applied Clay Science* 83–84 (2013): 144-52.
- Macfarlane, Allison M., and Marvin Miller. "Nuclear Energy and Uranium Resources." *Elements* 3, no. 3 (2007): 185-92.
- Mahoney, John J, Sonya A Cadle, and Ryan T Jakubowski. "Uranyl Adsorption onto Hydrated Ferric Oxide: A Re-Evaluation for the Diffuse Layer Model Database." *Environmental science & technology* 43, no. 24 (2009): 9260-66.
- Mangini, A, CH Sonntag, G Bertsch, and E Müller. "Evidence for a Higher Natural Uranium Content in World Rivers." *Nature* 278 (1979): 337-39.
- Marschner, Bernd, and Karsten Kalbitz. "Controls of Bioavailability and Biodegradability of Dissolved Organic Matter in Soils." *Geoderma* 113, no. 3 (2003/05/01/ 2003): 211-35.

- McKnight, Diane M, Elizabeth W Boyer, Paul K Westerhoff, Peter T Doran, Thomas Kulbe, and Dale T Andersen. "Spectrofluorometric Characterization of Dissolved Organic Matter for Indication of Precursor Organic Material and Aromaticity." *Limnology and Oceanography* 46, no. 1 (2001): 38-48.
- Mcnaughton, Christina. "Influence of Mercury-Dissolved Organic Matter (DOM) Complexation on Toxicity in Natural Waters." (2007).
- Mibus, Jens, Susanne Sachs, Wilfried Pflingsten, Cordula Nebelung, and Gert Bernhard. "Migration of Uranium (IV)/(VI) in the Presence of Humic Acids in Quartz Sand: A Laboratory Column Study." *Journal of contaminant hydrology* 89, no. 3 (2007): 199-217.
- Miller, Andrew W, Derrick R Rodriguez, and Bruce D Honeyman. "Simplified Behaviors from Increased Heterogeneity: I. 2-D Uranium Transport Experiments at the Decimeter Scale." *Journal of contaminant hydrology* 148 (2013): 39-50.
- Miller, Andrew W, Derrick R Rodriguez, and Bruce D Honeyman. "Upscaling Sorption/Desorption Processes in Reactive Transport Models to Describe Metal/Radionuclide Transport: A Critical Review." *Environmental science & technology* 44, no. 21 (2010): 7996-8007.
- Missana, T, M Garcia-Gutiérrez, and U Alonso. "Kinetics and Irreversibility of Cesium and Uranium Sorption onto Bentonite Colloids in a Deep Granitic Environment." *Applied Clay Science* 26, no. 1 (2004): 137-50.
- Morrison, Stan J, Robert R Spangler, and Vijay S Tripathi. "Adsorption of Uranium (VI) on Amorphous Ferric Oxyhydroxide at High Concentrations of Dissolved Carbon (IV) and Sulfur (VI)." *Journal of Contaminant Hydrology* 17, no. 4 (1995): 333-46.
- Mudd, Gavin M. "The Future of Yellowcake: A Global Assessment of Uranium Resources and Mining." *Science of the Total Environment* 472 (2014): 590-607.
- Nair, Sreejesh, and Broder J Merkel. "Effect of Mg-Ca-Sr on the Sorption Behavior of Uranium (VI) on Silica." In *The New Uranium Mining Boom*, 763-70: Springer, 2011.
- Nair, Sreejesh, and Broder J Merkel. "Impact of Alkaline Earth Metals on Aqueous Speciation of Uranium (VI) and Sorption on Quartz." *Aquatic Geochemistry* 17, no. 3 (2011): 209-19.
- Namkung, Eun, and Bruce E. Rittmann. "Soluble Microbial Products (Smp) Formation Kinetics by Biofilms." *Water Research* 20, no. 6 (1986): 795-806.
- Ni, Bing-Jie, Fang Fang, Bruce E Rittmann, and Han-Qing Yu. "Modeling Microbial Products in Activated Sludge under Feast–Famine Conditions." *Environmental science & technology* 43, no. 7 (2009): 2489-97.
- Ni, Bing-Jie, Fang Fang, Wen-Ming Xie, Min Sun, Guo-Ping Sheng, Wei-Hua Li, and Han-Qing

- Yu. "Characterization of Extracellular Polymeric Substances Produced by Mixed Microorganisms in Activated Sludge with Gel-Permeating Chromatography, Excitation–Emission Matrix Fluorescence Spectroscopy Measurement and Kinetic Modeling." *Water research* 43, no. 5 (2009): 1350-58.
- Ni, Bing-Jie, Bruce E Rittmann, Fang Fang, Juan Xu, and Han-Qing Yu. "Long-Term Formation of Microbial Products in a Sequencing Batch Reactor." *water research* 44, no. 13 (2010): 3787-96.
- Ni, Bing-Jie, Raymond J Zeng, Fang Fang, Wen-Ming Xie, Guo-Ping Sheng, and Han-Qing Yu. "Fractionating Soluble Microbial Products in the Activated Sludge Process." *Water Research* 44, no. 7 (2010): 2292-302.
- North, Nadia N, Sherry L Dollhopf, Lainie Petrie, Jonathan D Istok, David L Balkwill, and Joel E Kostka. "Change in Bacterial Community Structure During in Situ Biostimulation of Subsurface Sediment Cocontaminated with Uranium and Nitrate." *Applied and environmental microbiology* 70, no. 8 (2004): 4911-20.
- Ohno, Tsutomu, Aria Amirbahman, and Rasmus Bro. "Parallel Factor Analysis of Excitation–Emission Matrix Fluorescence Spectra of Water Soluble Soil Organic Matter as Basis for the Determination of Conditional Metal Binding Parameters." *Environmental science & technology* 42, no. 1 (2008): 186-92.
- Osiensky, James L, and Roy E Williams. "Factors Affecting Efficient Aquifer Restoration at in Situ Uranium Mine Sites." *Groundwater Monitoring & Remediation* 10, no. 2 (1990): 107-12.
- Papynov, EK, AS Portnyagin, AI Cherednichenko, IA Tkachenko, EB Modin, V Yu Maiorov, AN Dran'kov, *et al.* "Uranium Sorption on Reduced Porous Iron Oxides." Paper presented at the Doklady Physical Chemistry, 2016.
- Parkhurst, David L, and CAJ Appelo. "Description of Input and Examples for Phreeqc Version 3—a Computer Program for Speciation, Batch-Reaction, One-Dimensional Transport, and Inverse Geochemical Calculations." *US geological survey techniques and methods, book 6* (2013): 497.
- Payne, Tim. E., James. A. Davis, GR Lumpkin, R Chisari, and TD Waite. "Surface Complexation Model of Uranyl Sorption on Georgia Kaolinite." *Applied Clay Science* 26, no. 1–4 (8// 2004): 151-62.
- Payne, Tim E, V Brendler, M Ochs, B Baeyens, PL Brown, JA Davis, Christian Ekberg, *et al.* "Guidelines for Thermodynamic Sorption Modelling in the Context of Radioactive Waste Disposal." *Environmental modelling & software* 42 (2013): 143-56.
- Payne, Timothy E, James A Davis, Michael Ochs, Markus Olin, and Cherry J Tweed. "Uranium Adsorption on Weathered Schist—Intercomparison of Modelling Approaches."

- Radiochimica Acta* 92, no. 9-11 (2004): 651-61.
- Pelizza, MS. "In-Situ Recovery of Uranium." *Southwest Hydrol* 7, no. 6 (2008): 28-29.
- Phillippi, John M, Vijay A Loganathan, Melissa J McIndoe, Mark O Barnett, T Prabhakar Clement, and Eric E Roden. "Theoretical Solid/Solution Ratio Effects on Adsorption and Transport: Uranium (VI) and Carbonate." *Soil Science Society of America Journal* 71, no. 2 (2007): 329-35.
- Porro, Indrek, Meredith E. Newman, and Frank M. Dunnivant. "Comparison of Batch and Column Methods for Determining Strontium Distribution Coefficients for Unsaturated Transport in Basalt." *Environmental Science & Technology* 34, no. 9 (2000): 1679-86.
- Prikryl, James D., Alka Jain, David R. Turner, and Roberto T. Pabalan. "Uranium(VI) Sorption Behavior on Silicate Mineral Mixtures." *Journal of Contaminant Hydrology* 47, no. 2-4 (2001): 241-53.
- Reeder, Richard J., Melissa Nugent, C. Drew Tait, David E. Morris, Steve M. Heald, Kenneth M. Beck, Wayne P. Hess, and Anthony Lanzirotti. "Coprecipitation of Uranium(VI) with Calcite: Xafs, Micro-Xas, and Luminescence Characterization." *Geochimica et Cosmochimica Acta* 65, no. 20 (2001): 3491-503.
- Regberg, Aaron, Kamini Singha, Ming Tien, Flynn Picardal, Quanxing Zheng, Jurgen Schieber, Eric Roden, and Susan L Brantley. "Electrical Conductivity as an Indicator of Iron Reduction Rates in Abiotic and Biotic Systems." *Water resources research* 47, no. 4 (2011).
- Rittmann, Bruce E, and Perry L McCarty. *Environmental Biotechnology: Principles and Applications*. New York: McGraw-Hill, 2001.
- Seifert, Dorte, and Peter Engesgaard. "Sand Box Experiments with Bioclogging of Porous Media: Hydraulic Conductivity Reductions." *Journal of Contaminant Hydrology* 136-137, no. Supplement C (2012): 1-9.
- Seifert, Dorte, and Peter Engesgaard. "Use of Tracer Tests to Investigate Changes in Flow and Transport Properties Due to Bioclogging of Porous Media." *Journal of contaminant hydrology* 93, no. 1 (2007): 58-71.
- Sheng, Guo-Ping, and Han-Qing Yu. "Characterization of Extracellular Polymeric Substances of Aerobic and Anaerobic Sludge Using Three-Dimensional Excitation and Emission Matrix Fluorescence Spectroscopy." *Water Research* 40, no. 6 (2006): 1233-39.
- Sheppard, SC, and WG Evenden. "Critical Compilation and Review of Plant/Soil Concentration Ratios for Uranium, Thorium and Lead." *Journal of Environmental Radioactivity* 8, no. 3 (1988): 255-85.

- Stewart, Brandy D, Melanie A Mayes, and Scott Fendorf. "Impact of Uranyl– Calcium– Carbonato Complexes on Uranium (VI) Adsorption to Synthetic and Natural Sediments." *Environmental science & technology* 44, no. 3 (2010): 928-34.
- Tan, Kim H. *Principles of Soil Chemistry*. CRC press, 2010.
- Tian, Yu. "Behaviour of Bacterial Extracellular Polymeric Substances from Activated Sludge: A Review." *International Journal of Environment and Pollution* 32, no. 1 (2008): 78-89.
- Truax, Ryan A. "Generic Complexation Sorption and Downgradient Transport Modeling for the Smith Ranch Highland Uranium in-Situ Recovery Site in Wyoming, USA." Thesis, South Dakota School of Mines and Technology, 2015.
- USEPA. 1994. U.S. EPA Method 200.8, Methods for the Determination of the Trace Metals in Waters and Wastewaters. In *Methods for the Determination of Metals in Environmental Samples- Supplement 1*; EPA 600/R-94-111; U.S. Government Publishing Office: Washington DC, 1994.
- USGS. Reston, Virginia. 2009. "Groundwater Restoration at Uranium In-Situ Recovery Mines, South Texas Coastal Plain." Uranium 2009 Conference, Keystone CO.
- Waite, TD, JA Davis, TE Payne, GA Waychunas, and N Xu. "Uranium (VI) Adsorption to Ferrihydrite: Application of a Surface Complexation Model." *Geochimica et Cosmochimica Acta* 58, no. 24 (1994): 5465-78.
- Wang, Zhi-Ping, and Tong Zhang. "Characterization of Soluble Microbial Products (Smp) under Stressful Conditions." *Water Research* 44, no. 18 (2010): 5499-509.
- Wang, Zhi-Wu, Yu Liu, and Joo-Hwa Tay. "Biodegradability of Extracellular Polymeric Substances Produced by Aerobic Granules." *Applied microbiology and biotechnology* 74, no. 2 (2007): 462-66.
- Weishaar, James L, George R Aiken, Brian A Bergamaschi, Miranda S Fram, Roger Fujii, and Kenneth Mopper. "Evaluation of Specific Ultraviolet Absorbance as an Indicator of the Chemical Composition and Reactivity of Dissolved Organic Carbon." *Environmental Science & Technology* 37, no. 20 (2003): 4702-08.
- Wersin, Paul, Michael F Hochella, Per Persson, George Redden, James O Leckie, and David W Harris. "Interaction between Aqueous Uranium (VI) and Sulfide Minerals: Spectroscopic Evidence for Sorption and Reduction." *Geochimica et Cosmochimica Acta* 58, no. 13 (1994): 2829-43.
- Williams, Kenneth H, John R Bargar, Jonathan R Lloyd, and Derek R Lovley. "Bioremediation of Uranium-Contaminated Groundwater: A Systems Approach to Subsurface Biogeochemistry." *Current opinion in biotechnology* 24, no. 3 (2013): 489-97.

- Williams, Kenneth H, Philip E Long, James A Davis, Michael J Wilkins, A Lucie N'Guessan, Carl I Steefel, Li Yang, *et al.* "Acetate Availability and Its Influence on Sustainable Bioremediation of Uranium-Contaminated Groundwater." *Geomicrobiology Journal* 28, no. 5-6 (2011): 519-39.
- Xie, Wen-Ming, Bing-Jie Ni, Raymond J Zeng, Guo-Ping Sheng, Han-Qing Yu, Jing Song, De-Zhi Le, *et al.* "Formation of Soluble Microbial Products by Activated Sludge under Anoxic Conditions." *Applied microbiology and biotechnology* 87, no. 1 (2010): 373-82.
- Yabusaki, Steven B, Yilin Fang, Philip E Long, Charles T Resch, Aaron D Peacock, John Komlos, Peter R Jaffe, *et al.* "Uranium Removal from Groundwater Via in Situ Biostimulation: Field-Scale Modeling of Transport and Biological Processes." *Journal of contaminant hydrology* 93, no. 1 (2007): 216-35.
- Yuang, Paul-Cheng, and Yun-Hwei Shen. "Determination of the Surface Area of Smectite in Water by Ethylene Oxide Chain Adsorption." *Journal of Colloid and Interface Science* 285, no. 2 (2005): 443-47.
- Zhang, Fan, Jack C Parker, Scott C Brooks, Y-J Kim, Guoping Tang, Philip M Jardine, and David B Watson. "Comparison of Approaches to Calibrate a Surface Complexation Model for U (Vi) Sorption to Weathered Saprofite." *Transport in porous media* 78, no. 2 (2009): 185-97.
- Zhao, Weihong, Jiangtao Wang, and Meimei Chen. "Three-Dimensional Fluorescence Characteristics of Dissolved Organic Matter Produced by *Prorocentrum Donghaiense* Lu." *Chinese Journal of Oceanology and Limnology* 27 (2009): 564-69.
- Zhou, Ping, Hui Yan, and Baohua Gu. "Competitive Complexation of Metal Ions with Humic Substances." *Chemosphere* 58, no. 10 (2005): 1327-37.